Analyzing the role of cancer-associated adipocytes in breast tumor metastasis

Laura Garrido Jiménez

TESI DOCTORAL UPF / 2024

Work carried out under the supervision of Dr. Antonio García de Herreros in the Mechanisms of Tumorigenesis and Tumor Progression group from the Cancer Research Program, at the Hospital del Mar Research Institute (IMIM).

Barcelona 2024

Dr. Antonio García de Herreros
Thesis supervisor

Laura Garrido Jiménez
PhD Student

FACULTY OF MEDICINE AND LIFE SCIENCES

ABSTRACT

In breast cancer, the tumor microenvironment includes adipocytes and fibroblasts. When in contact with breast tumor cells, adipocytes undergo lipolysis and dedifferentiation. This thesis demonstrates that cancer-associated adipocytes (CAAs) shift gene expression towards progenitor, macrophage, and fibroblast phenotypes while decreasing the expression of genes related to lipid metabolism and adipogenesis. These changes support breast tumor cell migration and invasion. Exogenous lipid accumulation in tumor cells does not promote migration, but lipid uptake, lipolysis and catabolism are essential. Adipocytes alter tumor cell metabolism, increasing glucose consumption and reactive oxygen species production, and induce a partial epithelial to mesenchymal transition, with a Snail1 upregulation. Therefore, these findings highlight the crosstalk between adipocytes and breast tumor cells that promotes tumor progression.

RESUM

El microambient tumoral del càncer de mama inclou adipòcits i fibroblasts. Els adipòcits, en contacte amb les cèl·lules tumorals i fibroblasts, pateixen lipòlisi i desdiferenciació. Aquesta tesi demostra que els adipòcits associats al tumor (CAA) canvien l'expressió gènica cap a fenotips progenitors, macròfags i fibroblasts, alhora que disminueixen l'expressió de gens relacionats amb el metabolisme lipídic i l'adipogènesi. Aquests canvis donen suport a la migració i la invasió de cèl·lules tumorals de mama. Tot i que l'acumulació exògena de lípids no afavoreix la migració, la captació de lípids, la lipòlisi i el catabolisme són essencials. Els adipòcits alteren el metabolisme de les cèl·lules tumorals, augmentant el consum de glucosa i la producció d'espècies reactives d'oxigen, i induint una transició epiteli-mesènquima parcial marcada per l'increment de Snail1. Aquests resultats posen de manifest la diafonia entre els adipòcits i les cèl·lules tumorals de mama, afavorint la progressió del tumor.

TABLE OF CONTENTS

LIST OF FIGURES

INTRODUCTION

RESULTS

DISCUSSION

LIST OF TABLES

MATERIALS & METHODS

ACRONYMS AND ABBREVIATIONS

6-AN: 6-Aminonicotinamide

ACLY: ATP citrate lyase

ACSS2: Acyl-coenzyme A synthetase short-chain family member 2

ADFs: Adipocyte-derived fibroblasts

AMT: Adipocyte-to-mesenchymal transition

APN: Adiponectin

ATGL: Adipose triglyceride lipase

ATP: Adenosine triphosphate

AU: Arbitrary units

AZA: Azaserine

BCA: Bicinchoninic acid

BCs: Breast cancer cells

bHLH: basic Helix–Loop–Helix

BMDCs: Bone marrow-derived cells

BMS: BMS-309403

BODIPY: 4,4-Difluoro-1,3,5,7,8-Pentamethyl-4-Bora-3a,4a-Diaza-s-Indacene

BRCA1/2: Breast cancer-associated gene 1/2

BSA: Bovine serum albumin

C/EBP: CCAAT/enhancer-binding protein

CAAs: Cancer-associated adipocytes

CAFs: Cancer associated fibroblasts

CC: Direct co-culture

CCCP: Carbonyl cyanide 3-chlorophenylhydrazone

CD36: Cluster of differentiation 36

CHD: Coronary heart disease

CM: Conditioned media

CPT1: Carnitine palmitoyltransferase 1

CTCs: Circulating tumor cells

DCFDA: 2',7'-dichlorofluorescin diacetate

DMEM: Dulbecco's modified Eagle medium

DMSO: Dimethyl sulfoxide

DNL: De novo lipogenesis

DUBs: Deubiquitinating enzymes

ECAR: Extracellular acidification rate

ECM: Extracellular matrix

EMT: Epithelial-to-mesenchymal transition

ERK: Extracellular-regulated kinase

Eto: Etomoxir

EVs: Extracellular vesicles

FABPs: Fatty acid binding proteins

FADH: Flavin Adenine Dinucleotide

FAMEs: Fatty acid methyl esters

FAO: Fatty acid oxidation

FAs: Fatty acids

FASN: Fatty acid synthase

FATPs: Fatty acid transport proteins

FBS: Fetal bovine serum

FDR: False Discovery Rate

FFAs: Free fatty acids

G6PD: Glucose-6-phosphate dehydrogenase

GC-MS: Chromatography/electron ionization mass spectrometry

GFAT: Glutamine fructose-6-phosphate amidotransferase

GLUT4: Glucose transporter 4 (or Slc2a4)

GOBPs: Gene ontology biological processes

GPT: Glutamic-pyruvic transaminase

GSEA: Gene Set Enrichment Analysis

GSK-3β: Glycogen synthase kinase 3β

GSVA: Gene set variation analysis

HBSS: Hanks′ Balanced Salt Solution

HE: Hematoxylin & Eosin

HEPES: 4-(2-Hydroxyethyl)piperazine-1-ethanesulfonic acid

HIF1-α: Hypoxia-inducible factor 1-alpha

HK: Hexokinase

HPRT: Hypoxanthine Phosphoribosyltransferase 1

HRP: Horseradish peroxidase

HSL: Hormone-sensitive lipase

IBMX: Isobutyl-methyl-xanthine

IL: Interleukin

ISTD: Internal standard

JAK: Janus kinase

LB: Laemmli loading buffer

LDH: Lactate dehydrogenase

LDLs: Low-density lipoproteins

LDs: Lipid droplets

LIF: Leukemia inhibitory factor

MAGL: Monoacylglycerol lipase

MAPK: Mitogen-activated protein kinase

MET: Mesenchymal to epithelial transition

MMP: Matrix metalloprotease

MMTV-PyMT: Mammary mouse tumor virus polyoma middle-T

MSCs: Mesenchymal stem cells

mTOR: Mechanistic target of rapamycin

MTT: 3-(4,5-Dimethylthiazol-2-yl)-2,5-diphenyltetrazolium bromide

MUFAs: Monounsaturated fatty acids

NAC: N-acetyl-cysteine

NADH: Nicotinamide adenine dinucleotide

OCR: Oxygen consumption rate

ORO: Oil Red O

OXPHOS: Oxidative phosphorylation

PBS: Phosphate buffer saline

PDGFβ: Platelet-derived growth factor beta

PFA: Paraformaldehyde

PGI: Phosphoglucose isomerase

PI3K: Phosphatidylinositol-3-kinase

PI3K: Phosphoinositide 3-kinase

PPARɣ: Peroxisome proliferator-activated receptor gamma

PPP: Pentose phosphate pathway

PTMs: Post-translational modifications

PUFAs: Polyunsaturated fatty acids

PVDF: Polyvinylidene difluoride

PyMT: Polyoma Middle T antigen

RETN: Resistin

RNA: Ribonucleic acid

RNA-seq: RNA sequencing

ROS: Reactive oxygen species

RT: Room temperature

RT-qPCR: Real-time quantitative reverse transcription polymerase chain reaction

SCF: Skp-Culin-Fbox

SDS: Sodium dodecyl sulfate

SDS-PAGE: Sodium dodecyl sulfate polyacrylamide gel electrophoresis

SEM: Standard error of the mean

SIM: Selected ion monitoring

Slc2a4: Solute carrier family 2 member 4 (or Glut4)

STAT: Signal transducer and activator of transcription

TBST: Tris-buffered saline-Tween

TCA: Tricarboxylic acid

TF: Transcription factor

TGF-β: Transforming growth factor beta

TGs: Triacylglycerol s

TGS: Tris-Glycin-SDS

TME: Tumor microenvironment

TNF-α: Tumor necrosis factor alpha

TP53: Tumor Protein P53

Zeb: Zinc Finger E-Box Binding Homeobox

ZnF: Zinc finger domain

β-TrCP1: β-transducin-repeat containing protein

INTRODUCTION

1. CANCER OVERVIEW

Cancer originates from the uncontrolled growth of abnormal cells, which acquire the ability to invade and/or spread to other tissues and organs. In 2022, cancer caused nearly 9.7 million deaths, with lung cancer being the most common in men and breast cancer the most prevalent in women (Bray et al., 2024).

1.1. Cancer hallmarks

In 2000, Hanahan and Weinberg published a list of hallmarks or capabilities that regular cells acquire during tumor development (Hanahan and Weinberg, 2000). This list has been updated twice, once in 2011 and recently in 2022. The current core hallmarks of cancer include self-sufficiency in growth signals, insensitivity to growth suppressors, evading immune destruction, unlocking phenotypic plasticity, limitless replicative potential, capability to invade neighboring tissues and produce metastasis, senescence, capacity to resist cell death, sustained angiogenesis, and metabolic reprogramming (Hanahan and Weinberg, 2000; Hanahan and Weinberg, 2011; Hanahan, 2022) **(Figure I1)**.

The functional traits acquired by normal cells in their path to neoplastic states are not sufficient to explain cancer heterogeneity and pathogenesis. Thus, Hanahan and Weinberg in 2011 introduced the concept of “enabling characteristics”, which do not necessarily cause cancer but assist cells in the transition from normal to oncogenic. Current enabling characteristics of cancer include an inflammatory environment, non-mutational epigenetic reprogramming, genome instability, and polymorphic microbiomes (Hanahan and Weinberg, 2000; Hanahan and Weinberg, 2011; Hanahan, 2022) **(Figure I1).**

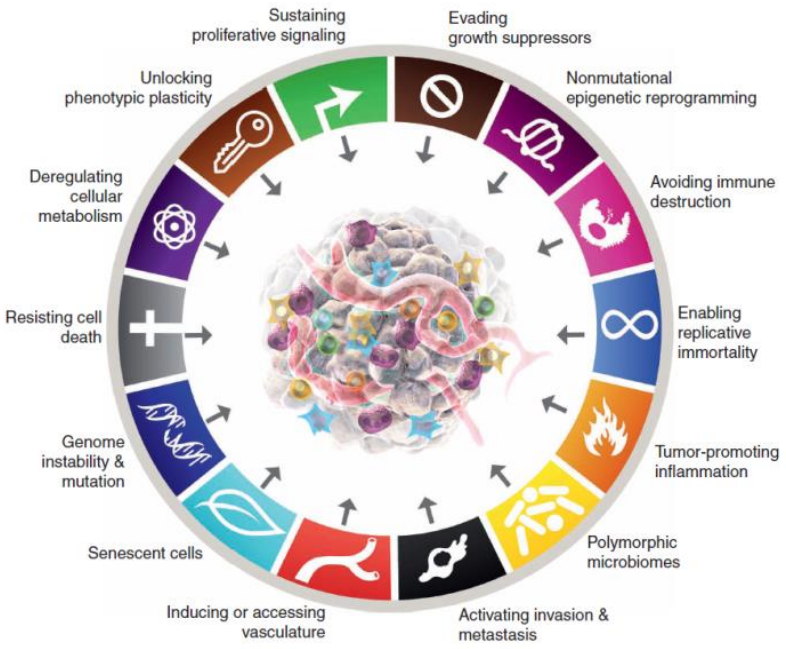

Figure I1. Hallmarks of cancer. Illustration of the core hallmarks and enabling characteristics proposed by Hanahan and Weinberg in 2011 (Hanahan and Weinberg, 2011), with the incorporation of the new emerging capabilities and characteristics proposed in 2022 (Hanahan, 2022).

Since their definition, the hallmarks of cancer have been a reference for understanding how this disease evolves and how scientists can develop more effective therapies to target cancer cells and treat human cancers.

1.2. Metastasis

Tumor development is a multistep process in which cells acquire somatic mutations and epigenetic changes that promote adaptive and proliferative advantages (Fares et al., 2020). During cancer

development, cells from the primary tumor gain the capacity to migrate and invade adjacent tissues, and hence travel to distant parts of the body, where they may generate new colonies and secondary tumors (Hanahan and Weinberg, 2000; Hanahan, 2022; Mehlen and Puisieux, 2006). The process that allows cancer cells from the primary tumor to travel far distances is described as the invasion-metastasis cascade (Hanahan and Weinberg, 2011; Mehlen and Puisieux, 2006) **(Figure I2)**.

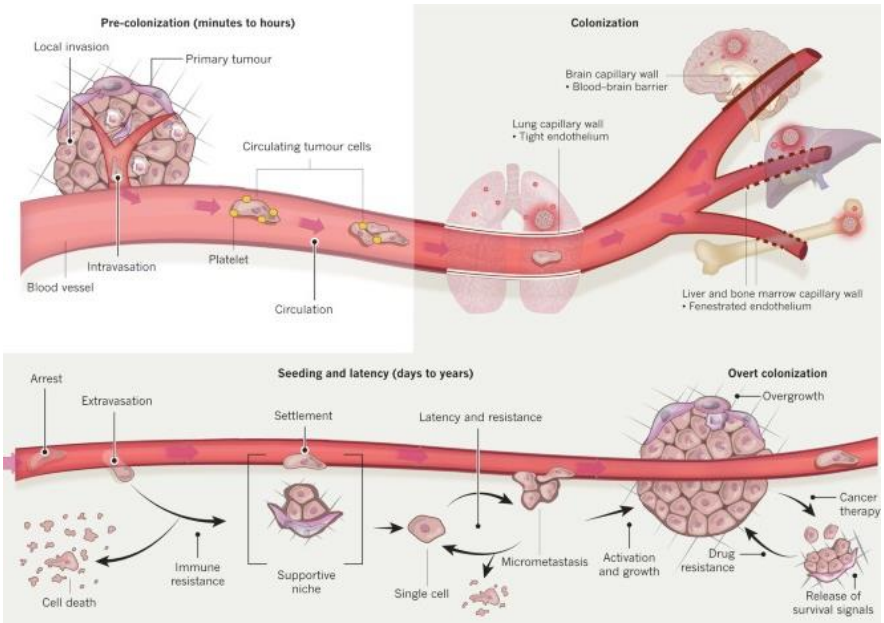

Figure I2. Metastatic colonization. The pre-colonization step can last from minutes to hours, during which cells invade the surrounding tissue and intravasate the local vasculature. Once in circulation, tumor cells move along the bloodstream until capillary arrest occurs in distant organs. Cells can extravasate and settle at secondary sites (Massagué and Obenauf, 2016).

The metastatic process is complex and begins with the invasion of adjacent tissues. This process requires tumor cell dissociation from the primary tumor and intravasation into blood vessels. During invasion, cells often acquire enhanced motility through activation of the epithelial-to-mesenchymal transition (EMT) (Ganesh and Massagué, 2021; Nieto et al., 2016). Cancer cells enter the circulatory system as single cells or clusters, and they must overcome several stressful events, such as mechanical forces, *anoikis* (programmed cell death induced by the lack of cell-matrix adhesion), attack of the immune system, and oxidative stress (Fares et al., 2020; Leone et al., 2018; Massagué and Obenauf, 2016; Piskounova et al., 2015). Often, cells are arrested in capillaries at distant sites and extravasate to begin colonization (Fares et al., 2020; Massagué and Obenauf, 2016). This step is highly affected by the local microenvironment that circulating tumor cells (CTCs) encounter.

Primary tumors can influence the microenvironment of distant organs prior to colonization, generating supportive premetastatic niches that promote cell survival in new tissues (Massagué and Obenauf, 2016). Primary tumor cells secrete soluble factors such as chemokines, cytokines, and hormones, as well as extracellular vesicles (EVs), which promote the recruitment of bone marrow-derived cells (BMDCs) to distant niches. These immune cells play a key role in remodeling remote tissues through the secretion of inflammatory cytokines, growth factors, and proangiogenic molecules, which aid CTCs colonization (Ganesh and Massagué, 2021; Liu and Cao, 2016).

1.3. Epithelial-to-Mesenchymal Transition (EMT)

EMT is a reversible and highly conserved cellular process, in which epithelial cells acquire mesenchymal traits. This process involves changes in several features, such as cell morphology, polarity, and cell-cell adhesion, which confer tumor cells with a more invasive phenotype (Nieto et al., 2016; J. Yang et al., 2020). EMT plays an important role in both physiological and pathological conditions, including embryogenesis, inflammation, fibrosis, wound healing, and cancer progression (J. Yang et al., 2020). EMT programs have been classified into three types: type I EMT is essential during embryonic development; type II EMT is observed during wound healing and tissue regeneration; and type III EMT occurs during carcinoma progression (Kalluri and Weinberg, 2009).

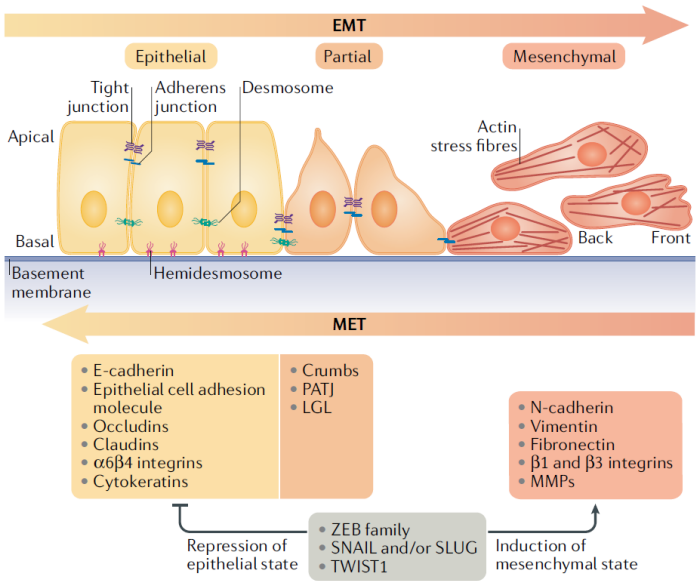

Figure I3. Epithelial-to-Mesenchymal Transition. Illustration of the EMT process, highlighting key markers regulated by EMT transcription factors. EMT is reversible and allows mesenchymal cells to return to their original epithelial state through a process known as mesenchymal-epithelial transition (MET) (Dongre and Weinberg, 2018).

During EMT **(Figure I3)**, polarized epithelial cells lose their adhesion properties because of the disassembly of adherens junctions and desmosomes. Consequently, the cells acquire a spindle-shaped morphology. Epithelial cells that activate the EMT program rarely advance to a fully mesenchymal state; they usually proceed to a hybrid epithelial/mesenchymal state in which they express a combination of markers. This phenotype confers cancer cells with tumor-initiating properties, motility, the ability to disseminate, and resistance to pro-apoptotic stimuli and chemotherapy (Dongre and Weinberg, 2018; J. Yang et al., 2020).

EMT is triggered by EMT-inducing transcription factors (EMT-TFs), which include the Snail family (Snail1 and Snail2), the Zeb family (Zeb1 and Zeb2/Sip1), and the bHLH family (including Twist1 and Twist2) (Díaz et al., 2014; Stemmler et al., 2019). These transcription factors induce the expression of genes that promote the mesenchymal cell state and repress the expression of genes that maintain the epithelial cell state. Genes associated with the epithelial state include those encoding claudins, cytokeratins, occludins, integrins, and E-cadherin, being the latter a key biomarker in EMT. On the other hand, genes associated with the mesenchymal state include vimentin, fibronectin, β1 and β3 integrins, and N-cadherin (Dongre and Weinberg, 2018).

The Snail family is the one that plays the most prominent role in controlling the EMT in most cells. It is comprised of three members: Snail1 (SNAI1), Snail2 (SNAI2 or SLUG), and Snail3 (SNAI3 or SMUC). This family is characterized by the presence of a SNAG box in its N-terminus domain, which is required for transcriptional repression, and by four to five zinc domains (ZnF) in its C-terminus, needed for DNA binding. Snail1 is the most relevant and studied

member of this family. Through the SNAG domain, Snail1 recruits co-repressors such as the Polycomb complex, which is involved in E-cadherin (CDH1) gene repression (García de Herreros, 2024; Herranz et al., 2008). Snail1 plays a crucial role in driving the EMT associated with the gain of the migratory phenotype, mainly by repressing the E-cadherin gene in cancer cells (Batlle et al., 2000; Cano et al., 2000). However, it also affects other cancer hallmarks since it reprograms metabolism (Kim et al., 2017), increases cell survival to proapoptotic insults (Escrivà et al., 2008), and provides tumor cells with cancer stem cell characteristics (Mani et al., 2008). Moreover, elevated Snail1 expression in tumors is associated with poor clinical prognosis (Kaufhold and Bonavida, 2014).

In addition to its role in EMT, Snail1 is involved in other cellular processes such as the activation of cancer-associated fibroblasts (CAFs) (Batlle et al., 2012) and regulation of adipogenesis (Batlle et al., 2012; Peláez-García et al., 2015). Adipogenesis is the process by which mesenchymal stem cells (MSC) differentiate into adipocytes. Remarkably, Snail1 plays a role in adipocyte differentiation because its downregulation is required for the generation of adipocytes from MSCs (Batlle et al., 2012). Overexpression of Snail1 leads to the downregulation of the nuclear receptor Nr2f6, which in turn promotes the expression of the anti-adipogenic cytokine IL-17 (Peláez-García et al., 2015).

Snail1 expression is controlled at multiple levels. *Snai1* transcription is regulated by transcription factors and epigenetic modifications (Baulida et al., 2019). Additionally, the stability of Snail1 mRNA is controlled by various microRNAs (Baulida et al., 2019). Notably, Snail1 is an inherently unstable protein with a half-life of 25 min and is highly susceptible to post-translational

modifications (PTMs) that control its protein stability (Baulida et al., 2019; Díaz et al., 2014; Kaufhold and Bonavida, 2014).

The Snail1 protein is regulated through ubiquitination and subsequent degradation by the 26S proteasome system (Díaz et al., 2014; Díaz and García de Herreros, 2016). Ubiquitination is a sequential process performed by ubiquitin-activating enzymes (E1), ubiquitin-conjugating enzymes (E2), and ubiquitin ligases (E3). Snail1 polyubiquitination involves the participation of several E3 ubiquitin ligases of the multimeric Skp-Culin-Fbox (SCF) subtype (Baulida et al., 2019; Díaz et al., 2014). The extensive involvement of E3 ligases ensures that Snail1 is almost undetectable in the adult epithelial cells. However, Snail1 stabilization supports its expression in adult tissues linked to wound healing, angiogenesis, and tumor development (Díaz and García de Herreros, 2016). Ubiquitination is a reversible process and the action of E3 ligases is antagonized by deubiquitinating enzymes (DUBs). Snail1 stabilization requires DUBs to recognize and remove ubiquitin molecules (Baulida et al., 2019).

Snail1 protein levels are also regulated by different post-translational modifications, with the most relevant being phosphorylation (Baulida et al., 2019). Snail1 can be phosphorylated by various kinases, either enhancing or inhibiting its function. For example, glycogen synthase kinase 3β (GSK-3β) phosphorylates Snail1 at different residues, triggering its nuclear export and β-transducin-repeat containing protein 1 (β-TrCP1)-mediated proteasomal degradation (Zhou et al., 2004).

2. BREAST CANCER

Breast cancer can be diagnosed in both women and men; however, its incidence in men does not reach 1% of all breast cancer patients. In 2022, an estimated 2.3 million women were newly diagnosed with breast cancer and around 666.000 women died as a consequence (Bray et al., 2024). In other words, breast cancer accounts for approximately 12% of all cancer cases and approximately 7% of all cancer deaths in 2022 (Bray et al., 2024).

The human breast is composed of skin, subcutaneous tissue, and breast tissue. The female breast tissue includes the breast parenchyma (ducts and lobules) and the supporting stroma, including white adipose tissue, a complex network of ligaments, nerves, arteries, veins, and lymphatic vessels (Bazira et al., 2022; Pandaya and Moore, 2011). The main function of the breast adipose tissue is to store and release excess energy when required by the body. Moreover, breast adipose tissue plays a major role in breast development and maturation. As a rich energy source, it aids in the development and progression of breast cancer (Kothari et al., 2020).

Breast cancer typically begins in epithelial cells in the ductal (85%) and lobular (15%) compartments. Initially, tumor growth is confined to the duct or lobule, where it has minimal capability to metastasize. Eventually, these *in situ* cancers become invasive when they invade the surrounding tissue. It can spread to nearby lymph nodes, causing regional metastasis, or to other organs in the body, causing distant metastasis (Polyak, 2007).

2.1. Breast cancer initiation and development

The exact etiology of breast cancer is currently unknown; however, several models have been proposed. The stochastic model suggests that several mutations in multiple epithelial cells may initiate tumor formation. In contrast, the cancer stem cell model states that a single cell with stem cell properties can grow in a clonal manner. However, these models are not mutually exclusive (Polyak, 2007; Zhang et al., 2017).

Although 90-95% of breast cancers are not inherited, 5-10% of the remaining cases can be explained by inherited genetic factors (Harbeck et al., 2019; Sun et al., 2017). For instance, mutations in BRCA1/2 (breast cancer-associated gene 1/2) follow an autosomal dominant inheritance pattern, which contributes to 20–25% of the hereditary risk (Harbeck et al., 2019; Mahdavi et al., 2018; Sun et al., 2017). BRCA proteins are involved in double-stranded DNA repair mainly through homologous recombination. Consequently, cells lacking functional BRCA proteins are particularly susceptible to DNA damage and cancer development (Cass et al., 2003).

Other genes are also involved in breast tumor initiation and progression. HER2 (Human epidermal growth factor receptor 2, encoded by ERBB2) is an important oncogene in breast cancer, as it is amplified in 13-15% of cases (Harbeck et al., 2019; Slamon et al., 1987). Belonging to the tyrosine kinase family, HER2 is a receptor whose activation results in increased proliferation and cell survival, thereby contributing to tumorigenesis (Harbeck et al., 2019; Oh and Bang, 2019). Other frequently mutated and/or amplified genes include TP53 (Tumor Protein P53), MYC, and EGFR (Epidermal Growth Factor Receptor) (Harbeck et al., 2019).

2.2. Obesity as a breast cancer risk factor

Several risk factors, besides sex, increase the probability of developing breast cancer. These include aging, family history of breast cancer, obesity, high-fat diet, tobacco exposure, and hormone levels (Britt et al., 2020; Harbeck et al., 2019; Sun et al., 2017).

It is estimated that 21% of breast cancer deaths can be attributed to the combined effects of alcohol use, overweight and obesity, and physical inactivity (Danaei et al., 2005).

Hormones such as estrogen and progesterone are drivers of breast cancer growth. Menopausal therapy and oral contraceptives increase the risk of breast cancer (Harbeck et al., 2019). Dysregulation of endogenous estrogen and progesterone levels also affects the incidence of breast cancer, which occurs during early menarche, late first birth, and late menopause (Colditz and Bohlke, 2015). Modern lifestyles include regular alcohol consumption, high-fat diet, and low physical activity. Higher levels of physical activity are associated with lower levels of sex hormones, whereas alcohol consumption is associated with higher levels of sex hormones (Friedenreich et al., 2010; Rinaldi et al., 2006). These findings may partially explain the association between physical activity, alcohol consumption, and the risk of breast cancer.

Diet is an important, modifiable risk factor. Diets with a high-fat percentage have been shown to increase the risk of breast cancer (Riboli, 2000). Some studies have suggested that the presence of certain fatty acid subtypes is more important than total fat intake (Romieu et al., 2017). However, the overall findings are conflicting. Diets high in monounsaturated fatty acids, such as olive oil, and

omega-3 polyunsaturated fatty acids, may reduce the risk of breast cancer. Nevertheless, diets high in saturated fatty acids and omega-6 polyunsaturated fatty acids seem to increase the risk of breast cancer (Buja et al., 2020; Romieu et al., 2017).

Obesity is a chronic disease in which excess body fat accumulates and negatively affects health (Dhurandhar, 2022). Obesity is the direct cause of many diseases. In particular, it is associated with the development of type 2 diabetes mellitus, coronary heart disease (CHD), hypercholesterolemia, hypertension, respiratory complications, osteoarthritis, and an increased incidence of several cancers (Quail and Dannenberg, 2018; Kopelman, 2000). Obesity increases the risk of cancer-specific mortality by approximately 17% (Pati et al., 2023). The association between body weight and the risk of breast cancer varies depending on menopausal status; obese women are at an increased risk of developing breast cancer if they are postmenopausal rather than premenopausal (Calle and Kaaks, 2004; Chan et al., 2014). Obesity increases the risk of breast cancer in postmenopausal women by 30-50% (Chan et al., 2014). Obesity has been associated not only with increased incidence, but also with increased progression and metastasis of breast tumors (Barone et al., 2020).

3. BREAST CANCER TUMOR MICROENVIRONMENT

A solid tumor is not only composed of tumor cells, but also includes infiltrating and host cells that are embedded in the extracellular matrix and surrounded by blood vessels, forming the tumor microenvironment (TME). The TME composition differs between tumor types but typically includes immune cells, fibroblasts, adipocytes, and cells from the vascular system (Anderson and Simon, 2020). The prevailing belief is that the TME is not a passive spectator but an active promoter of cancer progression. In the early stages of tumor growth, a reciprocal relationship develops between cancer cells and the components of the TME, facilitating cancer cell survival, local invasion, metastatic dissemination, angiogenesis, and immune evasion (Anderson and Simon, 2020) **(Figure I4)**.

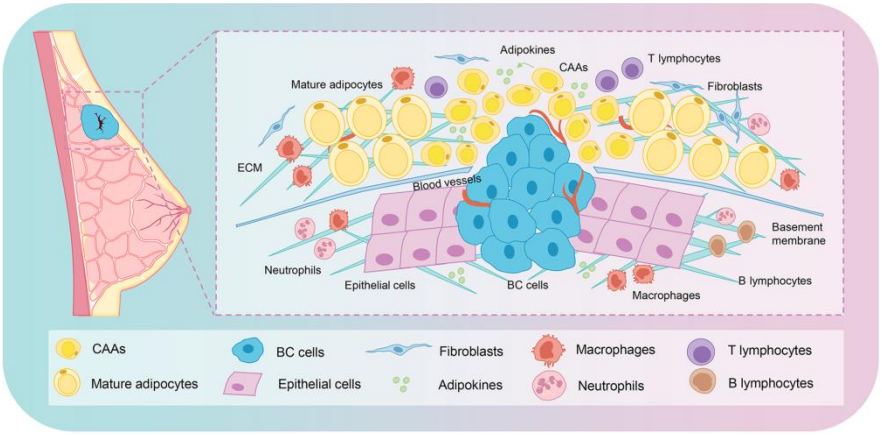

Figure I4. Breast tumor microenvironment. A depiction of cells present in the microenvironment of breast tumors. The breast niche is composed of many cellular types, including breast cancer cells (BC), adipocytes, epithelial cells, fibroblasts, and immune cells such as macrophages, neutrophils, T cells, and B cells (Zhao et al., 2020).

3.1. Cancer-associated adipocytes

Adipocytes are specialized cells that store excess energy as fat in the form of triacylglycerol (TG) and cholesterol esters within lipid droplets (LDs) (Mukherjee et al., 2022). Adipocytes are a significant component of breast, ovarian, and prostate TME. In these cancers, adipocytes situated in close proximity to tumor cells exhibit marked changes in both their phenotype and functionality. Histological examination of solid tumors has consistently revealed a reduction in both the number and size of adipocytes found at the invasive edge of the tumor when compared to adipocytes situated in further regions of the tumor (Dirat et al. 2011; Laurent et al. 2019; Nieman et al. 2013; Zhang et al. 2018; Zhu et al. 2022). These adipocytes close to the breast cancer cells are named as cancer-associated adipocytes (CAAs). Emerging evidence indicates bidirectional crosstalk between CAAs and surrounding breast cancer cells that supports tumor progression (Attané and Muller, 2020; Hoy et al., 2017; Rybinska et al., 2021; Zhao et al., 2020).

3.2. CAAs and tumor cells crosstalk in breast cancer

CAAs display distinct characteristics compared with normal adipocytes, such as reduced lipid content, decreased expression of adipocyte markers, and increased synthesis of cytokines (Balaban et al., 2017; Cai et al., 2023; Dirat et al., 2011; Laurent et al., 2019; Nieman et al., 2013; Zhang et al., 2018). It has been reported that adipocytes co-cultured with tumor cells *in vitro* decrease the expression of adipocyte differentiation markers such as hormone-sensitive lipase (HSL), adiponectin (APN), and resistin (RETN), as well as the transcriptional regulators CCAAT/enhancer-binding protein alpha (C/EBPα) and peroxisome proliferator-activated

receptor gamma (PPARɣ) (Dirat et al., 2011). This leads to a decrease in the number and size of lipid droplets due to increased lipolysis (Bochet et al., 2013; Dirat et al., 2011; Wang et al., 2017). Moreover, CAAs show an activated phenotype characterized by increased expression of pro-inflammatory cytokines, such as interleukin-6 (IL-6), interleukin-1 (IL-1), and tumor necrosis factor alpha (TNFα), as well as proteins involved in ECM remodeling, such as matrix metalloproteinase 11 (MMP11) (Dirat et al., 2011).

The presence of CAAs arises from the dedifferentiation of adipocytes, loss of lipid content, and the acquisition of an activated phenotype. Whether these processes are triggered by a single molecule released by tumor cells or are regulated independently requires further investigation. Currently, only a limited number of studies have suggested mechanisms responsible for initiating CAAs induction. In breast cancer models, activation of the Wnt/β-catenin pathway in mature adipocytes induces adipocyte dedifferentiation (Bochet et al. 2013; Gustafson and Smith, 2010). Other proposed mechanisms include lung cancer-derived extracellular vesicles containing IL-6, which are capable of inducing adipocyte lipolysis through the STAT3 pathway (Hu et al., 2019).

It has been proposed that the changes that mature adipocytes undergo in the presence of breast cancer cells contribute to tumor progression. Enhanced lipolysis causes the breakdown of lipid stores and the release of free fatty acids, which can be taken up by cancer cells (Balaban et al., 2017; Laurent et al., 2019; Nieman et al., 2011; Wang et al., 2017). These fatty acids can be used by cancer cells for energy production, cell membrane formation, and synthesis of lipid bioactive molecules (Anderson and Simon, 2020).

Fatty acid release from adipocytes occurs through the breakdown of TGs stored in LDs. Lipolysis relies on the sequential action of three lipases: adipose triglyceride lipase (ATGL), hormone-sensitive lipase (HSL), and monoacylglycerol lipase (MAGL), ultimately leading to the release of free fatty acids (FFAs) and glycerol (Attané and Muller, 2020). *In vitro* lipolysis has been observed in adipocytes directly co-cultured or treated with conditioned media from breast (Balaban et al., 2017; Wang et al., 2017), prostate (Laurent et al., 2019), pancreatic (Cai et al., 2023), ovarian (Nieman et al., 2011), and melanoma (Zhang et al. 2018) cell lines. After release by adipocytes, FFAs are transferred to cancer cells (Balaban et al., 2017; Laurent et al., 2019; Nieman et al., 2011; Wang et al., 2017).

Additionally, the enhanced secretion of metabolites, hormones, cytokines, and soluble factors by CAAs may also play a role in promoting proliferation, migration, invasion, and metastasis in breast cancer (Attané and Muller, 2020; Hoy et al., 2017). Adipokines are cytokines secreted by adipocytes with autocrine and paracrine functions, such as leptin and IL-6 (Dumas and Brisson, 2020; Hoy et al., 2017; Rybinska et al., 2021; Zhao et al., 2020). Leptin is a hormone that enhances proliferation (Yin et al., 2004) and promotes EMT (Wei et al., 2016) *in vitro* in breast cancer cell lines. Similarly, IL-6 triggers EMT in breast cancer cells by activating the STAT3 pathway (Gyamfi et al., 2018).

4. CANCER METABOLISM

Another hallmark of cancer proposed by Hanahan and Weinberg is reprogramming of metabolism in tumor cells. In subsequent sections, the mechanisms by which tumor cells alter their metabolic processes to promote proliferation, progression, and metastasis are discussed.

4.1. Glucose metabolism

Glucose serves as the primary energy source and is a key substrate for macromolecule biosynthesis **(Figure I5)**. Normal cells metabolize glucose to pyruvate via glycolysis in the cytosol. Pyruvate and NADH derived from glucose can be transported into the mitochondria to support respiration via oxidative phosphorylation (OXPHOS), or pyruvate can be reduced by NADH to produce lactate. The first process is glucose oxidation, which optimizes ATP production in the presence of oxygen. The second process, known as fermentation, occurs in the absence of oxygen, yielding lactate and less energy (Koppenol, 2011; Vander Heiden, 2009; Wang and Patti, 2023).

Interestingly, cancer cells convert most of their glucose to lactate even under oxygen-rich conditions. This phenomenon was first observed by Otto Warburg in 1923, who postulated that tumors have impaired respiration due to dysfunctional mitochondria (DeBerardinis and Chandel, 2020; Warburg, 1956). However, we now understand that this is not the case for most cancers (Vander Heiden, 2009; Wang, and Patti, 2023). Contrary to Warburg's hypothesis, we know now that aerobic glycolysis facilitates the conversion of glycolytic intermediates into various biosynthetic

pathways (Hanahan and Weinberg, 2011; Kocianova et al., 2022; Vander Heiden, 2009).

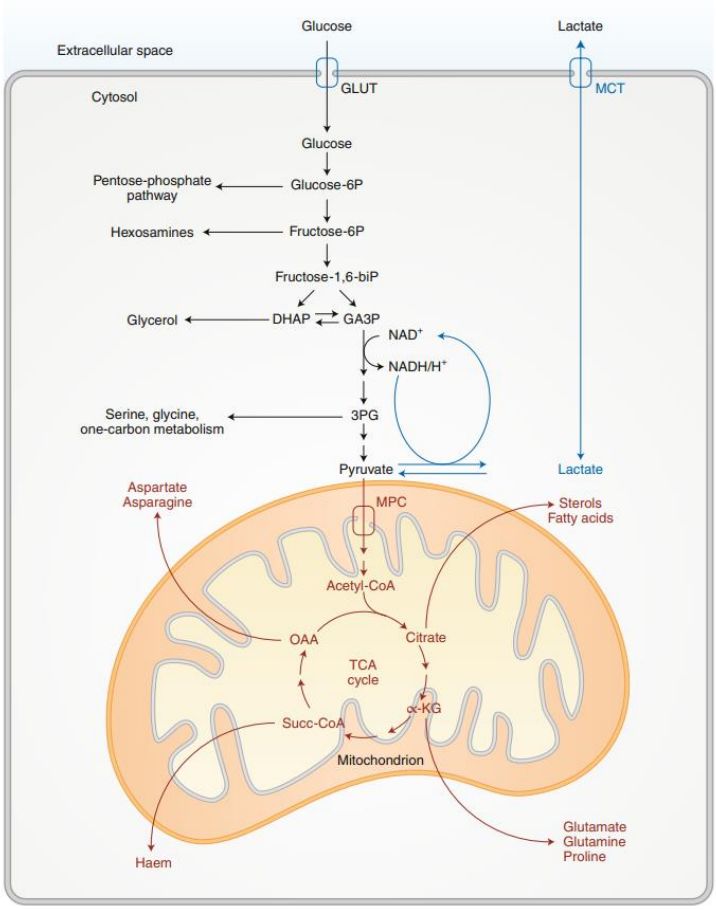

Figure I5. Glucose metabolism supplies biosynthetic intermediates. A simple representation of how glycolysis and the TCA cycle generate intermediates that serve as substrates for anabolic pathways (DeBerardinis and Chandel, 2020).

The glycolytic pathway involves the catabolism of glucose to pyruvate. First, glucose is imported into cells through GLUT transporters and phosphorylated by hexokinases (HK1 and HK2). Glucose 6-phosphate can be further converted into pyruvate or

enter the pentose phosphate pathway (PPP) to contribute to nucleotide synthesis and NADPH production. Glucose 6P is transformed into fructose 6-phosphate by phosphoglucose isomerase (PGI), and further converted into pyruvate or enter the hexosamine biosynthesis pathway to contribute to protein glycosylation. Fructose 6-phosphate first generates fructose-1,6-bisphosphate and pyruvate through a series of reactions. Pyruvate can either enter the tricarboxylic acid (TCA) cycle as acetyl-CoA, produce lactate by lactate dehydrogenase (LDH), or be converted to alanine via glutamic-pyruvic transaminase (GPT) (Nelson et al., 2021).

Oncogenes (such as RAS and MYC) and tumor suppressors (like TP53) are tightly connected to metabolic pathways via the regulation of metabolic enzymes, thereby promoting tumor growth and proliferation (Pascale et al., 2020). Pro-oncogenic genes can enhance glycolysis by activating the expression of enzymes, such as HK1, HK2, and LDH (Hsieh et al., 2015; Pascale et al., 2020). In addition, pro-oncogenic genes can promote biosynthetic pathways.

Downstream of AKT signaling, mTORC1 activation enhances glycolysis and the pentose phosphate pathway (Düvel et al., 2010). Additionally, glucose-6-phosphate dehydrogenase (G6PD), a key enzyme in the PPP, is regulated by several proteins including phosphoinositide 3-kinase (PI3K)/Akt, mammalian target of rapamycin (mTOR), and p53 (Patra and Hay, 2014).

Glucose plays a fundamental role in white adipose tissue metabolism. Glucose serves as a precursor for *de novo* lipogenesis (DNL), where it is converted into fatty acids and glycerol (Morigny et al., 2021). Glucose metabolism in white adipose tissue is intricately

linked to adipocyte differentiation and adipogenesis, highlighting its pivotal role in adipose tissue development and maintenance (Morigny et al., 2021). For instance, the differentiation of adult mouse primary preadipocytes relies on glucose supplementation (Griesel et al., 2021).

The pentose phosphate pathway is parallel to glycolysis, and produces ribose 5-phospate along with NADPH. PPP is important in rapidly dividing cells, such as tumor cells, which need ribose 5-phospate to make RNA and DNA. In other cells, NADPH is the relevant product of PPP, serving as a reducing agent in biosynthetic reactions, such as cholesterol synthesis, and protects cells against reactive oxygen species (ROS) (TeSlaa et al., 2023).

In the oxidative phase of PPP, glucose 6-phosphate is first oxidized by G6PD to form 6-phosphoglucono-δ-lactone. This reaction generates one NADPH molecule. Lactone is then hydrolyzed by lactonase, generating 6-phosphogluconate, which undergoes oxidation and decarboxylation by 6-phosphogluconate dehydrogenase to form ribulose 5-phosphate. This reaction generates a second molecule of NADPH. Finally, phosphopentose isomerase converts ribulose 5-phosphate into ribose (Nelson et al., 2021). In cancer, G6PD is upregulated in many tumors and correlates with poor prognosis (Mele et al., 2018).

In white adipocytes, PPP is crucial in the first steps of differentiation to increase the nucleotide and NADPH pools required for the expansion of preadipocytes and lipid synthesis, respectively (Griesel et al., 2021).

4.2. Lipid metabolism

In addition to glucose and glutamine, the importance of lipids in cancer progression has been gaining recognition. Lipid metabolism is highly altered in cancerous cells for energy production and membrane synthesis **(Figure I6)**. Consequently, tumor cells can increase fatty acid uptake and fatty acid oxidation (FAO) (Broadfield et al., 2021).

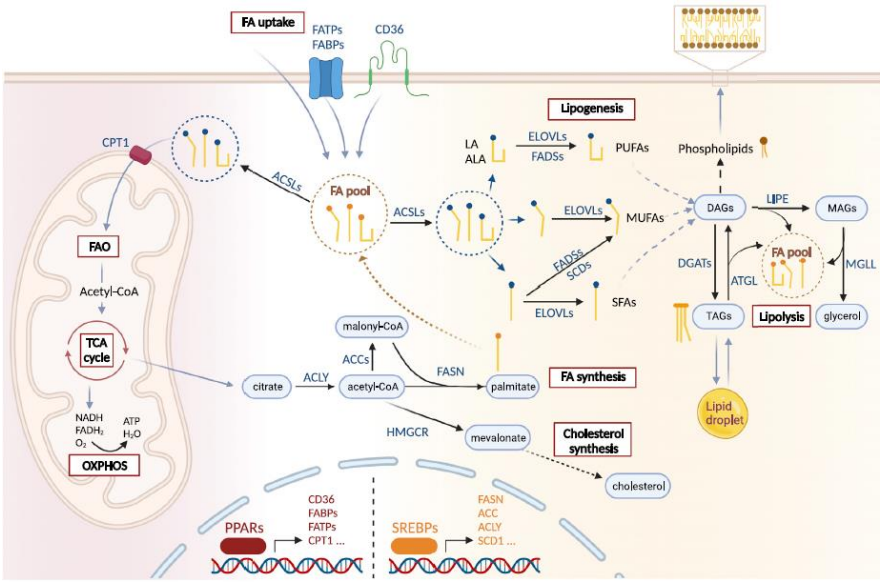

Figure I6. Major lipid metabolism pathways. Schematic representation of the lipid pathways involved in metastasis. Briefly, FAs can enter the cell through transporters, such as CD36, FATPs, and FABPs, or via passive diffusion. In the cytoplasm, contribute to the free fatty acid pool. FAs can be stored in lipid droplets in the form of TGs and released by lipolysis if needed. Moreover, FAs can be catabolized via FAO to generate acetyl-CoA, which enters the TCA cycle and ultimately generates ATP during OXPHOS. Citrate generated in the TCA cycle can be used to produce more lipids through DNL. Further modification of fatty acids generates more complex lipids (Martin-Perez et al., 2022).

Initially, most attention in cancer metabolism research was directed towards DNL. However, it has become evident that cancer cells can obtain lipids from exogenous sources. Recent studies have indicated that, instead of relying on DNL, cancer cells appear to primarily depend on exogenous FFAs as their main source of lipids (Attané and Muller, 2020; Balaban et al., 2019).

Cancer-associated adipocytes release FFAs, which can subsequently be transferred to tumor cells. The mechanism of this transfer remains elusive, but it is evident that several membrane transporters are involved in lipid uptake, such as CD36, fatty-acid binding proteins (FABPs), and fatty acid transport proteins (FATPs) (Broadfield et al., 2021; Martin-Perez et al., 2022; Nagarajan et al., 2021; Vasseur and Guillaumond, 2022). CD36 is a scavenger receptor primarily responsible for the absorption of long-chain fatty acids and oxidized low-density lipoproteins (LDL) (Guerrero-Rodríguez et al., 2022; Pepino et al., 2014). Breast cancer cells show increased CD36 expression and FFA import in the presence of adipocytes *in vitro* (Gyamfi et al., 2021). Additionally, CD36 in breast cancer cells induces EMT, promotes cell migration and invasion, favors cell proliferation, and confers stemness properties (Feng et al., 2023; Guerrero-Rodríguez et al., 2022; Gyamfi et al., 2021; Liang et al., 2018). CD36 is overexpressed in breast tumors compared with normal tissues (Gyamfi et al., 2021). High levels of CD36 are associated with increased adipocyte infiltration, suggesting that upregulation of CD36 in response to exogenous fatty acids may be an adaptive mechanism enhanced in tumorigenic breast cells (Gyamfi et al., 2021). Overall, in patient samples, the expression of CD36 is typically associated with poor prognosis and metastatic progression (Feng et al., 2023; Nath and Chan, 2016).

FATPs are transmembrane proteins that are involved in lipid uptake (Acharya et al., 2023). FATP1 has been identified as a key player in facilitating the transfer of FFAs from adipocytes to melanoma cells, thereby increasing their proliferation and invasiveness (Zhang et al., 2018). These processes can be disrupted by the pharmacological inhibition of FATPs with Lipofermata (Zhang et al., 2018). The role of FATP1 in the crosstalk between adipocytes and breast cancer cells has not yet been studied, although it has been reported that breast cancer patients with higher levels of FATP1 have lower overall survival and relapse-free survival (Mendes et al., 2019).

Other proteins are required for solubilization of FAs in the bloodstream. FABPs are small proteins that bind long-chain fatty acids and facilitate intracellular transport. There are different members of this family that have tissue-specific expression patterns, with FABP4 being primarily expressed in adipocytes (Guaita-Esteruelas et al., 2016). FABP4 is released from adipocytes and exerts its metabolic effects in a paracrine or exocrine manner (Guaita-Esteruelas et al., 2018). *In vitro* studies have shown that ovarian cancer cells exhibit increased FABP4 expression in the presence of adipocytes, and genetic ablation of FABP4 reduces adipocyte-promoted *in vitro* invasion and metastasis *in vivo* (Mukherjee et al., 2020; Nieman et al., 2011). The role of FABP4 in breast cancer has been less studied, but it has been reported to induce cell proliferation through the PI3K-AKT and MAPK-ERK pathways (Guaita-Esteruelas et al., 2016). Other FABPs are involved in FFA uptake into cancer cells, particularly FABP5, which has been reported to be upregulated in breast cancer, among others (Dumas and Brisson, 2020; Guaita-Esteruelas et al., 2018).

Recent investigations have shown that the transfer of lipids from adipocytes to cancer cells can also occur via EVs. The transfer of FAO enzymes and their substrates in EVs promotes the migration and invasion of melanoma cells *in vitro* (Clement et al., 2020; Lazar et al., 2016). In breast cancer, it has been described that adipocyte-secreted EVs promote EMT, growth, migration and invasion *in vitro* (La Camera et al., 2021).

Once in tumor cells, FFAs are substrates of various metabolic pathways or are stored in small LDs. This storage mechanism has been observed in many cancers, including breast (Wang et al., 2017), prostate (Laurent et al., 2019), ovarian (Nieman et al., 2011), and melanoma tumors (Clement et al., 2020). Storing FAs in LDs allows cells to have energy depots if needed, and supports *anoikis* resistance in gastric cancer cells (Li et al., 2020). These FAs are released from LDs through lipolysis. It has been reported that in the presence of adipocytes, the lipolytic activity of breast cancer cells increases both *in vitro* and *in vivo* due to elevated expression of ATGL (Wang et al., 2017). Moreover, FAs released from adipocytes can serve as substrates for the synthesis of new lipid families, such as phosphatidylethanolamines and ceramides (Adriá-Cebrián et al., 2021).

FFAs taken up by cancer cells or released from TGs stores are transported to mitochondria for oxidation. Carnitine palmitoyltransferase 1 (CPT1) is an enzyme involved in the uptake of FAs into the mitochondrial matrix. Once inside, FAs undergo oxidation in which the FA chains are broken down to generate acetyl-CoA. Acetyl-CoA enters the TCA cycle to generate ATP, NADH, and $FADH_2$ (Nelson et al., 2021). Breast and ovarian cancer cells co-cultured with adipocytes exhibit increased FAO (Miranda et

al., 2016; Wang et al., 2017). Moreover, activation of the CPT1A isoform in breast cancer cells increased the expression of EMT markers *in vitro*. Pharmacological inhibition of CPT1 with Etomoxir counteracted this effect (Wang et al., 2017). Furthermore, FAO can generate ROS, which are known to facilitate the EMT in various cancer cell lines (Castelli et al., 2021).

The upregulation of FA synthesis is a well-established metabolic alteration in cancer. Several enzymes involved in DNL are overexpressed in cancer cells and promote tumor progression. ATP citrate lyase (ACLY) activity is increased in lung cancer (Migita et al., 2008), while ACSS2 (Acyl-coenzyme A synthetase short-chain family member 2) is overexpressed in breast, ovarian, and lung cancers (Schug et al., 2016). FASN (Fatty acid synthase) is also upregulated in various cancers, including prostate (Swinnen et al., 2001), and liver (Calvisi et al., 2011).

Overall, the enhanced expression or activity of lipogenic enzymes is a prevalent characteristic observed in various cancer types.

4.3. Lipids in metastasis

Alterations in the composition of several lipids are associated with metastasis. Phospholipids are major components of cell membranes and alterations in their chemical composition can modify the fluidity of the plasma membrane. For instance, areas with low saturated fatty acids and cholesterol generate a fluid membrane that can promote cell motility and EMT *in vitro* in breast cancer cell lines (Zhao et al., 2016). Conversely, cancer cells with higher membrane saturation and cholesterol are less susceptible to lipid peroxidation and ferroptosis, thereby increasing the metastatic

capability of breast cancer cells (Liu et al., 2021). The mechanism by which cholesterol promotes metastasis remains unclear and the results are controversial. Cholesterol synthesis is increased in cancer cells (Ding et al., 2019), and high plasma cholesterol levels (hypercholesterolemia) have been linked to increased metastasis in breast cancer (Nelson et al., 2013) and prostate cancer (Hirano et al., 2020). One proposed mechanism involves the modulation of signaling pathways. Lipid rafts are domains present in cell membranes that are rich in cholesterol and sphingolipids, and serve as platforms for signaling proteins. Cancer cells show elevated levels of membrane lipid rafts and cholesterol, which can lead to downstream activation of signal transduction cascades that are crucial for cancer cell growth and proliferation (Mollinedo and Gajate, 2020).

Fatty acids can be either unsaturated or saturated and can contain one (monounsaturated, MUFAs) or more (polyunsaturated, PUFAs) carbon double bonds. Enzymes called desaturases generate double bonds, and their inhibition impairs the tumor initiation capacity of ovarian cancer stem cells *in vivo* (Li et al., 2017). In breast cancer, prolonged treatment of cells with palmitic acid leads to an increased tumor formation capacity *in vitro* (Liu et al., 2022). The degree of unsaturation confers different biological properties to fatty acids, affecting tumor progression differently (Martin-Perez et al., 2022). Oral squamous carcinoma cells exposed to palmitic acid, but not oleic or linoleic acid, generate highly metastatic tumors *in vivo* (Pascual et al., 2021). Accordingly, oleic acid (C18:1n9) has been found to reduce the migration and invasion capacity of hepatocellular carcinoma cells (Giulitti et al., 2021). Clinical studies support this finding, showing that oleic acid-enriched diets have a

beneficial effect on the primary prevention of breast cancer (Toledo et al., 2015). However, other studies have indicated that oleic acid promotes proliferation and migration of prostate cancer cells *in vitro* (Liotti et al., 2018).

Thus, the role of saturated and unsaturated fatty acids in metastasis remains unclear due to conflicting findings. FAs can follow various metabolic pathways within cells, and the complex metabolism of cancer cells can rewire these pathways to meet their requirements. However, it is evident that an increase in the systemic levels of FAs and dysregulation of cell homeostasis can have harmful consequences in cancer patients (Hoy et al., 2021; Martin-Perez et al., 2022; Vasseur and Guillaumond, 2022).

OBJECTIVES

Previous evidence has demonstrated that adipocytes near tumor cells lose their lipid content and dedifferentiate into fibroblast-like cells, thereby acquiring an activated phenotype. They enhance lipolysis, which leads to the release of free fatty acids that can then be utilized by cancer cells to promote tumor progression.

The aim of this thesis is to investigate the interplay between adipocytes and tumor cells, particularly focusing on how lipids released from adipocytes facilitate tumor progression. To achieve this, we outlined the following three objectives.

1. To elucidate the process of adipocyte dedifferentiation in response to tumor cells.
2. To examine the mechanism by which activated adipocytes contribute to tumor cell migration and invasion.
3. To assess the relevance of lipids in facilitating tumor cell migration.

RESULTS

1. ADIPOCYTES DEDIFFERENTIATE IN RESPONSE TO TUMOR CELLS

1.1. Adipocytes close to tumor cells are smaller than distant adipocytes in PyMT tumors

As indicated in the Introduction, the adipose tissue surrounding primary breast tumors differs from that close to normal mammary glands. Histological examinations reveal a reduction in both the number and size of adipocytes at the invasive edge of the tumor compared to those distant from the tumor. To confirm these findings, we obtained histological samples from PyMT mice. In this model, the polyomavirus middle T oncogene is expressed under the control of the mammary MMTV promoter, resulting in the spontaneous development of luminal B breast tumors (Guy et al., 1992).

As shown in **Figure R1**, adipose tissue contains large adipocytes in regions distant from the tumor. However, adipocytes close to or inside the tumor exhibit a smaller size. This observation corroborates with the reduction in adipocyte size near the primary tumor.

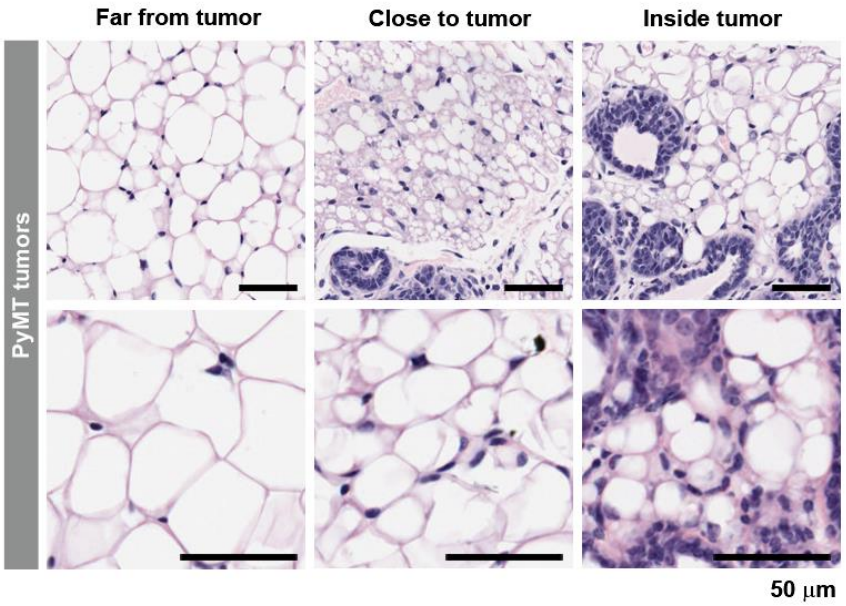

Figure R1. Adipocytes close to tumor cells are smaller than distant adipocytes in PyMT tumors. Once the tumors reached the carcinoma stage, the mice were sacrificed. Tumor-bearing mammary glands were extracted, fixed in 4% PFA, embedded in paraffin, and stained with Hematoxylin and Eosin (HE). Scale bar represents 50 μm.

1.2. 3T3-L1 adipocytes lose lipids in response to tumor cells

To molecularly study the differentiation process of white adipocytes *in vitro*, we used the 3T3-L1 murine preadipocyte cell line. These fibroblasts differentiate into adipocytes when provided with appropriate stimuli. The differentiation process lasts 10-12 days, and is induced by 4.5 g/L glucose DMEM containing isobutyl-methyl-xanthine (IBMX), dexamethasone, and insulin. Differentiation medium induces the expression of CCAAT enhancer binding protein (C/EBP) δ and C/EBPβ, which heterodimerize,

leading to the activation of both C/EBPα and peroxisome proliferator-activated receptor gamma (PPARγ) (Cave and Crowther, 2018). C/EBPα and PPARγ are the main transcription factors that initiate adipogenesis.

During differentiation, 3T3-L1 cells increase the expression of adipocyte markers and accumulate lipids in lipid droplets. This lipid accumulation can be detected using Oil Red O (ORO) or Bodipy 493/503 to stain neutral lipid droplets **(Figure R2A)**. To characterize this model, we performed a kinetic analysis of the differentiation process of 3T3-L1 adipocytes. We collected protein and RNA samples from the cells at various time points throughout the 10-12 day differentiation period. We assessed the expression of C/EBPα, PPARγ, solute carrier family 2 member 4 (Slc2a4 or Glut4), and hormone-sensitive lipase (Lipe) as differentiation markers. Additionally, we examined Snail1, given the role of this transcription factor in adipocyte differentiation.

During the first two days of differentiation, there was an increase in Snail1 protein levels **(Figure R2B)**, followed by a marked downregulation of Snail1 as adipogenesis progressed. As expected, the early adipogenesis markers C/EBPα and PPARγ were the first to be upregulated. Finally, in the later stages of differentiation, Glut4 (Slc2a4) expression was elevated.

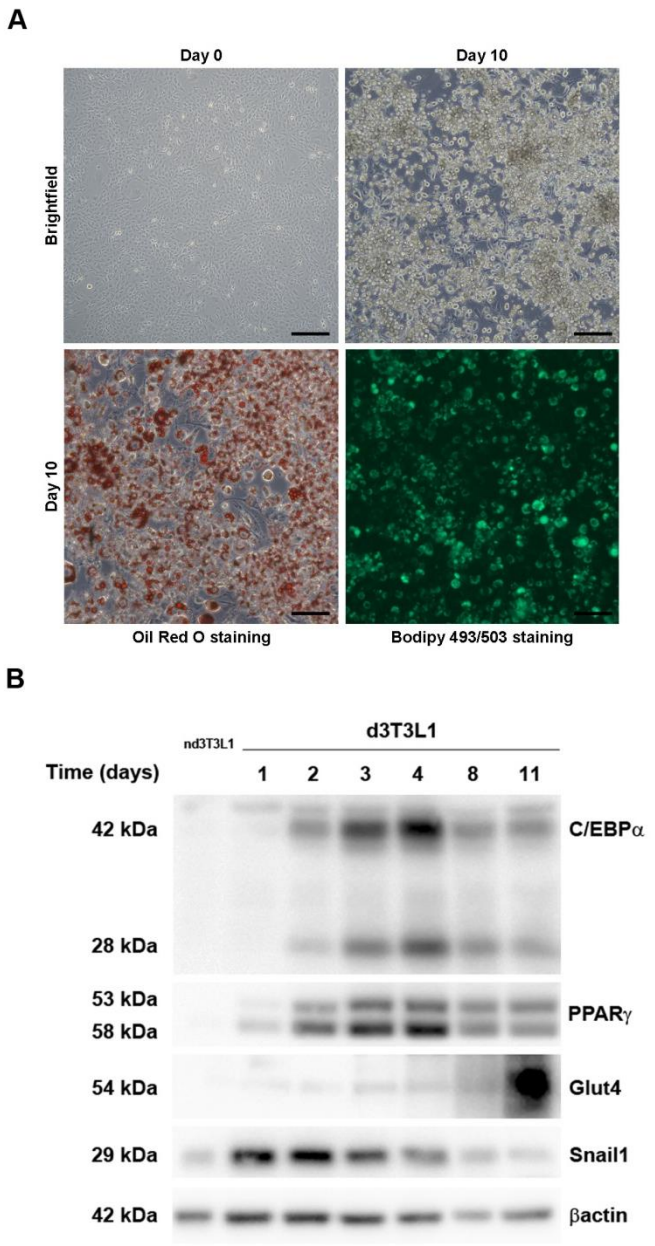

Figure R2. 3T3-L1 differentiation process. The differentiation of 3T3-L1 cells (nd3T3L1) was induced when the cells reached confluence. During the next 10-12 days, adipogenesis was assessed using ORO and Bodipy 492/503 staining **(A)** and Western blot for the indicated proteins **(B)**. In **A**, scale bar represents 50 µm.

mRNA analysis using real-time quantitative reverse transcription PCR polymerase chain reaction (RT-qPCR) yielded similar results **(Figure R3).** *Snai1* mRNA levels increased during the early stages of differentiation, followed by a strong downregulation. This was accompanied by an increase in the expression of *Cebpa* and *Pparg*, with *Lipe* and *Slc2a4* being upregulated at later stages.

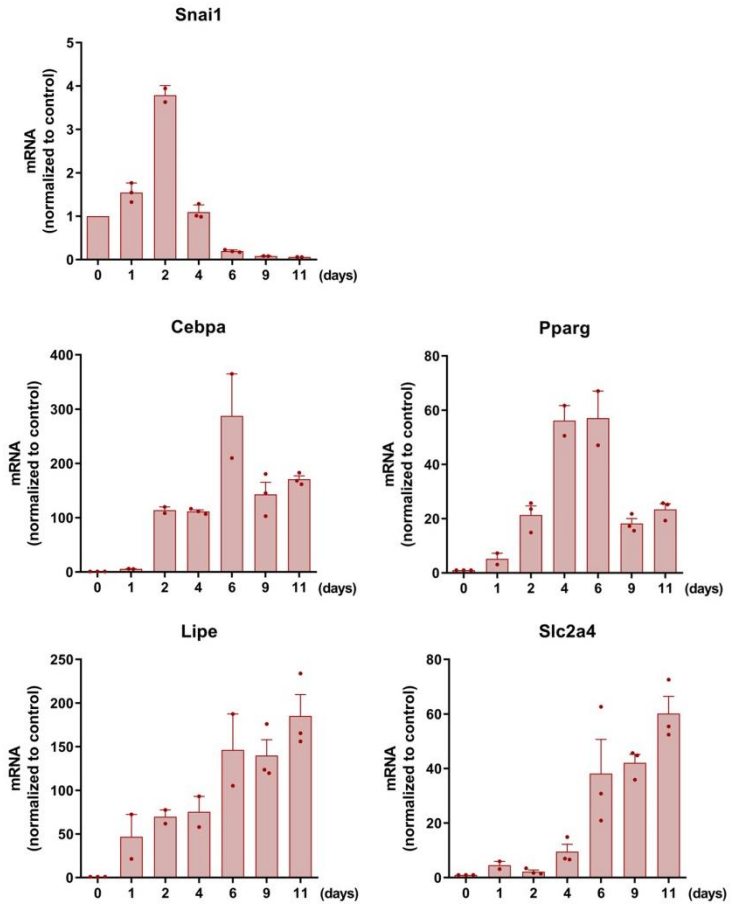

Figure R3. 3T3-L1 differentiation process. Differentiation of 3T3-L1 cells was induced when the cells reached confluence. During the next 10-12 days, adipogenesis was assessed using RT-qPCR. The control corresponds to day 0; the average ± SEM of at least two independent experiments is shown.

To study the crosstalk between adipocytes and tumor cells *in vitro*, we used three established tumor cell lines. AT3 and BTE136 are murine breast cancer cells generated from the breast tumors of MMTV-PyMT mice (Mestre-Farrera et al., 2021). MCF7 is a human breast cancer cell line that expresses estrogen, progesterone, and glucocorticoid receptors.

When we characterized these cell lines, we noted variations in the expression of epithelial and mesenchymal markers **(Figure R4)**. Specifically, AT3 cells showed a higher expression of E-cadherin and Cytokeratin 14, indicating an epithelial phenotype. In contrast, BTE136 cells showed higher levels of Fibronectin and Snail1, suggesting that they are more mesenchymal. MCF7 cells showed a higher expression of E-cadherin and lower levels of Snail1, indicating an epithelial phenotype similar to that of AT3 cells.

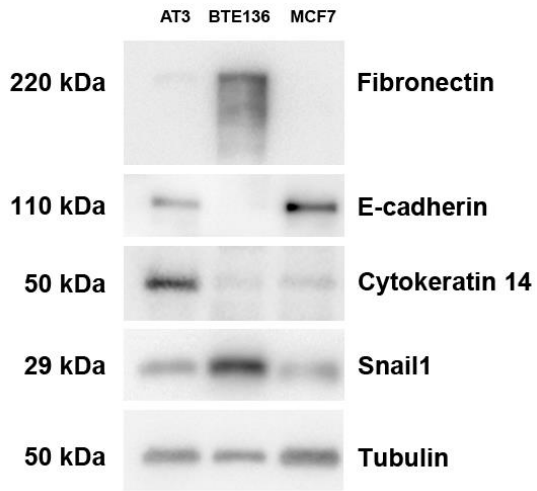

Figure R4. Breast tumor cells show differential expression of epithelial and mesenchymal markers. Protein levels of the indicated markers were determined by Western blot analysis in AT3, BTE136, and MCF7 cells.

To elucidate the process of adipocyte dedifferentiation in response to tumor cells, we established two main co-culture systems. The first is an indirect co-culture consisting of treating adipocytes with tumor cell-conditioned media from different cells (CM). The second method is direct co-culture, which involves seeding both cell populations in close contact using the Boyden chamber system.

Briefly, following adipocyte differentiation, tumor cells were added to a transwell **(Figure R5A)**. Direct co-culture of adipocytes with MCF7 cells for 3 or 7 days revealed a significant reduction in the lipid content **(Figure R5B)**. Additionally, this reduction in lipid content was time-dependent, as adipocytes co-cultured for 7 days exhibited lower lipid levels than those co-cultured for 3 days **(Figure R5C)**.

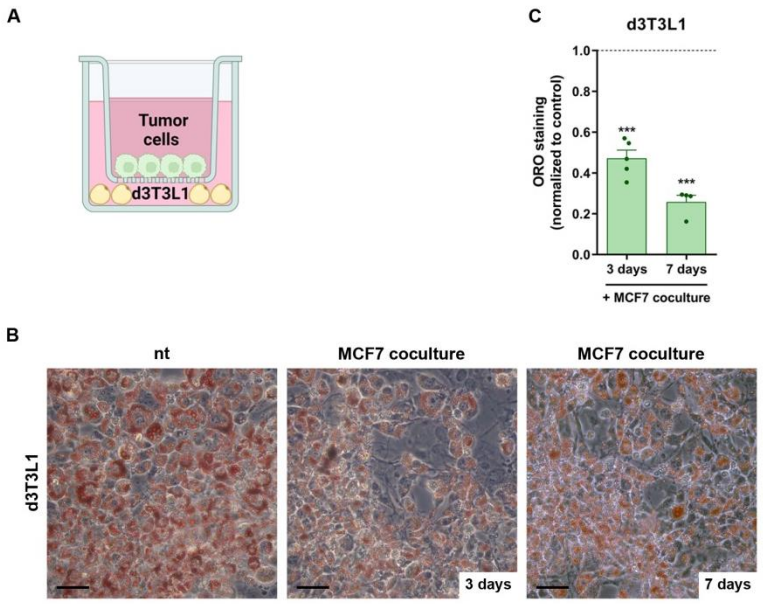

Figure R5. 3T3-L1 adipocytes lose lipids in response to MCF7 cells in a time-dependent manner. 3T3-L1 adipocytes were co-cultured with MCF7 cells for 3 or 7 days in direct co-culture **(A)**. Lipid loss was assessed by ORO staining **(B)** and quantified using ImageJ **(C)**. In **B**, scale bar represents 50 µm. In **C**, the control corresponds to non-co-cultured adipocytes; the average ± SEM of at least four independent experiments is shown. ***, $p < 0.001$.

Next, we evaluated whether breast cancer cells influence adipocyte activation differently, based on their phenotypes. Direct co-culture of adipocytes with AT3, BTE136, or MCF7 cells for 3 days **(Figure R6A**) revealed a significant reduction in lipid content across all three cell lines. The lipid loss observed in co-cultured adipocytes was similar for the three cell lines **(Figure R6B)**.

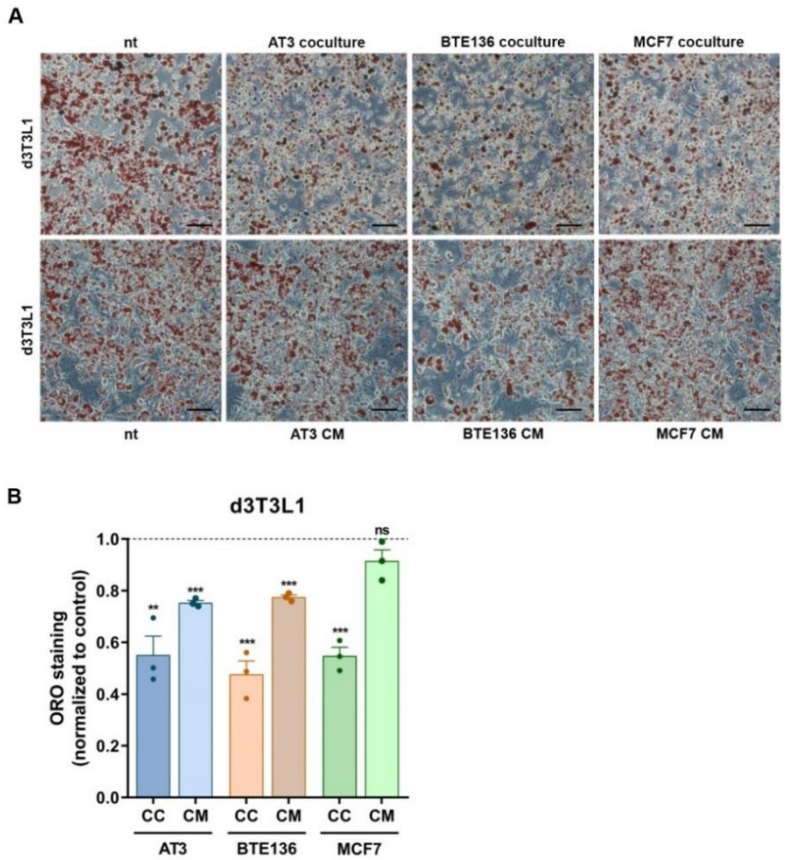

Figure R6. 3T3-L1 adipocytes lose lipids in response to tumor cells. 3T3-L1 adipocytes were co-cultured with AT3, BTE136, or MCF7 cells for 3 days in direct co-culture (CC) or indirect co-culture (CM). Lipid loss was assessed by ORO staining **(A)** and quantified using ImageJ **(B)**. In **A**, scale bar represents 50 µm. In **B**, the control corresponds to non-co-cultured adipocytes; the average ± SEM of three independent experiments is shown. ns, not significant; **, $p < 0.01$; ***, $p < 0.001$.

We also treated adipocytes with CM of the three breast cancer cell lines. This indirect co-culture of adipocytes for 3 days with AT3 and BTE136 CM also promoted lipid loss, although to a much lesser extent than the direct co-culture **(Figure R6B).**

We evaluated whether other cells present in the tumor microenvironment could promote lipid loss in adipocytes, particularly fibroblasts. We directly co-cultured adipocytes with L cells, CAFs, and NIH3T3 cells for 3 days (**Figure R7A**). We observed a significant reduction in lipid content similar for the three cell lines **(Figure R7B)**.

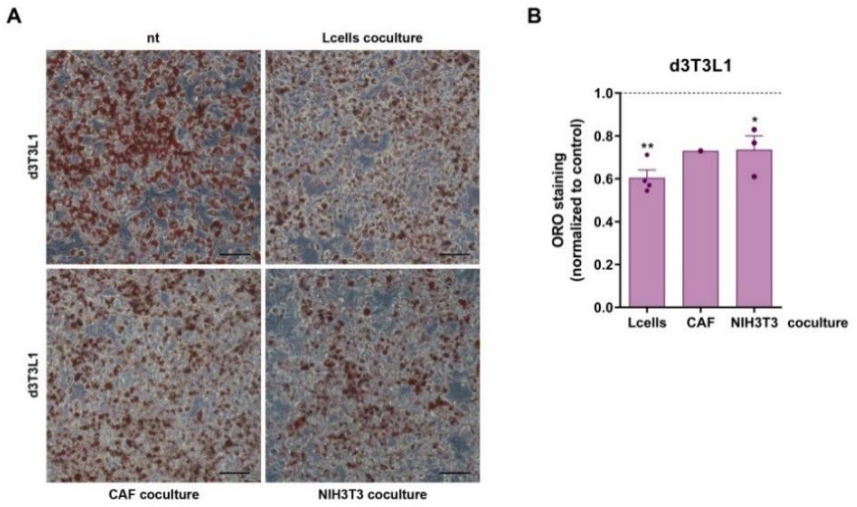

Figure R7. 3T3-L1 adipocytes lose lipids in response to fibroblasts. 3T3-L1 adipocytes were directly co-cultured with fibroblast cell lines (L cells, CAFs, or NIH3T3 cells) for 3 days. Lipid loss was assessed by ORO staining **(A)** and quantified using ImageJ **(B)**. In **A**, scale bar represents 50 µm. In **B**, the control corresponds to non-co-cultured adipocytes; the average ± SEM of at least three independent experiments is shown. *, $p < 0.05$; **, $p < 0.01$.

1.3. Inhibition of lipolysis partially prevents lipid loss

Next, we assessed whether the release of lipids from these LDs occurred through lipolysis. To achieve this, we used Atglistatin, a selective ATGL inhibitor.

Inhibition of lipolysis under non-co-culture conditions revealed a non-significant increase in lipid content **(Figure R8A)**. Adipocytes directly co-cultured with MCF7 cells for 3 days and treated with Atglistatin partially reversed the lipid loss observed in the MCF7 co-culture **(Figure R8B)**.

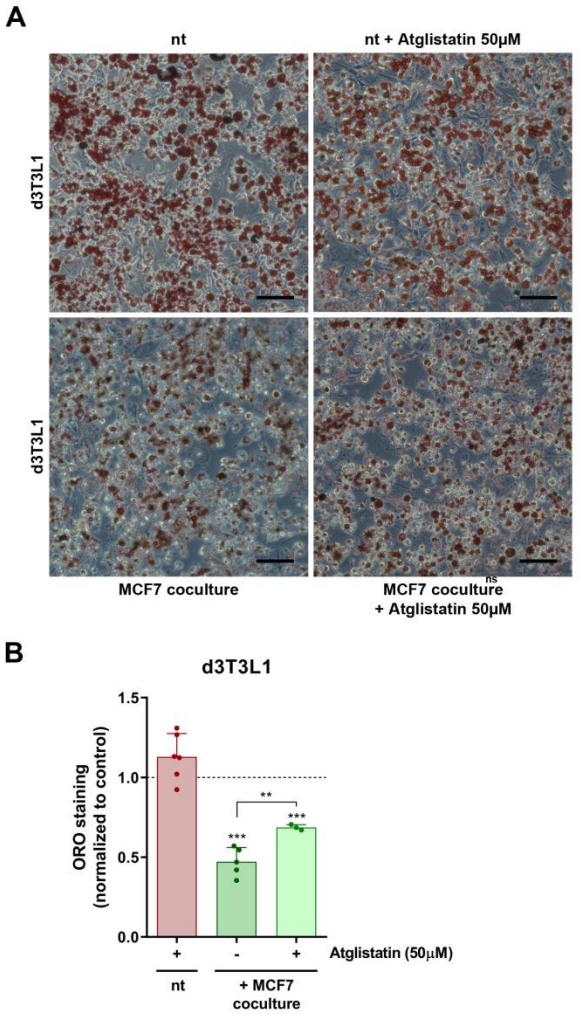

Figure R8. Co-cultured 3T3-L1 adipocytes partially lose lipids through lipolysis. 3T3-L1 adipocytes were treated with Atglistatin (50 µM) and directly co-cultured with MCF7 cells for 3 days. Lipid loss was assessed by ORO staining **(A)** and quantified using ImageJ **(B)**. In **A**, scale bar represents 50 µm. In **B**, the control corresponds to non-co-cultured untreated adipocytes; the average ± SEM of at least three independent experiments is shown. **, $p < 0.01$; ***, $p < 0.001$.

1.4. Adipocytes dedifferentiate in response to tumor cells

To assess whether tumor cells also promoted adipocyte dedifferentiation, we evaluated the downregulation of adipocyte markers. 3T3-L1 adipocytes were co-cultured directly (CC) or indirectly (CM) with breast tumor cells for 3 days, after which protein and RNA samples were collected.

Direct co-culture of adipocytes with breast tumor cells decreased the expression of adipocyte markers (C/EBPα, PPARγ, and Glut4) without modification in Snail1 **(Figure R9)**. Conversely, indirect co-culture of adipocytes with breast tumor cells did not promote a decrease in the expression of adipocyte markers or in Snail1 levels **(Figure R9)**.

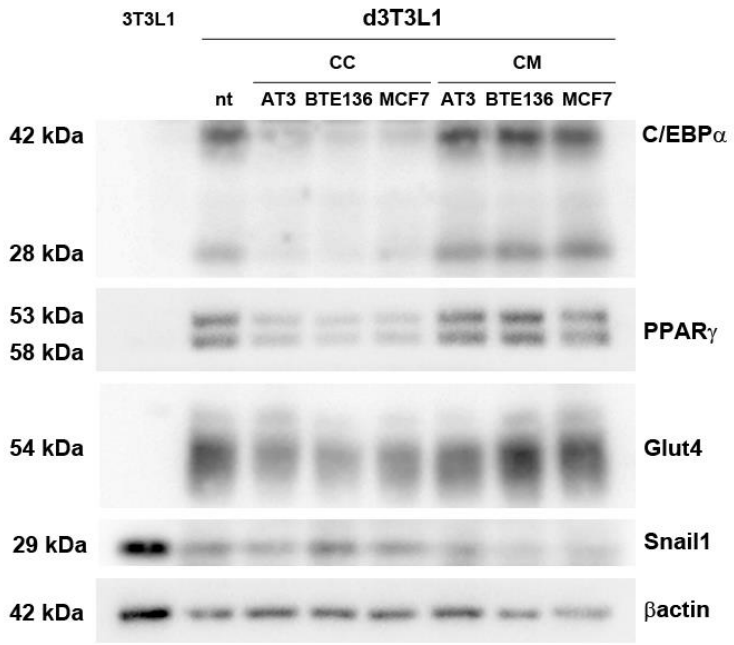

Figure R9. 3T3-L1 adipocytes dedifferentiate upon direct co-culture with breast tumor cells. 3T3-L1 adipocytes co-cultured directly (CC) or indirectly (CM) with breast tumor cell lines (AT3, BTE136, or MCF7) for 3 days. Adipocyte dedifferentiation was assessed by Western blot.

The mRNA analysis yielded similar results **(Figure R10)**.

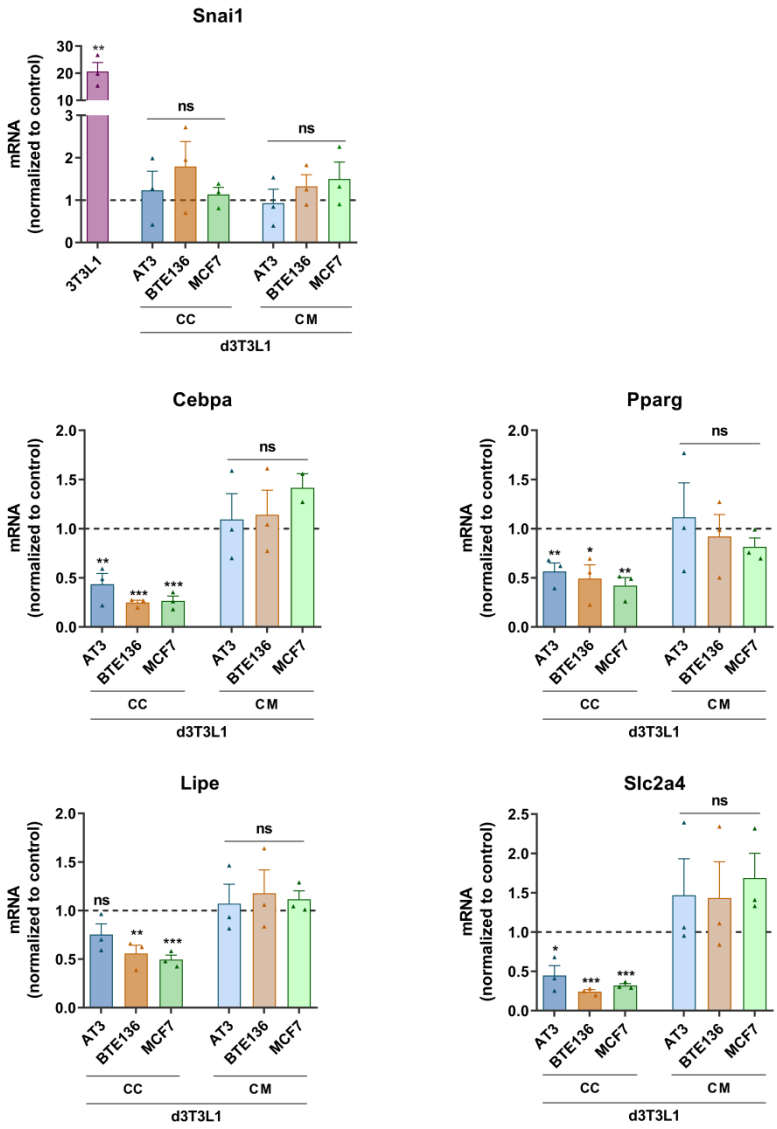

Figure R10. 3T3-L1 adipocytes dedifferentiate upon direct co-culture with breast tumor cells. 3T3-L1 adipocytes co-cultured directly (CC) or indirectly (CM) with breast tumor cell lines (AT3, BTE136, or MCF7) for 3 days. Adipocyte dedifferentiation was assessed using RT-qPCR. The control corresponds to non-co-cultured adipocytes; the average ± SEM of three independent experiments is shown. ns, not significant; *, $p < 0.05$; **, $p < 0.01$; ***, $p < 0.001$.

The co-culture with fibroblasts also promoted adipocyte dedifferentiation **(Figure R11)**.

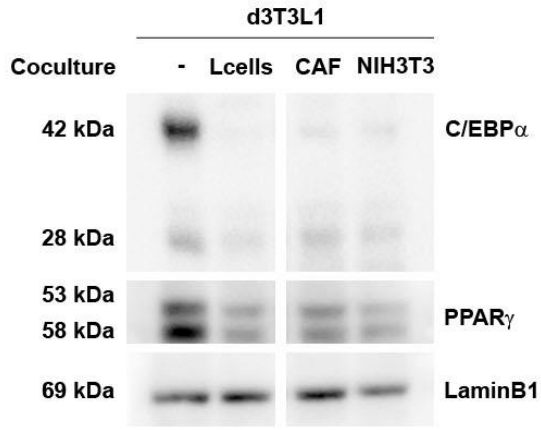

Figure R11. 3T3-L1 adipocytes dedifferentiate in response to fibroblasts. 3T3-L1 adipocytes were directly co-cultured with fibroblastic cell lines (L cells, CAFs, or NIH3T3) for 3 days. Adipocyte dedifferentiation was assessed by Western blot.

1.5. mRNA sequencing analysis reveals a pattern of de-differentiation in adipocytes

To gain a deeper understanding in the process of adipocyte dedifferentiation, we conducted a complete mRNA analysis of 3T3-L1 adipocytes co-cultured with MCF7 cells for 3 days (RNA-Seq).

We first examined the differential gene expression between activated adipocytes and non-co-cultured control cells. **Figure R12** highlights the ten most significantly upregulated and downregulated genes in the activated adipocytes.

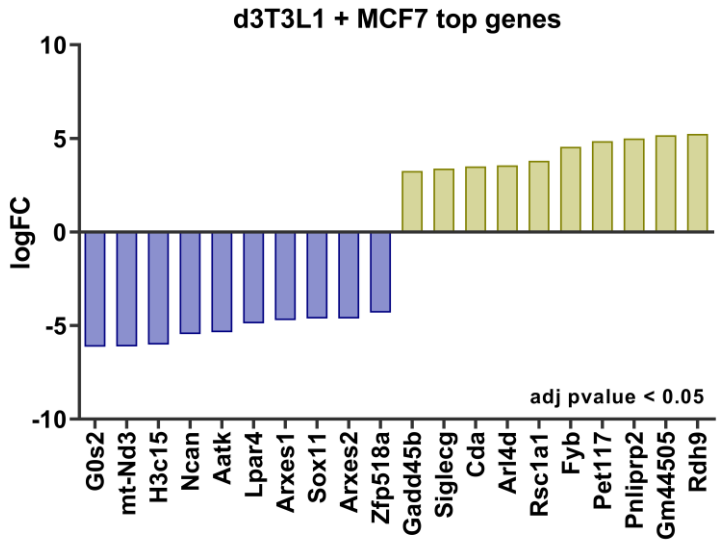

Figure R12. 3T3-L1 co-cultured adipocytes most modified genes. 3T3-L1 adipocytes were directly co-cultured with MCF7 cells for 3 days. Total RNA was collected and mRNA sequencing was performed, followed by bioinformatics analysis. The most significantly modified genes were selected based on an adjusted p-value < 0.05.

We validated the expression of selected genes in independent samples, specifically Gadd45b and Rdh9 using RT-qPCR. As in the RNA-seq analysis, both Gadd45b and Rdh9 were significantly upregulated in co-cultured adipocytes **(Figure R13)**.

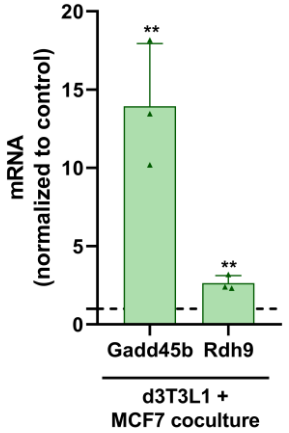

Figure R13. Gene validation using RT-qPCR. 3T3-L1 adipocytes were directly co-cultured with MCF7 cells for 3 days. Total RNA was collected, and RT-qPCR was performed. The control corresponds to non-co-cultured adipocytes; the average ± SEM of three independent experiments is shown. **, $p < 0.01$.

Gene Set Enrichment Analysis (GSEA) pathway enrichment analysis was performed to investigate the molecular processes modified during adipocyte activation induced by MCF7 cells. Gene Ontology analysis revealed a downregulation in biological processes (GOBPs) related to fatty acid metabolic processes, fatty acid catabolic processes, fatty acid beta-oxidation, and lipid biosynthetic processes **(Figure R14)**. Overall, these findings indicate significant suppression of fatty acid-related processes in activated adipocytes.

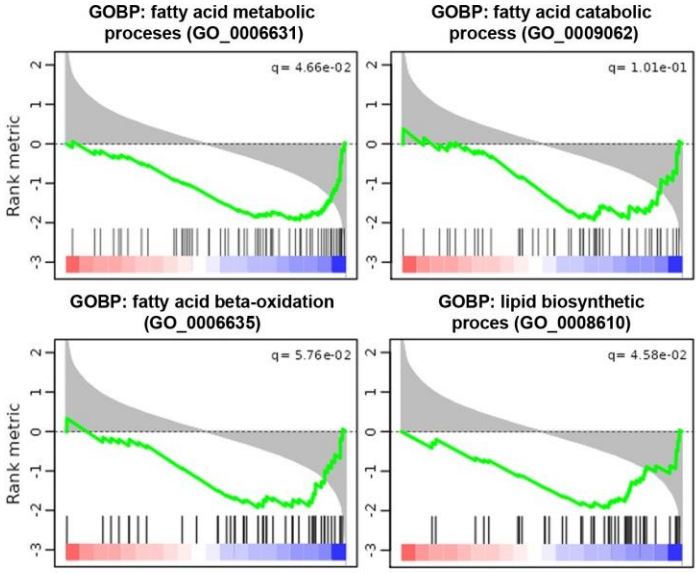

Figure R14. Activated adipocytes downregulate fatty acid-related processes. 3T3-L1 adipocytes were directly co-cultured with MCF7 cells for 3 days. Total RNA was collected for RNA-seq and subsequent bioinformatics analysis. GSEA analysis of GOBPs related to fatty acids with an FDR < 0.2.

Accordingly, GSEA revealed a downregulation of the adipogenesis hallmark **(Figure R15A)**. Adipocytes exhibited upregulation of Myc targets, apoptosis, and IL2-Stat5 signaling hallmarks **(Figure R15A)**. Among the top enriched genes associated with adipogenesis, RNA-seq showed downregulation in Fabp4 (Fatty acid binding protein 4), Lpl (Lipoprotein lipase), Lipe, and CD36 **(Figure R15B)**.

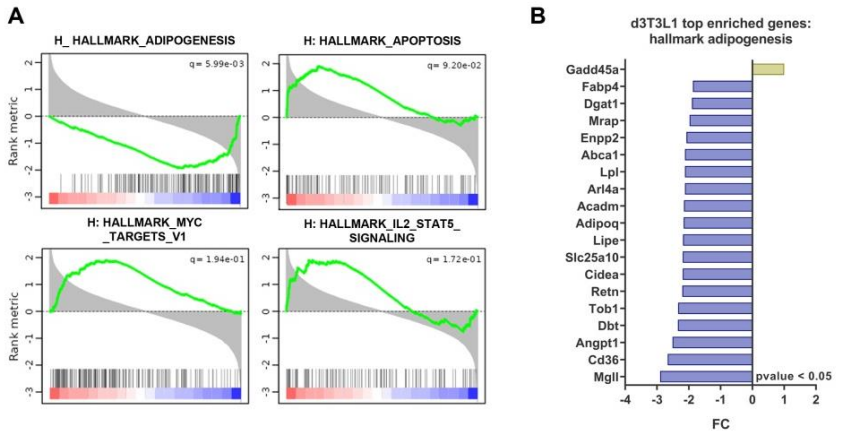

Figure R15. Activated adipocytes downregulate adipogenesis and upregulate Myc targets, apoptosis, and Stat5 signaling. 3T3-L1 adipocytes were directly co-cultured with MCF7 cells for 3 days. Total RNA was collected for RNA-seq and subsequent bioinformatics analysis. **(A)** GSEA of the top modified hallmarks with an FDR < 0.2. **(B)** List of the top differentially expressed genes within the adipogenesis hallmark shown in panel A, with a p-value < 0.05.

As mentioned in the Introduction, Stat3 activation via the IL-6 signaling pathway regulates adipocyte lipolysis. This, combined with our RNA-seq results, prompted us to investigate STAT activation in the activated adipocytes. Breast tumor cells increased Stat3 phosphorylation in adipocytes **(Figure R16)**.

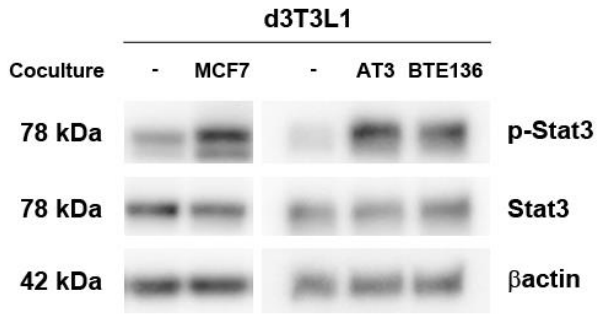

Figure R16. Enhanced Stat3 phosphorylation in activated 3T3-L1 adipocytes. 3T3-L1 adipocytes were directly co-cultured with the breast tumor cell lines (AT3, BTE136, or MCF7) for 3 days. Protein levels of the indicated markers were determined by Western blot analysis.

We also investigated whether activation of the JAK/STAT signaling pathway through external factors promoted adipocyte activation by treating differentiated 3T3-L1 adipocytes with various cytokines and growth factors. However, treatment of adipocytes with IL-6, LIF, PDGFβ, TGFβ, and TNFα, either alone or in combination, did not significantly reduce lipid content or decreased the expression of the adipogenic markers **(Figures R17A and B)**, despite Stat3 activation by LIF and IL-6 **(Figure R17C)**.

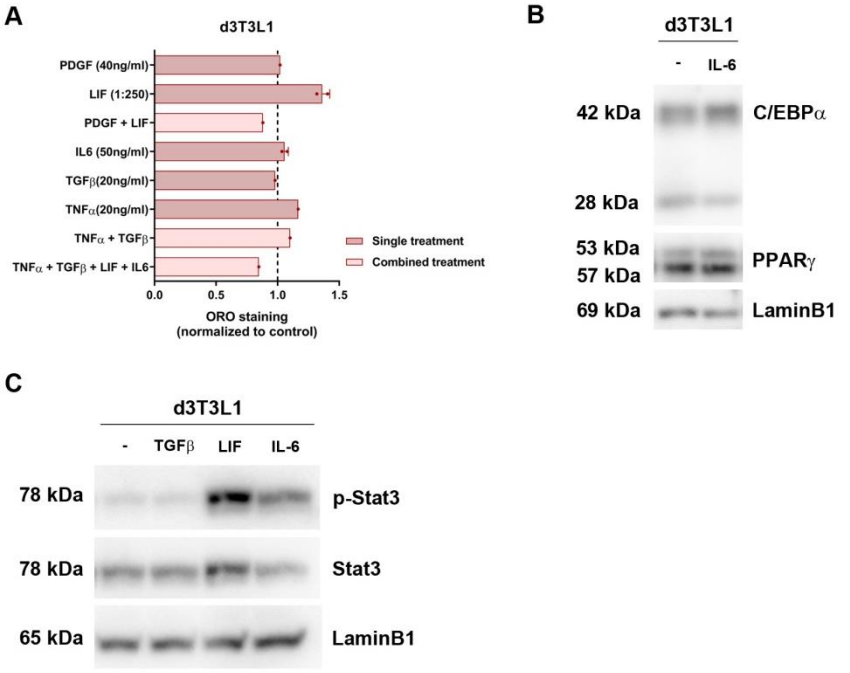

Figure R17. Cytokines do not promote lipid loss in 3T3-L1 adipocytes despite Stat3 activation. 3T3-L1 adipocytes were treated with the selected cytokines or growth factors for 3 days. **(A)** Lipid loss was assessed by ORO staining, and **(B)** adipocyte dedifferentiation and **(C)** Stat3 activation by Western blot. In **A**, the control corresponds to untreated adipocytes; the average ± SEM of one or two independent experiments is shown.

1.6. Activated adipocytes increase the expression of adipocyte progenitors, macrophage, and fibroblast marker genes

To further characterize the activated adipocytes, we analyzed our RNA-seq comparing our results with those published in human tumors. Related to a specific list of genes and markers found in Zhu et al. (2022), our results indicate that activated adipocytes show a decrease in the expression of mature adipocyte markers (Adipoq, Plin1, Fabp4) and adipogenic master regulators (Pparg, Cebpa, Lpl). Conversely, there was an overall increase in the expression of mesenchymal stem cell or adipocyte progenitor genes (Cd44, Ly6a, Cd24a, Cd9), macrophage markers (Lgals3), and fibroblast genes (Acta2, Vim, Serpinh1) **(Figure R18)**.

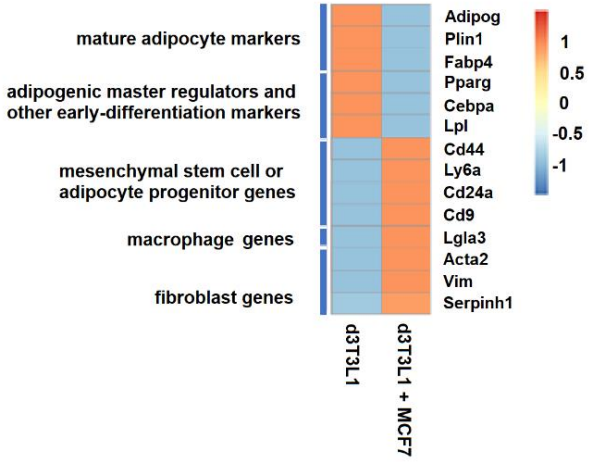

Figure R18. Activated adipocytes increase the expression of adipocyte progenitor, macrophage, and fibroblast markers. Heatmap depicting gene expression levels of mature adipocyte markers, early differentiation markers, adipocyte progenitor markers, and macrophage markers, and compared with genes expressed in 3T3-L1 adipocytes either non-co-cultured or directly co-cultured with MCF7 cells for 3 days.

1.7. Activated adipocytes show decrease glucose utilization

As mentioned in the Introduction, glucose is essential for white adipocytes as it serves as a precursor for de novo lipogenesis and is required for adipocyte differentiation. Our RNA-seq data revealed metabolic changes in activated adipocytes, particularly downregulation of lipid biosynthetic processes. We then investigated whether glucose metabolism was altered in the adipocytes activated by MCF7 cells. To explore this, we measured glucose concentration in the supernatants of co-cultured adipocytes, normalizing the data by cell number. We found that activated adipocytes consumed less glucose than non-co-cultured adipocytes **(Figure R19)**. This is probably related to the process of dedifferentiation, since non-differentiated 3T3-L1 cells (nd3T3L1) consumed less glucose than differentiated 3T3-L1 adipocytes.

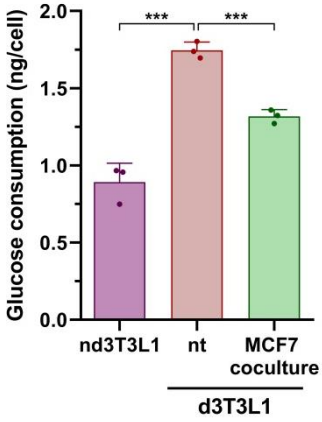

Figure R19. Activated adipocytes exhibit reduced glucose consumption. 3T3-L1 adipocytes were directly co-cultured with MCF7 cells for 3 days, whereas separate nd3T3L1 or d3T3L1 cells were maintained in culture for 3 days. Medium supernatants were obtained, followed by glucose determination and cell counting. The average ± SEM of three independent experiments is shown. ***, $p < 0.001$.

1.8. Glucose depletion mimics adipocyte activation

We reasoned that competition for glucose utilization between MCF7 cells and 3T3-L1 might be relevant for adipocyte dedifferentiation. Therefore, we reduced the glucose concentration in the media of differentiated 3T3-L1 adipocytes from 4.5 g/L (high glucose), to 1 g/L (low glucose), or 0.1 g/L (very low glucose). Glucose deprivation led to a reduction in lipid content **(Figure R20A)**. Adipocytes under very low glucose conditions exhibited significantly lower lipid content than those under low glucose conditions **(Figure R20B)**. Unlike direct co-culture with tumor cells, Atglistatin did not inhibit fatty acid loss during glucose deprivation **(Figure R20B)**.

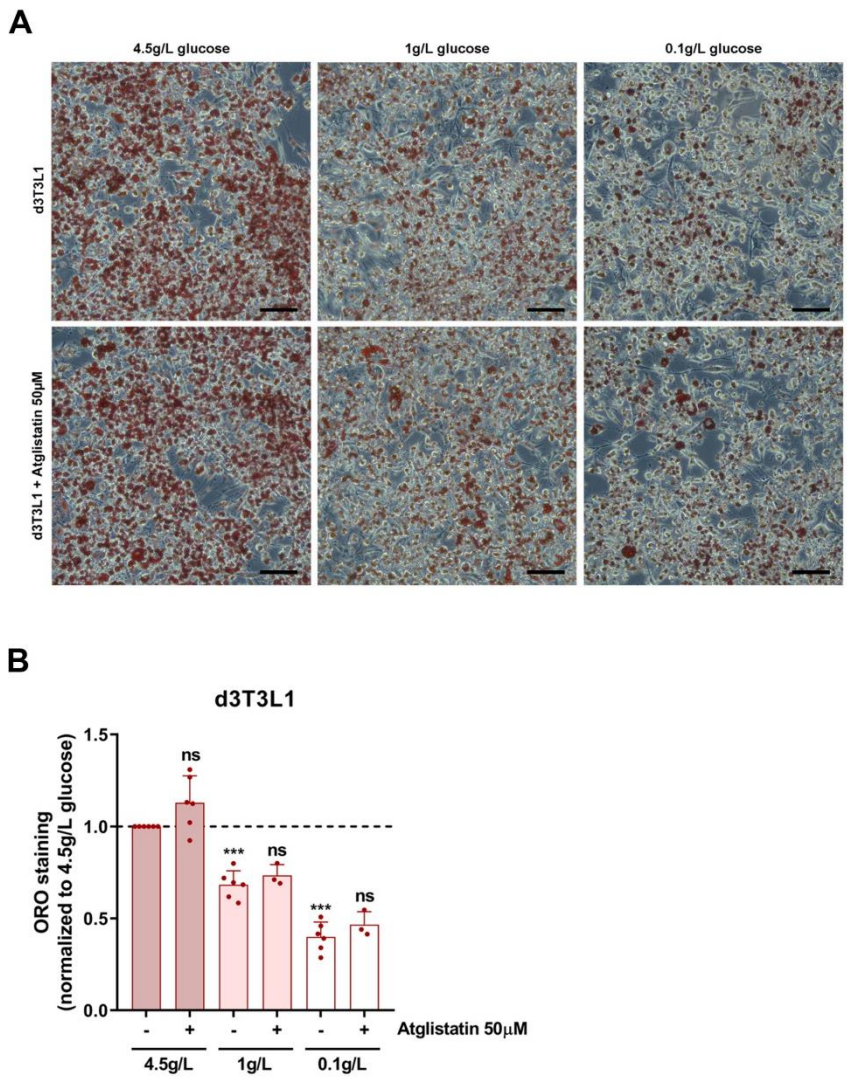

Figure R20. Glucose deprivation induces lipid loss in 3T3-L1 adipocytes. 3T3-L1 adipocytes were cultured in media containing 4.5 g/L glucose, 1 g/L glucose, or 0.1 g/L glucose for 3 days in control or with Atglistatin (50µM). Lipid loss was assessed by ORO staining **(A)** and quantified using ImageJ **(B)**. In **A**, scale bar represents 50µm. In **B**, the control corresponds to untreated adipocytes in 4.5 g/L glucose; the average ± SEM of at least three independent experiments is shown. ns, not significant; ***, $p < 0.001$.

Glucose deprivation promoted adipocyte dedifferentiation, as demonstrated by the analysis of different markers at protein **(Figure R21A)** and mRNA level **(Figure R21B)**. No differences were observed between low and very low glucose conditions.

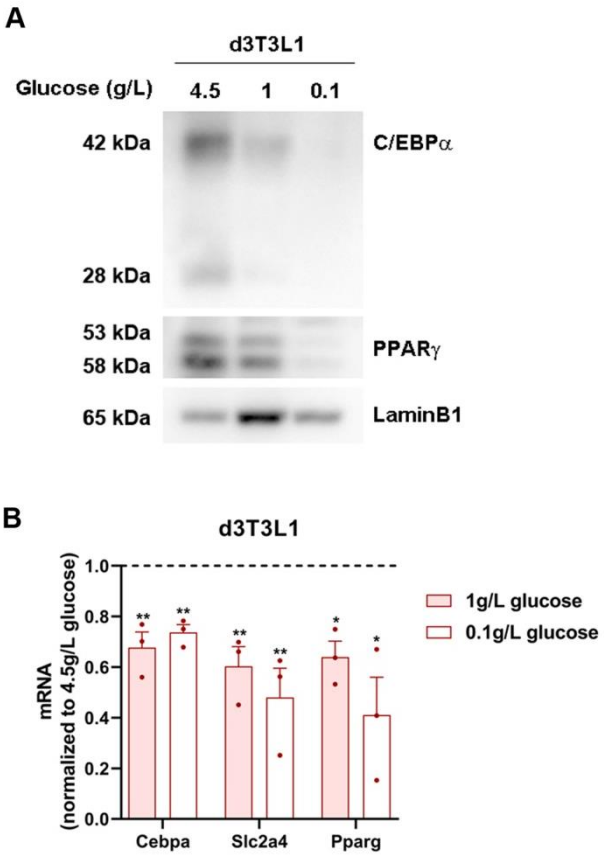

Figure R21. Glucose deprivation promotes 3T3-L1 adipocyte dedifferentiation. 3T3-L1 adipocytes were treated with 4.5 g/L glucose, 1 g/L glucose, or 0.1 g/L glucose for 3 days. Adipocyte dedifferentiation was assessed using Western blot **(A)** and RT-qPCR **(B)**. In **B**, the control corresponds to adipocytes in 4.5 g/L glucose; the average ± SEM of three independent experiments is shown. *, $p < 0.05$; **, $p < 0.01$.

We substituted glucose with another sugar, D-mannose, which can enter the glycolytic pathway and be converted to Fructose 6P *(see Introduction)*. D-mannose effectively prevented lipid loss under low glucose conditions **(Figure R22A and R22B)**.

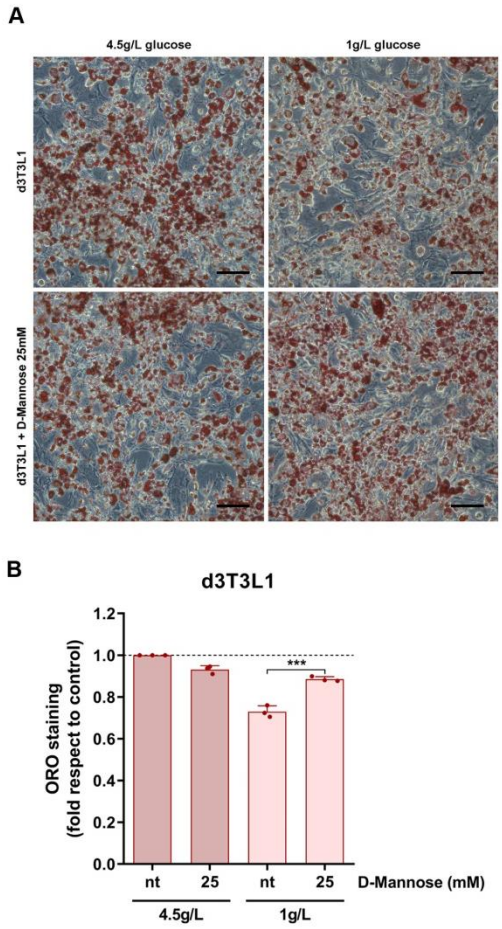

Figure R22. D-mannose prevents lipid loss in adipocytes in low glucose conditions. 3T3-L1 adipocytes were treated with 4.5 g/L glucose, or 1 g/L glucose for 3 days with or without D-mannose (25 mM). Lipid loss was assessed by ORO staining **(A)** and quantified using ImageJ **(B)**. In **A**, scale bar represents 50 µm. In **B**, the control corresponds to untreated adipocytes in 4.5 g/L glucose; the average ± SEM of three independent experiments is shown. ***, $p < 0.001$.

To better understand the alterations in glucose metabolism in activated adipocytes, we used inhibitors targeting two pathways involved in glucose utilization. Specifically, we used Azaserine (a Glutamine fructose-6-phosphate amidotransferase, GFAT, inhibitor) to inhibit the hexosamine pathway and 6-Aminonicotinamide (a G6PD inhibitor) to inhibit the pentose phosphate pathway.

The inhibition of glucose metabolism by Azaserine (Aza) or 6-Aminonicotinamide (6-AN) did not promote lipid loss **(Figure 23A and 23B)** or induce adipocyte activation **(Figure 23C)**.

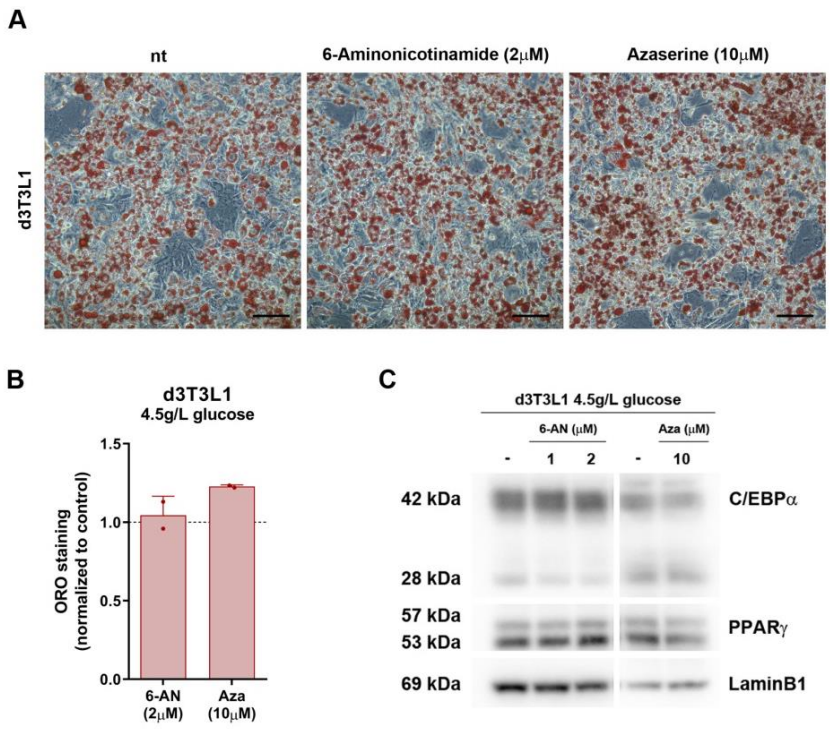

Figure R23. Inhibition of glucose metabolism did not induce adipocyte activation. 3T3-L1 adipocytes were cultured in media containing 4.5 g/L glucose for 3 days under control conditions or with 6-Aminonicotinamide (1-2 μM) or Azaserine (10μM). Lipid loss was assessed by ORO staining **(A)** and quantified using ImageJ **(B)**. Adipocyte dedifferentiation was assessed using Western blot **(C)**. In **A**, scale bar represents 50 μm. In **B**, the control corresponds to untreated adipocytes; the average ± SEM of two independent experiments is shown.

Although glucose deprivation promotes adipocyte dedifferentiation, this is not involved in the action of tumor cells. Supplementing adipocyte-tumor cells co-cultures with 4.5 g/L glucose every 24 h does not prevent lipid loss **(Figure R24A and R24B)** or adipocyte dedifferentiation **(Figure R24C)**.

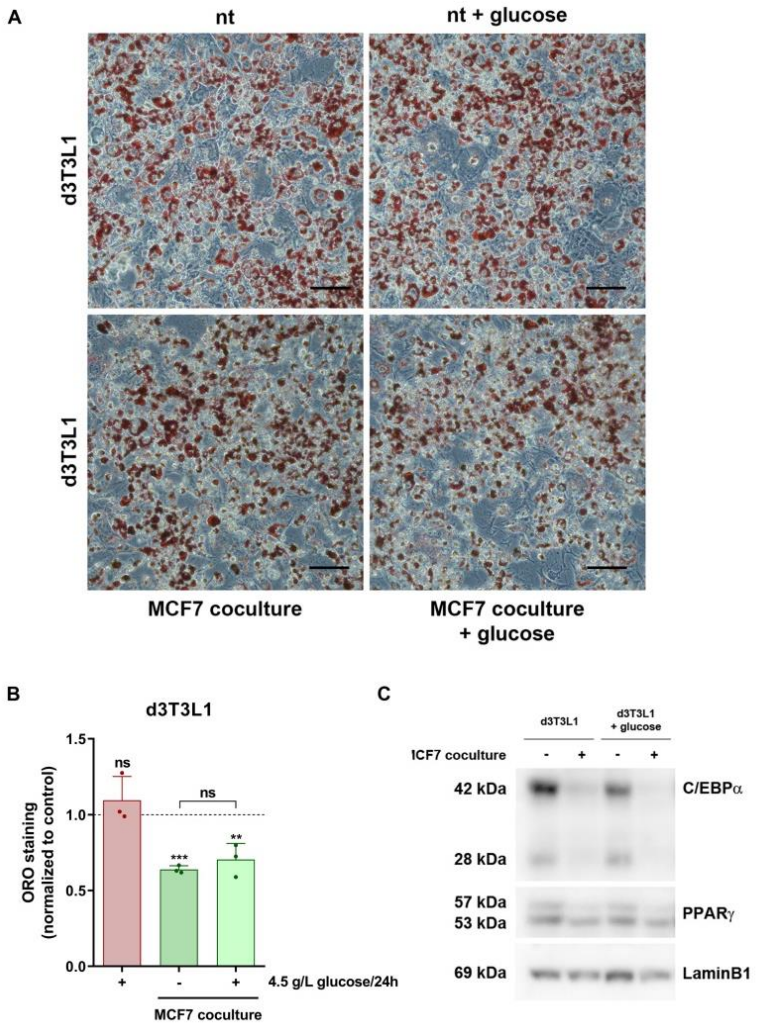

Figure R24. Glucose supplementation of direct co-culture did not prevent adipocyte activation. 3T3-L1 adipocytes were directly co-cultured with MCF7 cells for 3 days. Lipid loss was assessed by ORO staining **(A)**, and quantified using ImageJ **(B)**. Adipocyte dedifferentiation was assessed using Western blot **(C)**. In **A**, scale bar represents 50 µm. In **B**, the control corresponds to non-co-cultured untreated adipocytes; the average ± SEM of three independent experiments is shown. ns, not significant; **, $p < 0.01$; ***, $p < 0.001$.

2. ADIPOCYTES PROMOTE BREAST TUMOR CELLS MIGRATION AND INVASION

In previous experiments we demonstrated that adipocytes were activated in response to breast tumor cells and fibroblasts. Adipocyte activation involves loss of lipid content and downregulation of adipocyte markers. Additionally, RNA-seq and *in vitro* data showed that activated adipocytes altered their metabolism by decreasing lipid-related processes and glucose consumption. Thus far, we have focused on the mechanism by which tumor cells induce adipocyte activation. In the following sections, we explore the mechanisms by which activated adipocytes contribute to tumor cell migration and invasion.

2.1. 3T3-L1 adipocytes promote breast tumor cell migration and invasion

To investigate the effect of adipocytes on breast tumor cell migration and invasion, we used the Boyden Chamber system. Briefly, following adipocyte differentiation, tumor cells were added to a transwell and migration or invasion assays were performed in the presence of an FBS gradient.

Our results demonstrated that 3T3-L1 adipocytes enhanced the migration of AT3, BTE136, and MCF7 cells **(Figure R25A)** and also facilitated their invasion through matrigel **(Figure R25B)**.

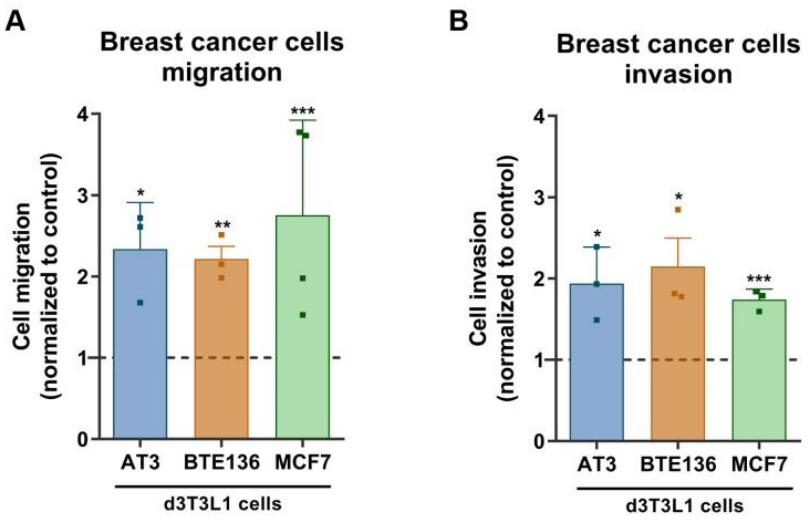

Figure R25. Enhanced breast tumor cell migration and invasion in the presence of 3T3-L1 adipocytes. Cell migration **(A)** or invasion **(B)** were measured as the ability of breast tumor cells to move from the upper to the lower compartment of Boyden Chambers through a porous membrane in the presence of adipocytes in the lower chamber. Controls represent the migration or invasion of tumor cells in the absence of adipocytes; the average ± SEM of at least three independent experiments is shown. *, $p < 0.05$; **, $p < 0.01$; ***, $p < 0.001$.

To determine whether a direct interaction between tumor cells and adipocytes is necessary to enhance migration, we conducted migration assays using adipocyte-conditioned medium in the bottom chamber.

Adipocyte CM (d3T3L1 CM) promotes MCF7 migration, although to a lesser extent compared to the direct presence of adipocytes (d3T3L1) **(Figure R26)**. This effect was not observed with 3T3L1 pre-adipocyte cells (nd3T3L1), confirming that the migration enhancement is specific of differentiated adipocytes **(Figure R26)**.

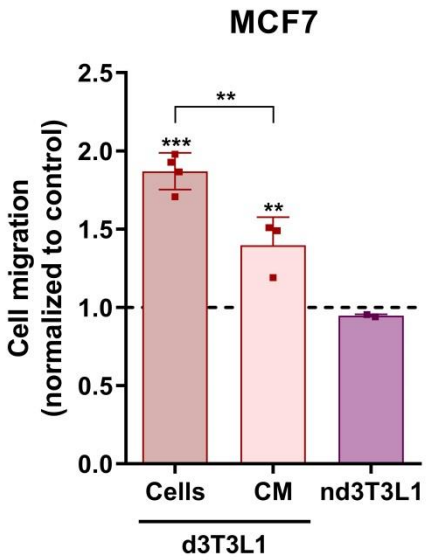

Figure R26. Enhanced breast tumor cell migration with 3T3-L1 adipocyte CM. MCF7 cell migration was measured in the presence of adipocytes, adipocyte CM, or nd3T3-L1 cells in the lower chamber. Controls represent the migration of MCF7 cells in the absence of cells or CM; the average ± SEM of at least two independent experiments is shown. **, $p < 0.01$; ***, $p < 0.001$.

We also explored the effect of adipocytes on tumor cell proliferation. We performed Crystal Violet staining of breast tumor cells cultured with adipocyte CM for three days. AT3 and BTE136 cells did not show increased proliferation in the presence of adipocyte CM; only MCF7 cells exhibited a small increase in proliferation **(Figure R27)**.

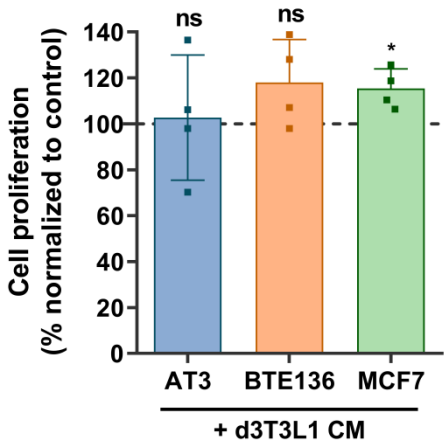

Figure R27. Co-cultured tumor cells do not show differences in proliferation. AT3, BTE136, and MCF7 cells were indirectly co-cultured with adipocytes (CM) for 3 days. Proliferation was assessed by Crystal Violet staining. Control represents cell proliferation of untreated breast tumor cells; the average ± SEM of four independent experiments is shown. ns, not significant; *, $p < 0.05$.

2.2. MCF7 cells accumulate lipids from adipocytes

Next, we investigated the role of fatty acids in tumor cell migration.

First, we examined whether MCF7 cells could store lipids in the LDs. We used Bodipy 493/503, which specifically stains neutral lipid droplets. MCF7 cells were incubated with adipocyte CM for three days and stained with Bodipy 493/503. The numbers of lipid droplet-positive and lipid droplet-negative cells were counted from the images using Qupath.

MCF7 cells incubated with adipocyte CM exhibited a higher number of lipid droplets **(Figure R28A and R28B)**.

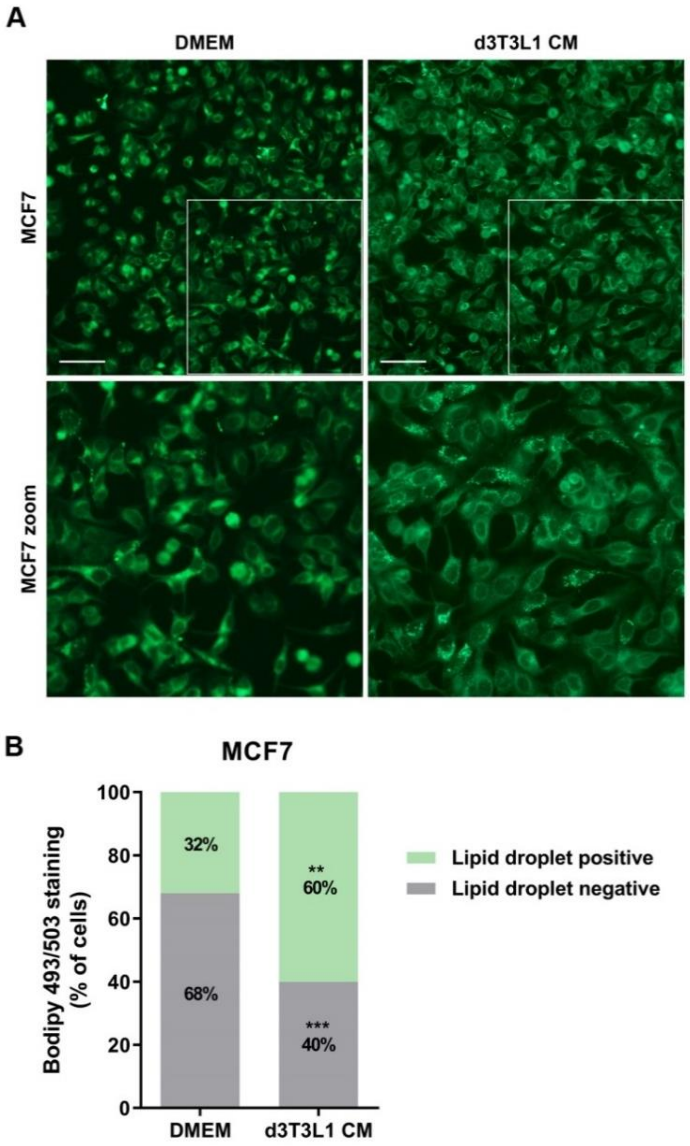

Figure R28. Indirectly co-cultured MCF7 cells have more lipid droplets than control cells. MCF7 cells were co-cultured with conditioned medium from adipocytes for 3 days and stained with Bodipy 493/503 for 10 min. **(A)** Random images were taken and **(B)** lipid droplet-positive and lipid droplet-negative cells were counted using Qupath. In **A**, scale bar represents 50 µm. In **B**, the average ± SEM of at least three independent experiments is shown. **, $p < 0.01$; ***, $p < 0.001$.

These experiments were repeated with primary adipocytes, and lipid storages were stained with ORO. MCF7 cells incubated with adipocyte CM and primary adipocytes exhibited higher lipid content **(Figure R29A and R29B)**. Strikingly, MCF7 cells directly co-cultured with 3T3-L1 adipocytes displayed the same lipid content as the controls **(Figure R29B)**.

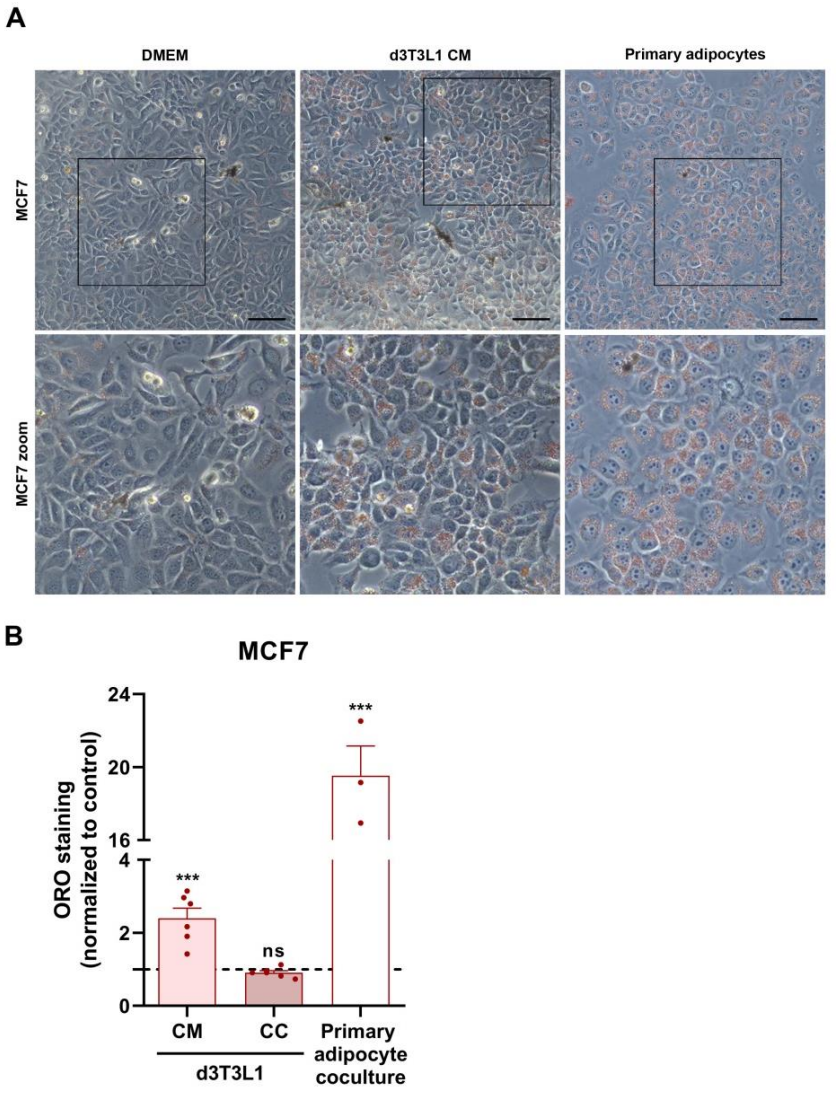

Figure R29. MCF7 cells have more lipid content in direct co-culture with primary adipocytes. MCF7 cells were indirectly co-cultured with adipocytes (CM), directly co-cultured with primary adipocytes, or directly co-cultured with 3T3-L1 adipocytes (CC) for 3 days. Lipid accumulation was assessed using ORO staining **(A)** and quantified by elution with isopropanol **(B)**. In **A**, scale bar represents 50 µm. In **B**, the controls correspond to non-co-cultured MCF7 cells; the average ± SEM of at least three independent experiments is shown. ns, not significant; ***, $p < 0.001$.

2.3. Analysis of fatty acids in adipocyte conditioned medium

MCF7 cells exhibit increased migration and invasion in the presence of adipocytes, which correlates with an elevated lipid content. To study the role of fatty acids in enhancing these capabilities, we analyzed the fatty acid content of adipocyte-conditioned media and investigated whether treating tumor cells with exogenous fatty acids could independently promote migration.

We cultured MCF7 cells with 3T3-L1 adipocytes conditioned medium for 2 days (MCF7 + d3T3L1 CM) or DMEM (MCF7 CM) and collected the supernatants. Additionally, we obtained adipocyte-conditioned medium (d3T3L1 CM) **(Figure R30A)**. The total fatty acid content of the supernatants was analyzed using gas chromatography coupled with electron ionization mass spectrometry (GC-MS). **Figure R30B** shows the differences in the fatty acid content of d3T3L1 CM compared to DMEM. Specifically, there was an increase in the concentrations of pentadecanoic acid (C15:0), palmitoleic acid (C16:1n7), and heptadecanoic acid (C17:0), and a decrease in linoleic acid (C18:2n6). We examined the differences in fatty acid content in MCF7 treated cells to identify fatty acids potentially utilized from the adipocyte CM. **Figure R30C** shows a decrease in the content of C15:0, C16:1n7, and C17:0 compared to the original adipocyte CM.

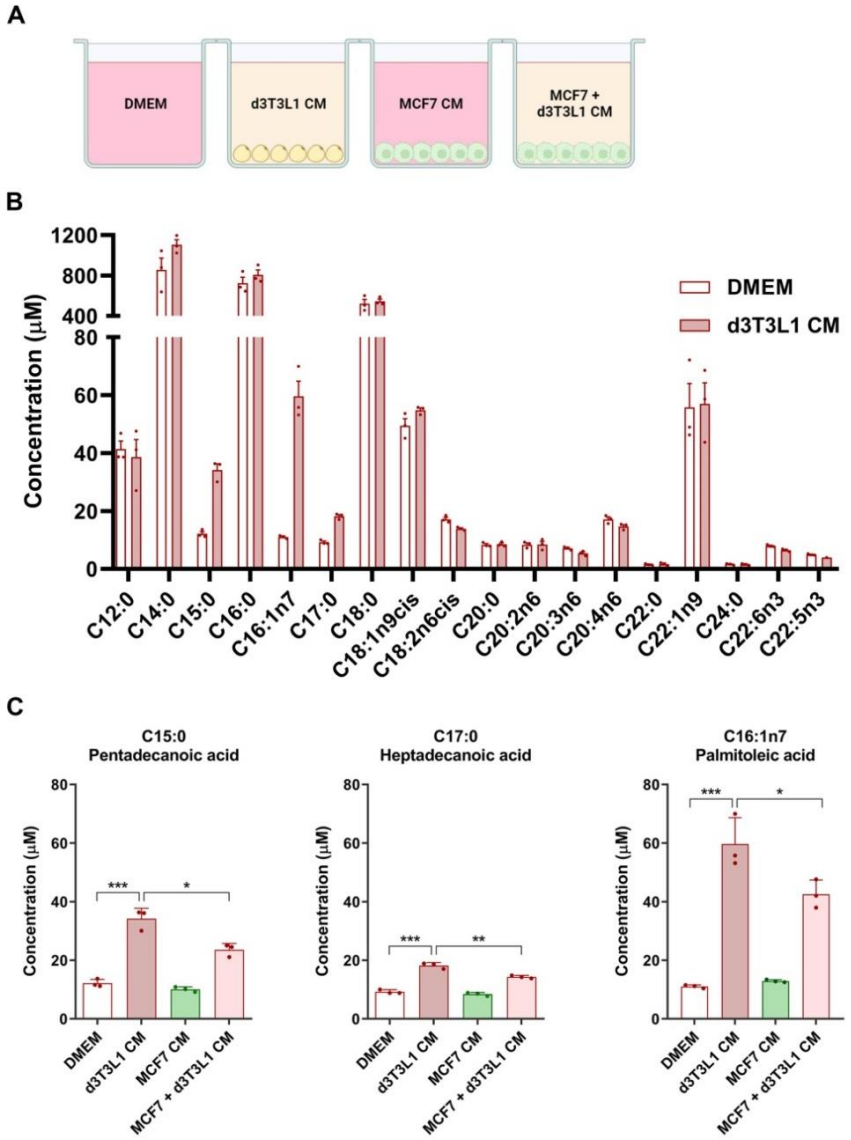

Figure R30. Adipocyte CM is enriched in C15:0, C17:0 and C16:1n7. Adipocyte conditioned media was obtained from 3T3-L1 adipocytes (d3T3L1 CM), and MCF7 cells were indirectly co-cultured with adipocytes (MCF7 + d3T3L1 CM) or DMEM (MCF7 CM) for 2 days **(A)**. Total fatty acid content was analyzed using GC-MS **(B, C)**. In **B** and **C**, the average ± SEM of three independent experiments is shown. *, $p < 0.05$; **, $p < 0.01$; ***, $p < 0.001$.

2.4. Lipid accumulation does not promote migration

Next, we investigated whether treating tumor cells with the selected exogenous fatty acids (C15:0 and C17:0) or others (palmitic acid, C16:0) could promote migration. MCF7 cells were treated with C15:0, C17:0, or C16:0 for 48 h, and their effects on cell migration were evaluated. Although MCF7 cells store exogenous fatty acids in LDs **(Figure R31A and R31B)**, exogenous fatty acid treatment did not enhance migration **(Figure R31C)**.

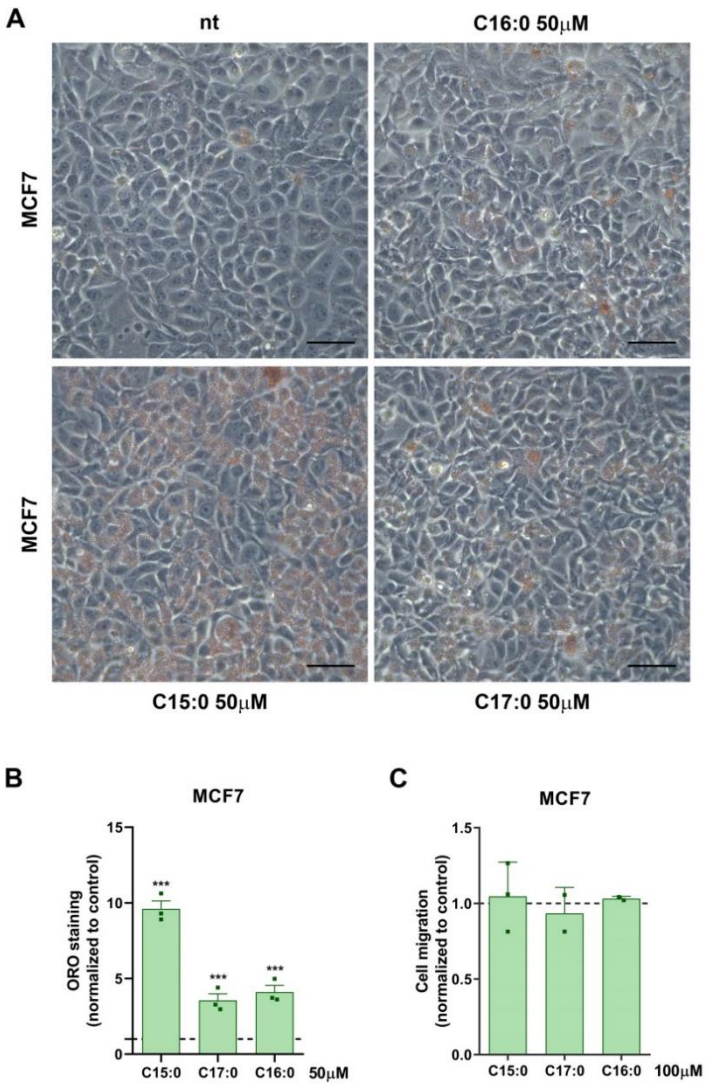

Figure R31. Exogenous fatty acid load does not enhance the migration of MCF7 cells. MCF7 cells were pretreated with Pentadecanoic (C15:0), Heptadecanoic (C17:0) or Palmitic Acid (C16:0) for 2 days. Lipid accumulation was assessed using ORO staining **(A)** and quantified by elution with isopropanol **(B)**. **(C)** MCF7 cell migration was measured in the presence of an FBS gradient. In **A**, scale bar represents 50 μm. In **B** and **C**, the controls correspond to untreated MCF7 cells; the average ± SEM of at least two independent experiments is shown. ***, $p < 0.001$.

2.5. Fatty acid metabolism is required for migration

To investigate this further, we explored whether fatty acid metabolism was essential for cell migration. We used three inhibitors of FA metabolism: Atglistatin to block triglyceride lipase and fatty acid release, Etomoxir to block fatty acid oxidation, and BMS-309403 (BMS), which, at the concentrations used, inhibits all FA binding proteins (FABPs) and thus FA uptake.

First, we evaluated the impact of these compounds on cell proliferation. Among the three drugs tested, MCF7 cells exhibited greater sensitivity to Atglistatin compared to BMS or Etomoxir **(Figure R32)**.

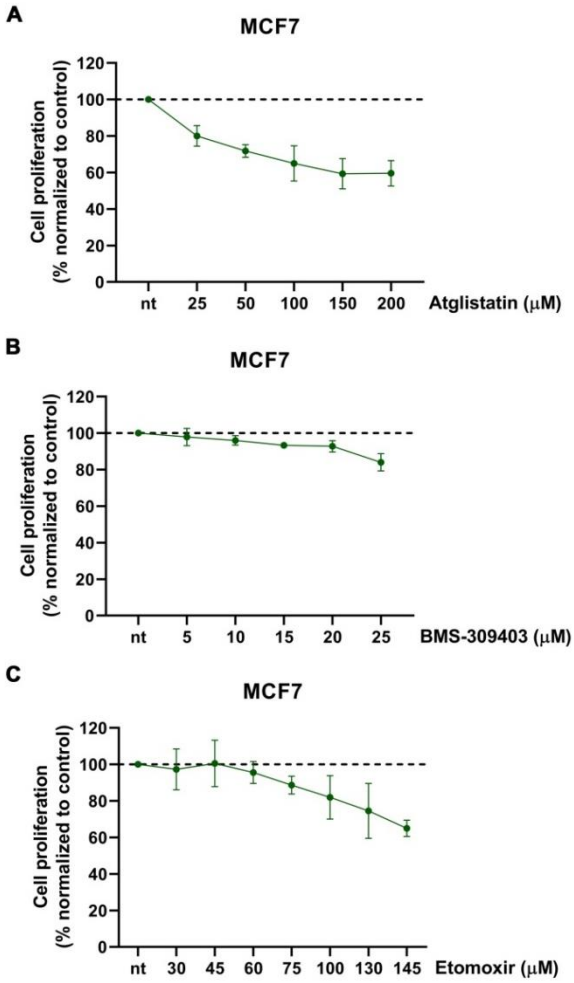

Figure R32. Impact of lipid metabolism inhibition on MCF7 cell proliferation. MCF7 cells were treated with Atglistatin, BMS-309403, or Etomoxir at specific concentrations for 2 days. Proliferation was assessed using Crystal Violet staining. Control represents cell proliferation of untreated MCF7 cells; the average ± SEM of three independent experiments is shown.

The three inhibitors significantly decreased MCF7 cell migration under basal conditions **(Figure R33A)**. When MCF7 cells were pretreated with a fatty acid mix containing C15:0, C17:0, and

C16:0, the inhibitory effect of BMS was reversed **(Figure 33B)**, which was expected since the cells had stored lipids and did not rely on the medium. These inhibitors also effectively prevented the enhanced migration observed in the presence of 3T3-L1 adipocytes **(Figure R33C)**.

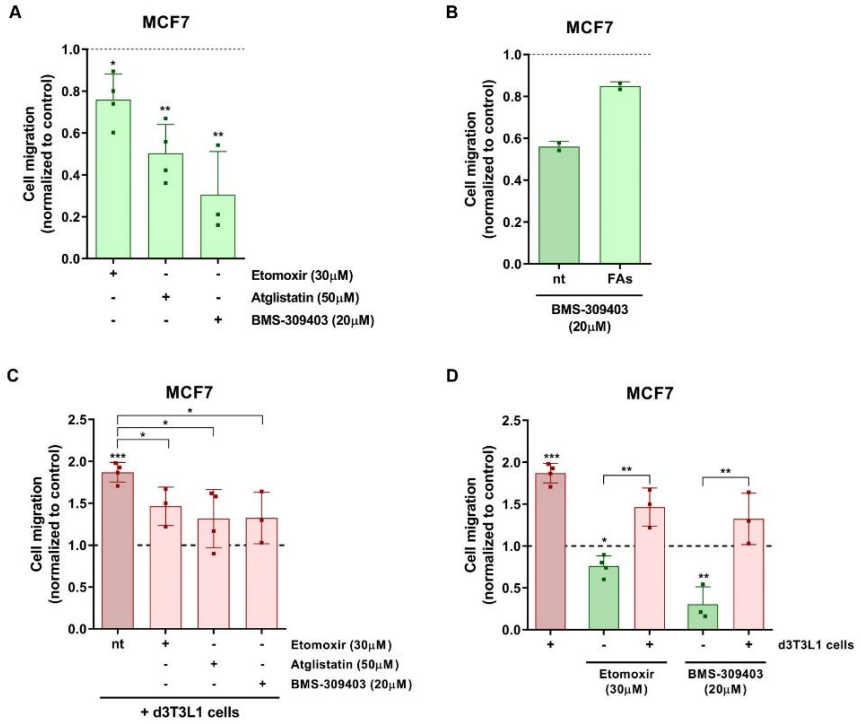

Figure R33. Inhibitors of fatty acid metabolism decrease MCF7 cell migration. MCF7 cell migration was measured **(A)** in the absence or **(C)** in the presence of 3T3-L1 adipocytes, without treatment (nt) or together with treatment with Atglistatin (50 µM), Etomoxir (30 µM), or BMS (20 µM). MCF7 cells were treated with the lipid mix (C15:0, C17:0, C16:0, all 50 µM) for 48 h. **(B)** MCF7 cell migration was measured in the absence or in the presence of BMS (20 µM). **(D)** Replot of the data presented in (A and C). Controls represent the migration of untreated MCF7 cells in the absence of 3T3-L1 adipocytes or any treatment; the average ± SEM of at least two independent experiments is shown. *, $p < 0.05$; **, $p < 0.01$; ***, $p < 0.001$.

It is important to remark than even in the presence of BMS or Etomoxir, co-culture with 3T3-L1 adipocytes increased MCF7 migration, indicating that part of the stimulation is independent on FABPs-mediated transport or FAO **(Figure 33D)**.

2.6. Adipocytes promote metabolic changes in MCF7 cells

We used Seahorse analysis to investigate changes in MCF7 cell metabolism in the presence of adipocytes. MCF7 cells were subjected to the Mito Stress Test after co-culture with adipocyte CM. This test measures the oxygen consumption rate (OCR) of cells in the presence of specific respiratory modulators. Seahorse analysis revealed no significant differences in the basal, ATP-linked, or maximal respiration of co-cultured MCF7 tumor cells compared with controls **(Figure R34A, R34B, and R34C)**.

Additionally, the Seahorse Cell Mito Stress Test allows for assessment of the extracellular acidification rate (ECAR) by detecting proton efflux. Specifically, it measures bulk acidification, including glycolysis and/or the TCA cycle (via CO_2). Seahorse analysis revealed significant differences in the ECAR of the co-cultured MCF7 cells **(Figure R34D)**.

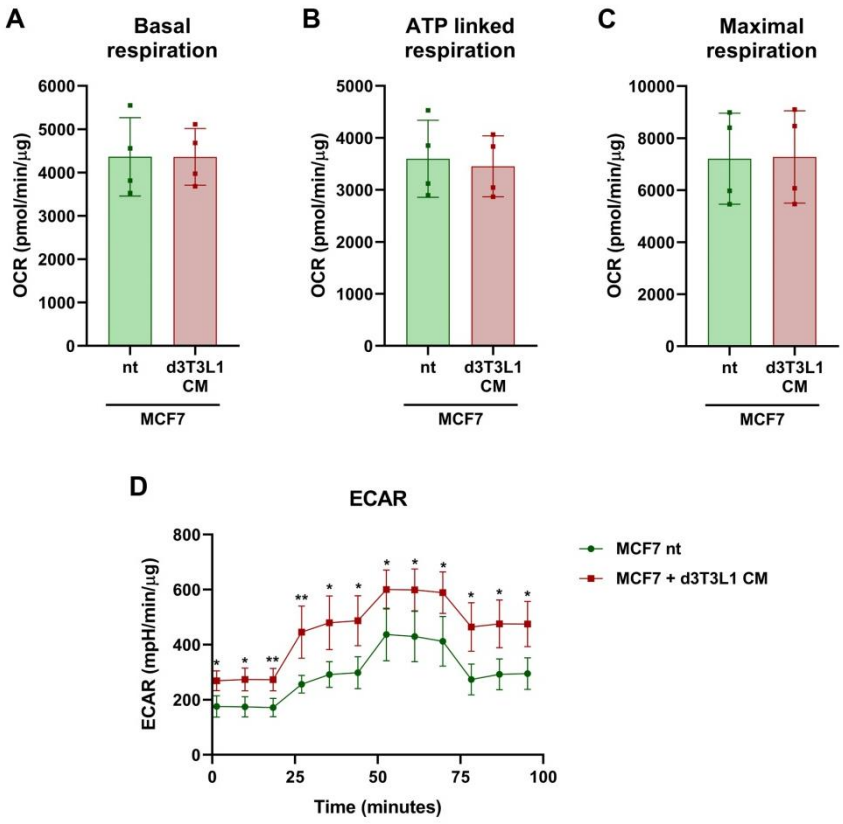

Figure R34. Adipocyte CM does not alter MCF7 cell ETC function, but increases ECAR. MCF7 cells were indirectly co-cultured with adipocytes (CM) for 3 days. Seahorse analysis was performed to assess mitochondrial function, specifically measuring **(A)** basal respiration, **(B)** ATP-linked respiration, **(C)** maximal respiration, and **(D)** extracellular acidification rate (ECAR). Data was normalized to protein concentration; the average ± SEM of at least three independent experiments is shown. *, $p < 0.05$; **, $p < 0.01$.

ECAR does not directly measure the glycolytic rate but serves as an indicator, prompting further investigation into the differences in glucose consumption by tumor cells.

Therefore, we determined the glucose concentration in the supernatants of MCF7 cells co-cultured directly and indirectly with adipocytes, normalizing the data by cell number. MCF7 cells cultured with adipocyte CM showed increased glucose consumption compared to controls **(Figure R35, left)**. Furthermore, direct co-culture with adipocytes led to higher glucose consumption by MCF7 cells compared to the controls **(Figure R35, right)**.

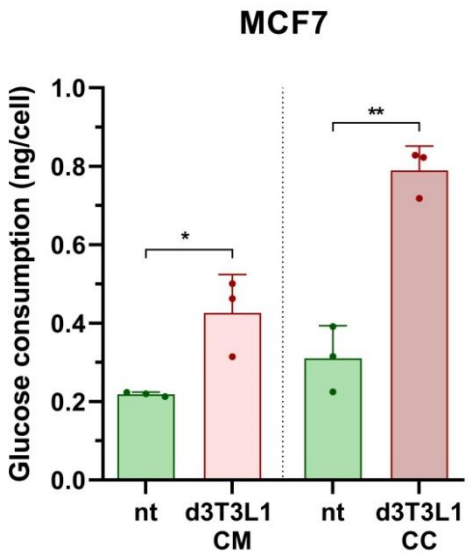

Figure R35. Co-cultured MCF7 cells increase glucose consumption. MCF7 cells were indirectly (CM) or directly (CC) co-cultured with adipocytes for 3 days. Medium supernatants were obtained, followed by glucose determination and cell counting. The average ± SEM of three independent experiments is shown. *, $p < 0.05$; **, $p < 0.01$.

Reactive oxygen species (ROS) are involved in various cellular processes, including proliferation, survival, and metastasis, and their levels are often elevated in cancer cells (Wu et al., 2024). To explore the impact of adipocytes on ROS production in MCF7 cells, we measured ROS levels in MCF7 cells indirectly co-cultured with adipocytes for three days. The co-cultured MCF7 cells exhibited a threefold increase in ROS production compared with the control cells **(Figure R36)**.

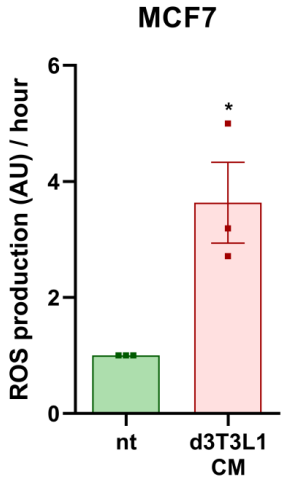

Figure R36. Co-cultured MCF7 cells increase their ROS production. MCF7 cells were indirectly co-cultured with adipocytes (CM) for 3 days. ROS production was measured, followed by cell counting. Data is expressed as fluorescence/cell arbitrary units (AU) per hour; the average ± SEM of three independent experiments is shown. *, $p < 0.05$.

2.7. Gene expression alterations in MCF7 activated by adipocytes

To gain a deeper understanding of the transcriptomic changes in breast tumor cells in the presence of adipocytes, we performed an extensive mRNA analysis of MCF7 cells directly co-cultured with 3T3-L1 adipocytes for 3 days.

We first examined the differential gene expression between co-cultured MCF7 cells and non-co-cultured control cells. **Figure R38** highlights the ten most significantly upregulated and downregulated genes in the co-cultured MCF7 cells.

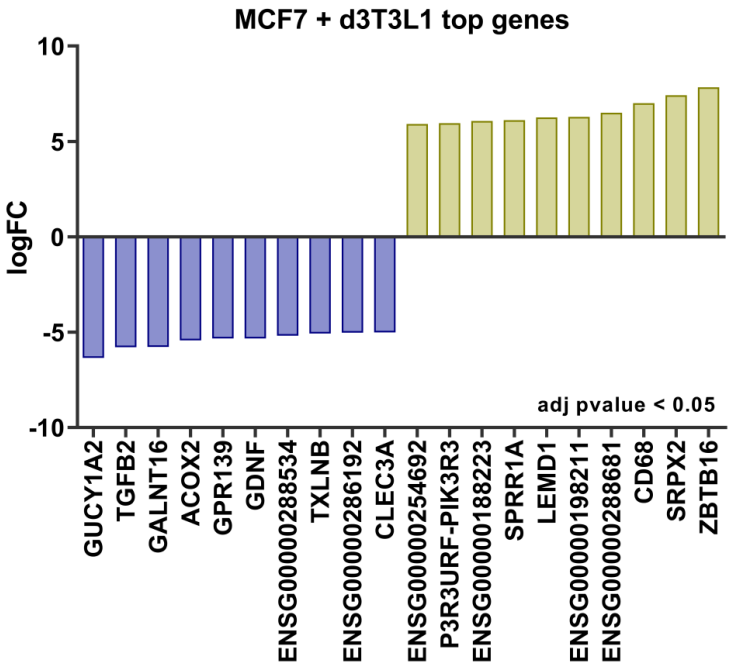

Figure R37. Co-cultured MCF7 cells most modified genes. MCF7 cells were directly co-cultured with 3T3-L1 adipocytes for 3 days. Total RNA was collected, and mRNA sequencing was performed, followed by bioinformatics analysis. The most significantly modified genes were selected based on an adjusted p-value < 0.05.

Next, we validated the expression of selected genes in independent samples, specifically CD68, MYC, and GADD45 using RT-qPCR. As in the RNA-seq analysis, both CD68 and GADD45 were significantly upregulated in co-cultured adipocytes, whereas MYC was downregulated **(Figure R38)**.

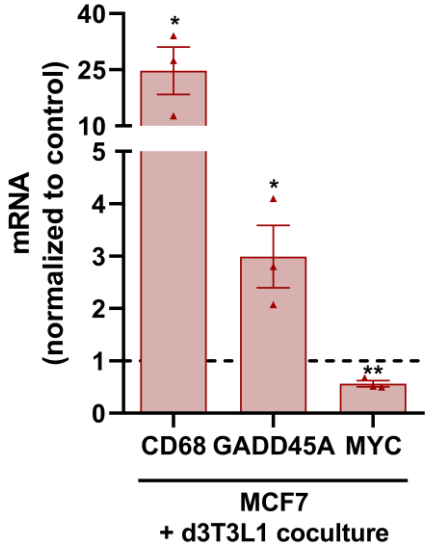

Figure R38. Gene validation using RT-qPCR. MCF7 cells were directly co-cultured with 3T3-L1 adipocytes for 3 days. Total RNA was collected, and RT-qPCR was performed. Control corresponds to non-co-cultured MCF7 cells; the average ± SEM of three independent experiments is shown. *, $p < 0.05$; **, $p < 0.01$.

Gene Set Enrichment Analysis (GSEA) pathway enrichment analysis was performed to investigate the molecular processes altered during MCF7 co-culture with adipocytes. Gene Ontology analysis revealed upregulate in biological processes (GOBPs) related to glycolytic processes **(Figure R39)**.

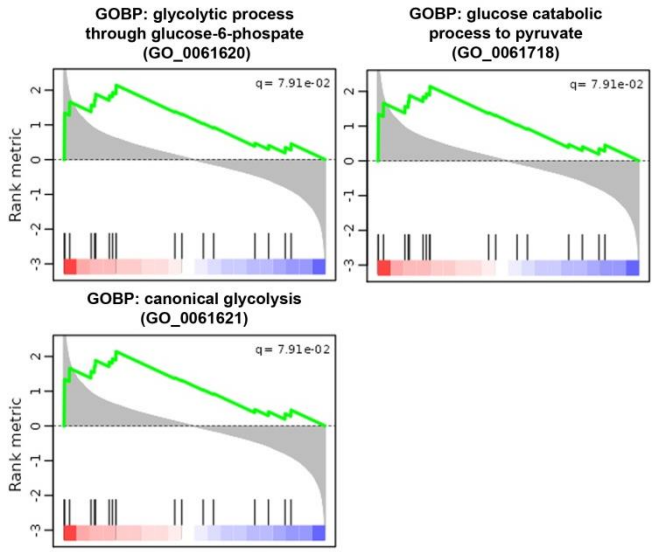

Figure R39. Co-cultured MCF7 cells increase glycolytic-related processes. MCF7 cells were directly co-cultured with 3T3-L1 adipocytes for 3 days. Total RNA was collected, and mRNA sequencing was performed, followed by bioinformatics analysis. GSEA of the top modified GOBPs with an FDR < 0.2.

Moreover, GSEA revealed an upregulation of hallmarks associated with Hypoxia, Apoptosis, Epithelial to Mesenchymal Transition and Cholesterol Homeostasis, together with downregulation of MYC Target hallmarks **(Figure R40)**.

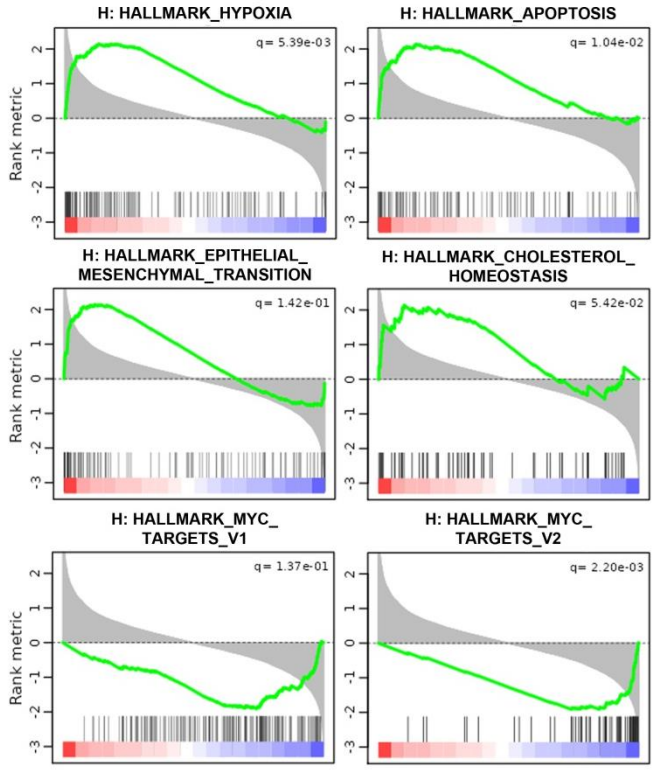

Figure R40. Co-cultured MCF7 cells show increased hypoxia, apoptosis, EMT and cholesterol homeostasis hallmarks, while MYC targets are decreased. MCF7 cells were directly co-cultured with 3T3-L1 adipocytes for 3 days. Total RNA was collected, and mRNA sequencing was performed, followed by subsequent bioinformatics analysis. GSEA of the top modified hallmarks with an FDR < 0.2.

Snail1 is a protein critically involved in inducing EMT *(see Introduction).* Therefore, we analyzed its levels in our cells. Direct co-culture of tumor cells with 3T3-L1 adipocytes led to an increase in Snail1 protein levels in breast cancer cell lines **(Figure R41A)** with minimal changes in other epithelial and mesenchymal markers. At mRNA level, MCF7 cells showed increased Snai1 expression **(Figure R41B)**.

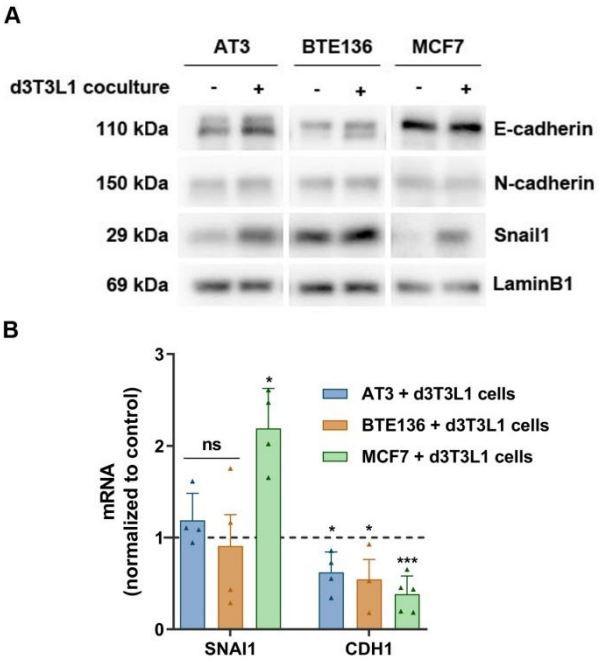

Figure R41. 3T3-L1 adipocytes increase Snail1 protein levels in breast cancer cells. Breast tumor cell lines were directly co-cultured with 3T3-L1 adipocytes for 3 days. Indicated markers were determined **(A)** at protein level using Western blot, or **(B)** at mRNA level using RT-qPCR. In **B**, control corresponds to non-co-cultured tumor cells; the average ± SEM of at least three independent experiments is shown. ns, not significant; *, $p < 0.05$; ***, $p < 0.001$.

The increase in Snail1 protein in MCF7 cells was not rapid and was detected between 48-72 hours **(Figure R42)**.

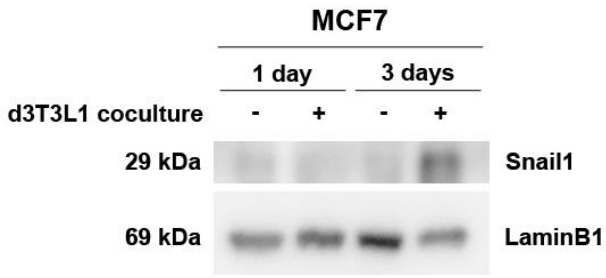

Figure R42. 3T3-L1 adipocytes increase Snail1 protein levels after 24 hours. MCF7 cells were directly co-cultured with 3T3-L1 adipocytes for 3 days. Protein levels of the indicated markers were determined by Western blot analysis.

Tumor cells directly co-cultured with primary adipocytes also showed increased Snail1 protein **(Figure R43A)** and mRNA in MCF7 cells **(Figure R43B)**.

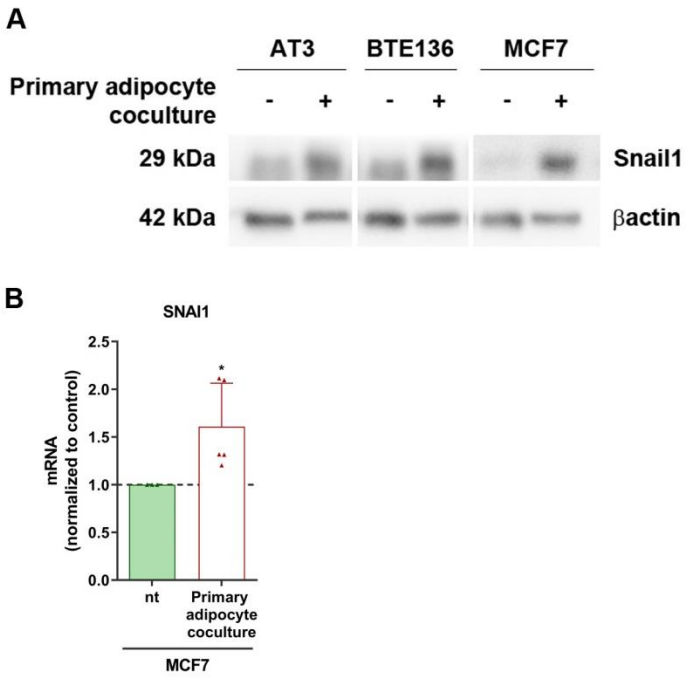

Figure R43. Primary adipocytes increase Snail1 protein levels in breast cancer cells. Breast tumor cell lines were directly co-cultured with primary adipocytes for 3 days. Indicated markers were determined **(A)** at protein level using Western blot, or **(B)** at mRNA level using RT-qPCR. In **B**, the control corresponds to non-co-cultured MCF7 cells; the average ± SEM of five independent experiments is shown. *, $p < 0.05$.

Moreover, epithelial tumor cells (AT3 and MCF7) cultured with 3T3-L1 adipocyte CM exhibited increased Snail1 protein **(Figure R44A)** and mRNA **(Figure R44B)**. Indirect co-culture also increased the mRNA levels of CD68 and GADD45 in MCF7 cells **(Figure R44B)**.

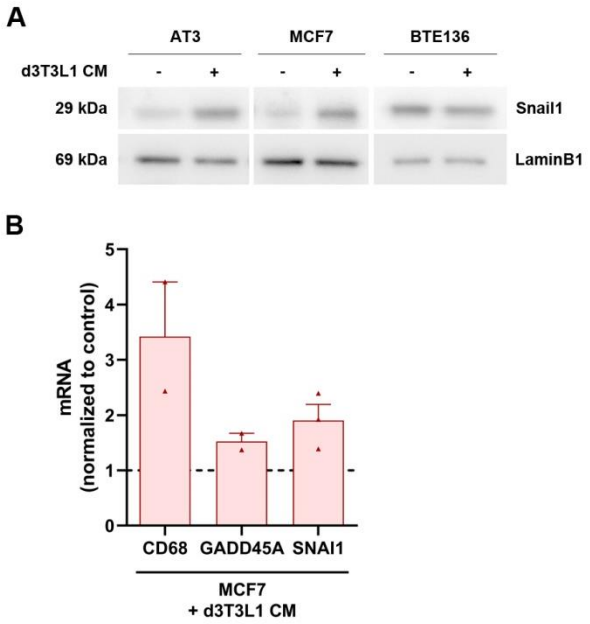

Figure R44. Co-culture with 3T3-L1 adipocyte CM increases Snail1 protein levels in epithelial-like breast cancer cells. Breast tumor cell lines were directly co-cultured with 3T3-L1 adipocyte CM for 3 days. Indicated markers were determined **(A)** at protein level using Western blot, or **(B)** at mRNA level using RT-qPCR. In **B**, the control corresponds to non-co-cultured MCF7 cells; the average ± SEM of two independent experiments is shown.

The upregulation of Snail1 in tumor cells by direct co-culture with 3T3-L1 adipocytes was partially reversed by Etomoxir **(Figure R45A)** and NAC **(Figure R45B)**, suggesting that this is partly a consequence of the elevated ROS caused by the increased FA metabolism of MCF7 cells incubated with adipocytes.

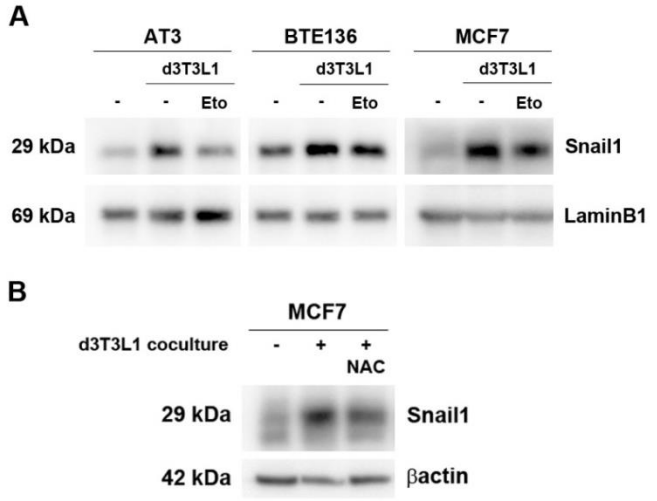

Figure R45. Etomoxir and NAC reverse the Snail1 increase in breast cancer cells. Breast tumor cell lines were directly co-cultured with 3T3-L1 adipocytes for 3 days and treated with Etomoxir (Eto, 30 µM) or NAC (1 mM). Protein levels of the indicated markers were determined by Western blot analysis.

Next, we aimed to elucidate the pathways involved in these changes. The JAK–STAT3 signaling pathway plays a pivotal role in cancer development within tumor cells (Yu et al., 2014). IL-6 has been shown to induce the EMT phenotype in breast cancer cells through activation of the STAT3 pathway (Gyamfi et al., 2018). Upon direct co-culture with adipocytes, MCF7 cells activated the STAT3 pathway, as evidenced by the increased phosphorylation of STAT3 **(Figure R46)**. Snail1 was also increased by these cytokines as observed earlier.

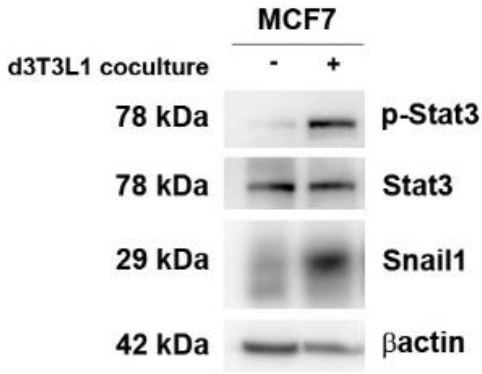

Figure R46. Co-cultured MCF7 cells increase Stat3 pathway activation. Protein levels of the indicated markers were determined by Western blot analysis in MCF7 cells directly co-cultured with adipocytes for 3 days.

DISCUSSION

Adipocytes play a crucial role in the tumor microenvironment of breast, ovarian, and prostate cancers. Adipocytes close to the tumor are referred to as cancer-associated adipocytes (CAAs), and engage in bidirectional crosstalk with neighboring cancer cells. This interaction appears to support tumor progression in breast cancer, which was the focus of my research. My thesis has investigated the molecular mechanisms underlying the transformation of adipocytes into CAAs and their subsequent effects on tumor cells.

1. ADIPOCYTES ARE ACTIVATED IN RESPONSE TO TUMOR CELLS

Histological examination of PyMT tumors reveal a reduction in the size of adipocytes at the invasive edge of the tumor. Previous studies (Dirat et al., 2011; Laurent et al., 2019; Nieman et al., 2013; Zhang et al., 2018; Zhu et al., 2022) have indicated that this reduction in size is also linked to a decrease in the number of adipocytes. However, due to their small size in sections close to the tumor, we were unable to measure the adipocyte area or accurately quantify them. Interestingly, the reduction in size of adipocytes has also been documented in cachexia, a pathology commonly associated to many neoplasms (Han et al., 2018; Hu et al., 2019).

We successfully developed an adipocyte model that closely resembled mature white adipocytes to investigate the crosstalk between adipocytes and breast tumor cells *in vitro*. We established two co-culture systems to study adipocyte activation by breast tumor cells, using tumor cells with distinct phenotypes to determine if adipocyte activation varied accordingly. Our findings indicate that breast tumor cells promote lipid loss in directly co-cultured

adipocytes in a time-dependent manner, regardless of phenotype **(Figure R5 and R6)**. This observation aligns with the discoveries of Bochet et al. (2013) and Dirat et al. (2011). Similar mechanisms have been described in other cancer types such as ovarian cancer (Nieman et al., 2011), pancreatic cancer (Cai et al., 2023), prostate cancer (Laurent et al., 2019), and melanoma (Zhang et al., 2018).

Adriá-Cebrián et al. (2021) reported that conditioned media (CM) from different breast cancer cell lines, including MCF7 cells, induced lipid loss in adipocytes. Similarly, Wang et al. (2017) described that CM from ZR-75-1 and SUM159PT breast cancer cell lines promoted lipolysis in adipocytes. However, in our model, direct crosstalk between the two cell populations seemed necessary for adipocyte activation, as indirect co-culture promoted minimal or no lipid loss **(Figure R6)**. This discrepancy may be attributed to the glucose concentration in the conditioned medium. It is possible that ZR-75-1 and SUM159PT cells have higher proliferative rates than MCF7 cells, potentially altering the glucose concentrations in the CM and explaining the observed lipid loss described by others since we reported that glucose deprivation promotes adipocyte dedifferentiation. We also observed adipocyte lipid loss when directly co-cultured with fibroblasts, suggesting that components of the TME other than tumor cells, can promote adipocyte activation.

The observed lipid loss likely originates from lipids stored in lipid droplets through lipolysis. Our findings indicated that the significant lipid loss observed in direct co-culture of adipocytes with MCF7 cells was not entirely attributable to ATGL activity **(Figure R8)**. This implies that lipid transport mechanisms other than lipolysis also play a relevant role. In this context, Clement et al. (2020) described

that adipocytes release extracellular vesicles (EVs) containing fatty acids independently of lipolytic stimuli, which are then taken up by melanoma cells. Recently, an alternative mechanism known as lipophagy has been identified for releasing stored lipids in LDs. Lipophagy involves the degradation of LDs via autophagy through the lysosomal pathway (Cruz et al., 2020; Zhang et al., 2022). Inhibition of autophagy blocks lipid accumulation and differentiation in 3T3-L1 cells (Liu and Czaja, 2012). Therefore, we suggest that activated adipocytes in co-culture lose lipids from LDs through both lipolysis and alternative mechanisms such as lipophagy or release of lipid-loaded vesicles.

However, our results were based on the use of Atgilstatin. Atglistatin inhibits TG hydrolase activity by 78% in mouse white adipose tissue, suggesting that other TG hydrolases, such as HSL, are also involved in lipolysis (Mayer et al., 2013).

Adipocyte dedifferentiation is also characterized by the loss of adipocyte markers. Our findings indicate that both breast tumor cells and fibroblasts promote adipocyte dedifferentiation when directly co-cultured with adipocytes **(Figure R9-R11)**. This effect was absent in the indirect co-culture, reinforcing the necessity of direct crosstalk between cell populations for adipocyte activation. Downregulation of key adipogenic factors and repression of lipogenic factors in adipocytes have been observed in cachectic mice (Bing et al., 2006). Dirat et al. (2011) reported a loss of several adipocyte markers in adipocytes directly co-cultured with breast tumor cells. However, this effect has not been studied using conditioned media from tumor cells. Direct co-culture allows the two populations to be in close proximity, facilitating full activation, likely through the constant signaling of molecules secreted by both

cell types. Additionally, this proximity ensures that stimulated cells secrete other molecules that would not be produced if they were unstimulated.

Total mRNA sequencing analysis indicated that co-cultured adipocytes halt fatty acid-related processes, including catabolism and synthesis, ceasing to function as adipocytes, as evidenced by the downregulation of adipogenesis. Other authors (Cai et al., 2023) performed RNA-seq analysis of adipocytes co-cultured with pancreatic cancer cells and described a marked increase in gene sets corresponding to the insulin signaling and JAK-STAT3 pathways, along with suppression of adipogenesis and fatty acid catabolic and anabolic processes, in close parallel with our results. Additionally, other pathways stimulated in our cells, such as c-Myc, are periodically expressed during the early phase of adipogenesis (Deisenroth et al., 2014). Constitutive overexpression of c-Myc inhibits the differentiation of 3T3-L1 cells (Kami et al., 2016). These findings, along with our data, suggest that activated adipocytes initiate transcription programs similar to those active during the early stages of differentiation.

Stat3 activation via the IL-6 signaling pathway can promote adipocyte lipolysis in the context of cachexia (Han et al., 2018; Hu et al., 2019). Moreover, STAT3 phosphorylation was increased in co-culture with pancreatic cancer cells (Cai et al., 2023). Hence, we investigated whether adipocyte activation could be promoted by Stat3 activation. IL-6 (interleukin-6) and LIF (leukemia inhibitory factor) are potent activators of Stat3 via the IL-6 receptor (IL-6R) and LIF receptor (LIFR), respectively (Jones and Jenkins, 2018). Other cytokines, such as PDGFβ and TGFβ, also promote activation of the JAK/STAT3 signaling pathway (Tzavlaki and

Moustakas, 2020; Zou et al., 2022). Independently of STAT signaling, it has been described that TNFα is a potent stimulator of lipolysis in adipocytes (Chen et al., 2009). Moreover, TNF-α inhibits adipogenesis in 3T3L1 by preventing the induction of PPARγ and C/EBPα expression (Cawthorn and Sethi, 2007). However, in our cell system, and despite Stat3 activation, none of the tested cytokines or growth factors, alone or in combination, significantly reduced lipid content. This reinforces the need for direct contact between adipocytes and tumor cells.

Further characterization of our activated adipocytes revealed a decrease in the expression of mature adipocytes and adipogenic master regulators, along with an increase in the expression of mesenchymal stem cell or adipocyte progenitor genes and macrophage- and fibroblast-like genes. Zhu et al. (2022) proposed that in the presence of breast tumor cells, adipocytes undergo an adipocyte-to-mesenchymal transition (AMT). This transition is characterized by the loss of adipocyte identity and acquisition of features typical of other cell types, including myofibroblasts and macrophages. Similarly, Bochet et al. (2013) described that breast cancer cells induce mature adipocytes to become fibroblast-like cells, referred to as adipocyte-derived fibroblasts (ADFs). Additionally, Charrière et al. (2003) demonstrated that the 3T3-L1 preadipocyte cell line could be converted into a functional macrophage-like cell type when injected into the peritoneal cavity of mice. These findings support our hypothesis that activated adipocytes undergo dedifferentiation and initiate transcription programs similar to those in the early stages of differentiation, eventually acquiring new cellular identities. Adipocyte dedifferentiation remains a largely unexplored research area.

Currently, and besides the cytokines mentioned above, only Wnt3a has been documented to induce the dedifferentiation of mature adipocytes (Bochet et al., 2013; Gustafson and Smith, 2010). Therefore, there is a critical need to identify molecules that can effectively promote full adipocyte activation.

Although dedifferentiated 3T3-L1 cells consume less glucose, we considered that the competition between differentiated adipocytes and MCF7 might be relevant for the process of activation. Glucose deprivation led to a reduction in lipid content, which was not prevented by Atglistatin, and promoted adipocyte dedifferentiation **(Figure R20-R21)**. Our findings suggest that glucose is essential for the maintenance of adipocyte identity and the expression of adipocyte markers. Lipid loss caused by glucose depletion was partially prevented by D-mannose treatment. Inhibition of the hexosamine or pentose phosphate pathways does not trigger adipocyte activation, indicating that, under high glucose conditions, glucose is not predominantly utilized in these biosynthetic pathways. Instead, glucose is most likely to be used as a substrate for lipid synthesis.

However, glucose deprivation alone does not directly activate adipocytes, as evidenced by lipid loss, despite daily glucose supplementation in the co-cultures. We hypothesized that under normal conditions with abundant glucose, adipocytes use glucose for lipid synthesis. Increasing glucose levels in the co-culture does not inhibit adipocyte activation, as dedifferentiated adipocytes do not require as much glucose. Instead, they undergo dedifferentiation into fibroblasts or other cell types with different metabolic demands and lower glucose requirements.

This may also explain why tumor cell CM induces a slight lipid loss in adipocytes but does not necessarily lead to adipocyte dedifferentiation. CM may contain low levels of glucose, which promotes lipid loss but is insufficient to induce full dedifferentiation of adipocytes.

In conclusion, although glucose deprivation mimics some aspects of direct co-culture with tumor cells, it does not fully replicate the conditions, as adipocyte activation appears to occur independently of glucose supplementation.

2. ADIPOCYTES PROMOTE BREAST TUMOR CELLS MIGRATION AND INVASION

Our results also reproduce results from other researchers because adipocytes promote tumor cell migration and invasion both *in vitro* and *in vivo* in breast (Dirat et al., 2011; Wang et al., 2017), ovarian (Nieman et al., 2011), pancreatic (Cai et al., 2023), and prostate cancers (Laurent et al., 2019).

Our results showed that adipocytes enhance breast tumor cell migration and invasion without significantly affecting their proliferation. Similarly, Dirat et al. (2011) and Wang et al. (2017) observed no significant increase in tumor cell proliferation when co-cultured with adipocytes. Of the four breast tumor cell lines studied by Dirat et al. (2011), only SUM159PT showed increased cell proliferation upon co-culture with adipocytes, suggesting that adipocytes only promote proliferation in specific cell lines.

Both Dirat et al. (2011) and our findings showed that adipocytes stimulate tumor cell migration, whereas preadipocytes do not. Our

findings indicate that adipocytes promote greater migration than adipocyte CM. Similarly, Nieman et al. (2011) reported that in ovarian cancer, adipocyte CM enhanced tumor cell migration and invasion to a lesser degree than direct adipocyte exposure.

However, it is important to note that our experimental methodology differs from those of some of the studies cited above (Cai et al., 2023; Dirat et al., 2011; Laurent et al., 2019; Wang et al., 2017). According to these authors, tumor cells are typically pre-co-cultured with adipocytes (directly or indirectly), trypsinized, and then assessed for migration or invasion. In our experiments, tumor cells were assessed by migration or invasion assays with either adipocytes or adipocyte CM in the lower chamber, following a methodology similar to that of Nieman et al. (2011), and with a more physiological setting. Additionally, proliferation experiments were conducted using the adipocyte CM. Whether tumor cells proliferate differently in direct co-culture with adipocytes should be investigated.

Wang et al. (2017) in breast tumor cells and Nieman et al. (2011) in ovarian tumor cells have both reported that cancer cells accumulate lipids in the presence of adipocytes. Similarly, MCF7 cells exhibited higher lipid content with adipocyte CM and primary adipocyte culture, but not when directly co-cultured with 3T3-L1 adipocytes. MCF7 cells co-cultured directly with 3T3-L1 adipocytes were placed in a transwell, whereas those treated with adipocyte CM or co-cultured with primary adipocytes were placed in a well. Directly co-cultured MCF7 cells exhibited migratory behavior, unlike MCF7 cells under other conditions. The reduction in lipid content observed in directly co-cultured MCF7 cells may be attributed to the utilization of lipids during migration.

However, lipid accumulation alone is insufficient to promote cell migration. MCF7 cells can accumulate palmitic acid when this FA is added to the medium; however, this pretreatment does not promote migration. Exogenous palmitic acid has been described to promote tumor migration *in vitro* in prostate cancer (Laurent et al., 2019); however, we did not observe this effect in our breast cancer cell line. Our migration assays were performed at high glucose concentrations (4.5 g/L) and with an FBS gradient. Under these conditions, MCF7 cells likely obtain enough lipids from their own synthesis and from the culture media, and do not need an additional source.

Although lipid accumulation itself does not promote migration of MCF7 cells, lipid metabolism is essential for this process. Inhibition of fatty acid oxidation (FAO), or FABP-mediated transport reduces migration, both under basal conditions and in the presence of adipocytes. Wang et al. (2017) noted that Etomoxir has no effect under basal conditions but decreases migration in breast cancer cells co-cultured with adipocytes. However, other studies have shown that Etomoxir has no effect on adipocyte-induced migration of prostate cancer cells (Laurent et al., 2017). It is possible that lipids may be utilized for purposes other than energy production, such as incorporation into cell membranes to modify fluidity and enhance migration. Nevertheless, adipocytes may promote migration independent of lipids, potentially through the release of cytokines and chemokines.

Adipocyte CM promotes changes in MCF7 metabolism. Although it does not alter MCF7 cell electron transport chain function, it enhances its glycolytic capabilities, as evidenced by increased glucose consumption in MCF7 co-cultured with adipocytes. To

better assess the glycolytic capacity of MCF7 cells, we could measure the production of lactate in the supernatants.

Laurent et al. (2021) described that prostate cancer cells co-cultured with adipocytes showed increased production of Reactive Oxygen Species (ROS). Similarly, culturing MCF7 cells with adipocyte CM increased ROS production. This mimics the effect of Snail1 expression; in fact, similar to Snail1, the elimination of ROS decreases migration (Pastor et al., unpublished observations).

Total mRNA sequencing analysis indicated that co-cultured MCF7 cells upregulated GOBPs related to glycolytic processes and hallmarks associated with Hypoxia, Apoptosis, Epithelial to Mesenchymal Transition and Cholesterol Homeostasis, and downregulated MYC Target hallmarks. Similarly, Cai et al. (2023) used mass spectrometry and bioinformatics analysis to show that co-cultured pancreatic cells increase the overrepresentation of hallmark pathways involved in hypoxic signaling, glycolysis, fatty acid metabolism, EMT, and cholesterol homeostasis.

c-MYC contributes to tumor progression by promoting cell proliferation, ribosomal biosynthesis, glycolysis, mitochondrial function, and differentiation (Okuyama et al., 2010). Therefore, c-Myc is known to be overexpressed in many cancers. Okuyama et al. (2010) showed that tumor cells under hypoxic and glucose-deprived conditions have reduced c-MYC protein levels. We described that directly and indirectly co-cultured MCF7 cells had decreased c-Myc mRNA levels. Since c-Myc promotes apoptosis (Meyer and Penn, 2008), we hypothesized that downregulation of the Myc pathway in co-cultured tumor cells could be a mechanism for survival under stress conditions.

Dirat et al. (2011) reported that breast cancer cells co-cultured with adipocytes exhibit decreased E-cadherin expression without a concurrent increase in mesenchymal markers expression. Similarly, Wang et al. (2017) found that breast cancer cells co-cultured with adipocytes showed reduced E-cadherin expression and increased Snail1 protein levels. Other studies have also shown that adipocytes can promote the expression of mesenchymal markers in breast cancer cells (Gyamfi et al., 2018). Our RNA-seq data indicate an increase in the EMT hallmark, although our *in vitro* experiments suggest that this transition is partial.

We observed elevated Snail1 protein levels in breast cancer cells co-cultured directly with both 3T3L1 adipocytes and primary adipocytes as well as in cells cultured with adipocyte CM. This increase in Snail1 protein was also reflected in the increase in Snai1 mRNA levels in MCF7 cells. While there was a decrease in E-cadherin mRNA levels in MCF7 cells, E-cadherin protein levels remained unchanged. Notably, Snail1 protein levels were not significantly altered in co-cultured BTE136 cells, as the basal levels of Snail1 were already high in these cells. These findings suggest the occurrence of an incomplete epithelial-mesenchymal transition that increases breast cancer cell migration and invasion capabilities.

Moreover, Snail1 might regulate cellular metabolism. Yang et al. (2020) described that Snail augments FAO by suppressing the acetyl-coA carboxylase beta (ACC2) enzyme. It has also been reported that Snail regulates glycolytic activity by switching glucose flux to PPP (Kim et al., 2017; J.H Yang et al., 2020). Snail1 upregulation in co-cultured breast cancer cells was abrogated by Etomoxir and the antioxidant N-acetylcysteine (NAC). Similarly,

Wang et al. (2017) reported that Etomoxir reduced Snail1 protein levels in co-cultured breast cancer cells. These findings suggest that FAO is partially responsible for this EMT phenotype, as Etomoxir also inhibited MCF7 cell migration under both basal conditions and in the presence of adipocytes. Furthermore, the effect of NAC on co-cultured MCF7 cells could be explained by FAO, that produces high levels of ROS, which could also contribute to this EMT phenotype. Accordingly, Laurent et al. (2017) described that migration of prostate cancer cells in the presence of adipocytes can be reversed by NAC treatment. Therefore, an increase in ROS production in tumor cells as a consequence of FAO could promote a partial EMT.

STAT3 phosphorylation is increased in pancreatic cancer cells co-cultured with adipocytes (Cai et al., 2023). Leptin secreted by adipocytes can induce the EMT phenotype in endometrial cancer cells through the activation of the STAT3 pathway (Shen et al., 2023). Moreover, IL-6 has been shown to induce the EMT phenotype in breast cancer cells through activation of the STAT3 pathway (Gyamfi et al., 2018) and STAT3 pathway is tightly linked to lipid metabolism since it promotes FAO in breast cancer stem cells (Wang et al., 2018). It needs to be investigated if these factors are also relevant in our cellular system.

3. SUMMARY

Based on the data discussed above, we propose an *in vitro* model to illustrate the crosstalk between adipocytes and the surrounding tumor cells, which drives tumor progression. This model is depicted in **Figure D1**.

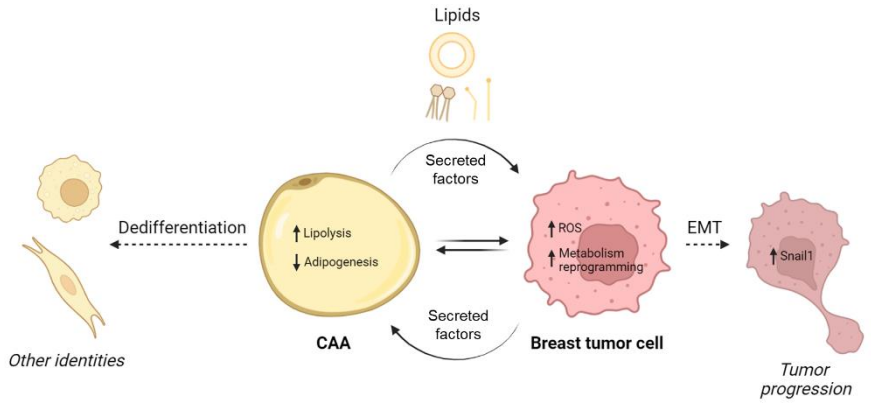

Figure D1. Simplified model of crosstalk between adipocytes and breast tumor cells. Adipocytes and the surrounding breast tumor cells mutually stimulate each other, resulting in adipocyte activation and enhanced tumor progression. Cancer-associated adipocytes (CAAs) increase lipid release and reduce adipogenesis, leading to dedifferentiation and acquisition of other identities. Consequently, tumor cells reprogram their metabolism and acquire migratory capabilities through epithelial-to-mesenchymal transition (EMT) via Snail1 upregulation.

In this model, the two cell populations mutually stimulate each other, resulting in significant changes that alter adipocyte identity and reprogram the metabolism of both cell types. Adipocytes become activated and transform into cancer-associated adipocytes (CAAs), which are characterized by lipid release and

downregulation of adipogenesis-associated processes such as lipid and glucose metabolism. Further dedifferentiation may lead CAAs to acquire additional phenotypes such as fibroblasts and macrophages. Lipolysis, among other mechanisms, facilitates the release of lipids from lipid droplets in the CAAs.

Tumor cells stimulated by adipocytes can incorporate these released lipids and reprogram their metabolic machinery to their own benefit. This is accompanied by increased glucose consumption and enhancement of the glycolytic pathway. Through this metabolic reprogramming, tumor cells acquire metastatic features via a partial EMT characterized by Snail1 upregulation, a process closely linked to lipid metabolism. Furthermore, altered tumor metabolism results in increased ROS production.

CONCLUSIONS

My general conclusion is that there is crosstalk between adipocytes and tumor cells in co-culture, inducing relevant changes in both cell types that are mutually amplified. More specifically:

1. Adipocytes lose lipids and dedifferentiate in response to breast tumor cells and fibroblasts.
2. Dedifferentiated adipocytes downregulate lipid metabolic processes and upregulate the expression of adipocyte progenitor, macrophage, and fibroblast marker genes.
3. Tumor-activated adipocytes increase Stat3 signaling pathway activity.
4. Glucose depletion promotes adipocyte dedifferentiation and lipid loss.
5. Adipocytes promote breast tumor cell migration and invasion without significantly affecting their proliferation.
6. Tumor cells accumulate lipids from adipocytes.
7. Exogenous lipid accumulation does not promote tumor cell migration; however, lipid uptake, lipolysis and lipid catabolism are required for cell migration.
8. Adipocytes induce metabolic changes in MCF7 cells, increasing glucose consumption and ROS production.
9. In the presence of adipocytes, MCF7 cells undergo a partial epithelial-to-mesenchymal transition characterized by Snail1 upregulation, which can be partially blocked by inhibitors of fatty acid oxidation and antioxidants.

MATERIALS & METHODS

1. CELL CULTURE

1.1. Cell lines

Cells were grown in Dulbecco's modified Eagle's medium (DMEM, Invitrogen) supplemented with 4.5 g/L of glucose, 100 U/ml penicillin, 100 μg/ml streptomycin, 2 mM glutamine, and 10% fetal bovine serum (FBS) (all from Gibco). All cell lines were maintained at 37°C in a humidified atmosphere with 5% CO_2 and periodically tested to verify that they remained mycoplasma-free.

The cell lines used in this thesis are listed in **Table M1**.

Cell line	Origin	Characteristics
3T3-L1	Mouse fibroblasts	Fibroblastic morphology
AT3	PyMT mouse tumors	Epithelial morphology
BTE136	PyMT mouse tumors	Mesenchymal morphology
CAFs	Cancer associated fibroblasts from PyMT mouse tumors	Fibroblastic morphology
L cells	Mouse fibroblasts	Fibroblastic morphology
MCF7	Human mammary adenocarcinoma	Epithelial morphology
NIH3T3	Mouse fibroblasts	Fibroblastic morphology

Table M1. Cell lines used and their morphology.

3T3-L1 cell line was provided by Dr. Antonio Zorzano, Institut d'Investigació Biomèdica de Barcelona (Barcelona, Spain). AT3 and BTE136 tumor cell lines were provided by Dr. Antoni Celià (Institut Hospital del Mar d'Investigacions Mèdiques, Barcelona, Spain) and Dr. M. Quintela (Centro Nacional de Investigaciones

Cardiovasculares, Madrid, Spain), respectively. Both AT3 and BTE136 cell lines were isolated from spontaneous luminal B breast tumors of MMTV-PyMT mice bearing a polyomavirus middle T oncogene that is expressed under the control of the mammary MMTV promoter (Mestre-Farrera et al., 2021). CAFs were previously established in our laboratory (Alba-Castellón et al., 2016). The L cells were obtained from the American Type Culture Collection (ATCC). The MCF7 and NIH3T3 cell lines were acquired from the repository stock of our center (IMIM Cell Bank).

Cells were maintained in a complete medium until required. For seeding, the medium was removed, cells were washed once with PBS, and detached with 0.5% trypsin (25300062, Gibco). Cells were re-seeded into the flask at a diluted concentration to maintain the stock. For the experiments, cells were counted using an optical microscope and a Neubauer chamber, and trypan blue was added to the resuspension mix to determine cell viability. The number of seeded cells was dependent on the experiment performed.

1.2. 3T3-L1 cell differentiation

3T3-L1 is a cell line derived from 3T3 cells obtained from Swiss mouse embryo tissue. The 3T3-L1 preadipocyte cell line differentiates under an appropriate hormonal media into mature white adipocytes (Green and Kehinde, 1975). These cells are morphologically similar to fibroblastic preadipose cells found in the stroma of adipose tissue; once differentiated, they exhibit characteristics associated with adipocytes present in the adipose tissue.

Prior to seeding, plates were coated with gelatin 1% to enhance cell attachment. Briefly, gelatin 1% (G1890, Sigma-Aldrich) was prepared in PBS and sterilized in an autoclave. Before seeding, 1% gelatin was added to the desired plates, which were incubated at 37°C for 30 min, and then washed twice with PBS. For adipocyte differentiation, 3T3-L1 cells were plated at a concentration of 2.5 x 10^5 cells per well in 6-well plates or 3 x 10^4 cells per well in 24-well plates, and cultured for one day. Differentiation was induced by the addition of DMEM (4.5 g/L glucose) supplemented with 10% FBS and 0.5 mM isobutyl-methyl-xanthine (I5879, Sigma-Aldrich), 0.2 µM dexamethasone (D4902, Sigma-Aldrich) and 10 µg/ml insulin (I1882, Sigma-Aldrich). The differentiation medium was added when cells reached confluence and replenished every three days for a period of 10-12 days.

1.3. Primary adipocytes isolation

As indicated below, all the animal procedures of the thesis were previously approved by the Animal Research Ethical Committee from the PRBB and by the Generalitat de Catalunya.

To obtain primary adipocytes, C57Bl/6J 30-week-old mice were sacrificed, and subcutaneous and visceral adipose tissues were removed and placed in HBSS. Adipose tissue was cut into pieces using a scalpel and digested with collagenase type I 2 mg/ml (9001-12-1, VWR International Eurolab) at 37°C for 1 h on a rocker. Cells were then filtered through a 100 µm-mesh (352360, Corning) and centrifuged for 10 min at 1200 rpm. After filtration, there was a thin white floating layer of adipocytes at the top. The adipocytes were taken, and centrifuged twice 10 min at 1200 rpm.

This protocol was adapted from the literature (Fernyhough et al., 2004; Ruan et al., 2003). After the last centrifugation, adipocytes were used for the indicated experiments in DMEM F12 supplemented with 10% FBS (12634-010, Gibco).

1.4. Cell treatments

The treatments used in this thesis are detailed in **Table M2**. For the low glucose conditions, cells were cultured in 1 g/L glucose Dulbecco's modified Eagle's medium (DMEM, 11054020 Gibco) supplemented with 100 U/ml penicillin, 100 μg/ml streptomycin, 2 mM glutamine, and 10% FBS (all from Gibco).

Treatment	Reference	Supplier	Conc
6-Aminonicotinamide	HY-W010342	MedChemExpress	1-2 μM
Atglistatin	SML1075	Sigma-Aldrich	50 μM
Azaserine	HY-B0919	MedChemExpress	10 μM
BMS-309403	HY-101903	MedChemExpress	20 μM
D-Mannose	M6020	Sigma-Aldrich	25 mM
Etomoxir	236020	Selleckchem	30 μM
Heptadecanoic acid	H3500	Sigma-Aldrich	50 - 100 μM
IL6 (mouse)	216-16	Peprotech	50 ng/ml
LIF	ESG1107	Millipore	1:250
N-acetyl-cysteine	A9165	Sigma-Aldrich	1 mM
Sodium palmitate	P9767	Sigma-Aldrich	50 - 100 μM
PDGFβ	100-14B	Peprotech	40 ng/ml
Pentadecanoic acid	W433400	Sigma-Aldrich	50 - 100 μM
TGFβ	100-21	Peprotech	20 ng/ml
TNFα	300-01A	Peprotech	20 ng/ml

Table M2. Cell culture treatments.

For very low glucose conditions, cells were cultured in Dulbecco's modified Eagle's medium (DMEM, A1443001 Gibco) supplemented with 0.1 g/L glucose, 100 U/ml penicillin, 100 µg/ml streptomycin, 2 mM glutamine, 110 mg/L sodium pyruvate, and 10% FBS (all from Gibco).

1.4.1. Fatty acid preparation

Fatty acid preparation for *in vitro* use involves the saponification of commercial fatty acid salts. Palmitic acid was prepared at a stock concentration of 2 mM and diluted as required for experimental use. Briefly, sodium palmitate was prepared at 2 mM by dissolving in 150 mM NaCl at 80°C until clear. The fatty acid solution was coupled with fatty acid-free bovine serum albumin (BSA; A8806, Sigma-Aldrich) at a molar ratio fatty acid/BSA of 5:1. Previously, 4% BSA was prepared in 150 mM NaCl at 37°C. The clear solution of palmitate was added dropwise to the BSA solution and left for 1 h at constant stirring at 37°C. The final stock solution was filtered through a 0.4 5µm filter (SLHP033RS, Millipore) and stored at -20°C. Before the experiments, palmitic acid was prewarmed for 1 h at constant stirring at 37°C.

Heptadecanoic acid and pentadecanoic acid were directly diluted in ethanol to prepare 5 mM stock solutions that were stored at 4°C.

1.5. Adipocyte-tumor cells coculture

1.5.1. Indirect coculture

Indirect co-cultures were performed by culturing tumor cells (AT3, BTE136, or MCF7 cells) with conditioned media of adipocytes, or culturing adipocytes with conditioned media of tumor cells (AT3, BTE136, or MCF7 cells).

Adipocyte-conditioned media was obtained from 3T3-L1 cell line (d3T3L1 CM). After 10-12 days of differentiation, the differentiation medium was removed, cells were washed once with PBS and medium was replaced with DMEM plus 1% FBS. d3T3L1 CM was recovered after 48 h and stored at -80°C until use.

Tumoral-conditioned media was obtained from AT3, BTE136, and MCF7 cell lines. Cells were cultured until they reached 80% confluence, and then medium was replaced with DMEM plus 1% FBS. Tumoral CM was recovered after 72 h and stored at -80°C until use.

1.5.2. Direct coculture

Direct co-cultures were performed by seeding 3T3-L1 cells in 6-well plates. After reaching confluence and differentiated for 10-12 days, direct co-culture was performed by using the Boyden chamber system. 7 x 10^5 tumor cells (AT3, BTE136, or MCF7 cells) or fibroblasts (L cells, CAFs, or NIH3T3) were seeded on top of 8 µm transwells (782746, BRAND) in DMEM plus 10% FBS for 3 days.

2. PROTEIN ANALYSIS

2.1. Protein extraction

Culture medium was removed from the culture plates or transwells, and cells were washed twice with cold PBS. Then, cells were scrapped with 2% SDS lysis buffer to solubilize all cellular components. Volume of lysis buffer depended on the cell type, confluence, and culture plate size. Cell lysates were boiled at 95ºC for 10 min and centrifuged at 16,000 x g for 5 min.

2.2. Protein quantification

2.2.1. Lowry assay

Protein concentration for Western Blot was determined using the Lowry method (5000111 DC Protein Assay kit, Bio-Rad). Briefly, samples were added to a 96-well plate together with 25 µl of a mix of Reagent A-Reagent S (20 µl of reagent S to each ml of reagent A). Simultaneously, a BSA (23209, Thermo Fisher) standard curve was established and mixed with 25 µl of the Reagent A-Reagent S mix. Next, 200 µl of reagent B was added to each well. After 15 min at room temperature (RT), the absorbance was quantified in an Infinite M200 microplate Reader (Tecan) at 750 nm.

2.2.2. BCA assay

Protein concentration from the Seahorse experiment was determined using the Pierce BCA protein assay (23225, Thermo Fisher). Previously, cells were lysed with 50 µl 0.1% Triton in PBS, and protein quantification was performed with the whole extract. Briefly, samples were added to a 96-well plate, and a BSA standard curve was established. 200 µl of a mix of Reagent A-

Reagent B (196 µl of reagent A with 4 µl of reagent B) was added to all samples. After 15 min at 37°C, absorbance was quantified using a Tecan Sunrise microplate reader at 550 nm.

2.3. Western Blot

Western blot technique was used for protein analysis. Protein samples were mixed with Laemmli loading buffer and boiled at 95ºC for 5 min. Protein samples were loaded onto 10-12% SDS-polyacrylamide electrophoresis gels and run in Tris-Glycine-SDS buffer (TGS 1X) using a Mini-Protean III/Tetra System (Bio-Rad). Precision Plus Protein Dual Color Standards (1610394, Bio-Rad) was used for accurate molecular weight estimation on the gel. Resolved proteins were transferred to a Polyvinylidene difluoride (PVDF) membrane (IPVH00010, Millipore), previously activated with methanol for 1 min, in transfer buffer at a constant voltage (100 V) for 60 min.

Before immunoblotting, the PVDF membrane was blocked with TBS-Tween (TBST) containing 1% BSA (A7906, Sigma-Aldrich) for 60 min at RT. Membranes were incubated with the primary antibody diluted in TBST containing 0.1% BSA overnight at 4ºC. Membranes were then washed three times with TBST for 5 min each and incubated with the appropriate secondary antibody (HRP-conjugated anti-IgG) for 1 h at RT. Finally, membranes were washed three times with TBST and developed with Immobilon Western Chemiluminescent HRP Substrate (WBKLS0500, Millipore) in an Alliance Q9 (UVITEC) chemiluminescent imager. The primary and secondary antibodies used in this thesis are listed in **Table M3**.

Antibody	Host	Dilution	Reference	Supplier
Anti-Mouse	Go	1:10000	31430	Invitrogen
Anti-Rabbit	Go	1:10000	ab205718	Abcam
β-Actin	Rb	1:10000	ab8227	Abcam
C/EBPα	Rb	1:1000	D56F10	Cell Signaling
Cytokeratin 14	Rb	1:1000	ab181595	Abcam
E-cadherin	Ms	1:2000	610182	Transduction Labs
Fibronectin	Rb	1:10000	ab2413	Abcam
Glut4	Rb	1:1000	ab33780	Abcam
LaminB1	Rb	1:2000	ab16048	Abcam
N-cadherin	Ms	1:1000	610920	Transduction Labs
PPARɣ	Rb	1:1000	C26H12	Cell Signaling
p-Stat3 (Tyr705)	Rb	1:1000	9145S	Cell Signaling
Snail1	Rb	1:1000	SN9H2	Cell Signaling
Stat3	Rb	1:1000	D3Z2G	Cell Signaling

Table M3. Primary and secondary antibodies used for Western blot analysis.

3. RNA ANALYSIS

3.2. RNA extraction

For RNA extraction, phenol-chloroform RNA extraction method was used. First, cells were washed twice with ice-cold PBS and lysed using TRIzol reagent (15596018, Invitrogen). The volume of TRIzol reagent was dependent on the culture plate surface. Lysates were then mixed with 200 µl of chloroform, vortexed, and incubated for 2 min at RT. Samples were then centrifuged at 12,000 x g for 20 min at 4°C. The aqueous phase was transferred into a new Eppendorf tube and mixed with 500 µl of RNase-free isopropanol. Eppendorfs were incubated for 15 min at RT and centrifuged at 12,000 x g for 20 min at 4° to

precipitate RNA. Supernatant was discarded, and the pellet was washed with 1 ml ethanol 75% and centrifuged at 12,000 x g for 20 min at 4°C. Ethanol was completely removed, and the RNA pellet was resuspended in 20-60 µl RNase-free water. Samples were then quantified using a NanoDrop and stored at -80°C until use.

3.2. Real-time quantitative reverse transcription coupled to polymerase chain reaction (RT-qPCR)

For quantitative analysis, 1-2 µg of RNA was retrotranscribed using the Transcriptor First Strand cDNA Synthesis Kit (04897030001, Roche) following manufacturer's instructions. 40 ng of cDNA were amplified with specific primers **(Table M4)** using the LightCycler 480 SYBR Green I Master Real Time System (04887352001, Roche). The amount of amplified cDNA was normalized to that of the housekeeping gene Hypoxanthine Phosphoribosyltransferase 1 (HPRT). All analyses were performed in triplicate.

Gene		Sequence
Mouse		
Cebpa	Fw	TTCGGGTCGCTGGATCTCTA
	Rv	TCAAGGAGAAACCACCACGG
Cdh1	Fw	TTCAACCCAAGCACGTATCA
	Rv	ACGGTGTACACAGCTTTCCA
Gadd45b	Fw	TAGAGGAACGCTGAGACCCA
	Rv	TCCCAGAAGGTATCACGGGT
Lipe	Fw	GGAGCTCCAGTCGGAAGAGG
	Rv	GTCTTCTGCGAGTGTCACCA
Rdh9	Fw	TGACCATCCCTCCCTGAAAAC
	Rv	GACTCACCAACCTAGCAGCA
Slc2a4	Fw	ATCCGGAACCTGGAGGGGCC
	Rv	TGGCTCAGCTGCAGCACCAC
Snai1	Fw	GCGCCCGTCGTCCTTCTCGTC
	Rv	CTTCCGCGACTGGGGGTCCT
Pparg	Fw	GGCTGCAGCGCTAAATTCTT
	Rv	TGCGAGTGGTCTTCCATCAC
Human		
CD68	Fw	GGATTCACCAGTTCTGCCCA
	Rv	CCGCCATGTAGCTCAGGTAG
CDH1	Fw	GAACGCATTGCCACATACAC
	Rv	ATTCGGGCTTGTTGTCATTC
GADD45A	Fw	CACTGTCGGGGTGTACGAAG
	Rv	GTTGATGTCGTTCTCGCAGC
MYC	Fw	AACACACAACGTCTTGGAGC
	Rv	GCACAAGAGTTCCGTAGCTG
SNAI1	Fw	GTGCCTCGACCACTATGCC
	Rv	GCTGCTGGAAGGTAAACTCTGG
Hprt/HPRT	Fw	GGCCAGACTTTGTTGGATTTG
	Rv	TGCGCTCATCTTAGGCTTTGT

Table M4. Primers used for RT-qPCR.

3.3. Total RNA-sequencing

RNA extraction from the samples was conducted following the phenol-chloroform RNA extraction method described in *Section 3.1*. Subsequent total RNA-sequencing and analysis were performed at Centre Nacional d'Anàlisi Genòmica (CNAG, Barcelona, Spain).

Total RNA was quantified using the Qubit® RNA BR Assay Kit (Thermo Fisher Scientific) and RNA integrity was assessed using the RNA 6000 Nano Bioanalyzer 2100 Assay (Agilent). The RNA-Seq libraries were prepared with the KAPA Stranded mRNA-Seq Kit for Illumina Platforms (Roche) according to the manufacturer's recommendations. Briefly, 500 ng of total RNA was used for poly-A fraction enrichment. The blunt-ended double-stranded cDNA was 3'-adenylated, and Illumina platform-compatible adaptors with unique dual indexes and unique molecular identifiers (Integrated DNA Technologies) were ligated. The ligation product was then enriched through 15 cycles of PCR, and the final library was validated using an Agilent 2100 Bioanalyzer with the DNA 7500 Assay. The libraries were sequenced on a NovaSeq 6000 (Illumina) in paired-end mode with a read length of 2x51 bp, following the manufacturer's protocol for dual indexing. Image analysis, base calling, and quality scoring of the run were processed using the manufacturer's Real Time Analysis (RTA 3.4.4) software, followed by the generation of FASTQ sequence files.

RNA-seq reads were mapped against the Homo sapiens (GRCh38) and Mus musculus (GRCm39) reference genomes with STAR/2.7.8a (Dobin et al., 2021) using ENCODE parameters. Gene

quantification was performed with RSEM/1.3.0 (Li and Dewey, 2011) using gencode.v42 and gencode.vM31 annotations. Differential expression analysis was performed with limma (Ritchie et al., 2015) using the voom (Law et al., 2014) transformation of the counts. Functional enrichment of the differentially expressed genes was performed using g:Profiler (Kolberg et al., 2023). Pathway enrichment analysis was performed using OmicsPlayground (BigOmics Analytics) (Akhmedov et al., 2019).

3.4. Bioinformatics analysis

A heatmap illustrating the expression of various markers in d3T3-L1 and d3T3-L1 + MCF7 was generated using the GSVA package in RStudio (Hänzelmann S et al., 2013). The markers include mature adipocyte markers (Adipoq, Plin1, Fabp4), adipogenic master regulators and early differentiation markers (Pparg, Cebpa, Lpl), mesenchymal stem cell or adipocyte progenitor genes (Cd44, Ly6a, Cd24a, Cd9), macrophage markers (Lgals3), and fibroblast genes (Acta2, Vim, Serpinh1). The gene list was sourced from (Zhu et al., 2022).

4. CELL STAINING

The following stainings were used to detect neutral lipid droplets in both adipocytes and tumoral cells.

4.1. Oil Red O (ORO)

Culture medium was removed from the culture plates and cells were washed twice with cold PBS. Cells were fixed with 4% paraformaldehyde (PFA) for 15 min at RT. Then, 4% PFA was

removed, cells were washed twice with cold PBS, and a filtered solution of 60% Oil Red O (01391, Sigma-Aldrich) with 40% H_2O was added for 15 min at RT. Finally, Oil Red O solution was removed and cells were washed with cold PBS until Oil Red O solution was completely removed. Random pictures were taken using an Inverted Microscope Axio Vert.A1 (491237-0002-000, Carl Zeiss). To quantify the ORO staining of the 3T3-L1 cells, ImageJ software (Schneider et al., 2012) was used to measure the stained area. Red color was selected using the Color Threshold tool (Hue 20-235, pass selected), and the percentage of the selected area was obtained for each image.

Alternatively, to quantify the ORO staining of the tumoral cells, isopropanol was added to elute the dye. The volume of isopropanol was dependent on plate surface. Absorbance was quantified using an Infinite M200 microplate Reader (Tecan) at 510 nm.

4.2. BODIPY 493/503

Culture medium was removed from the culture plates and cells were washed once with PBS. BODIPY 493/503 (D3922, Invitrogen) was added at a final concentration of 1 µg/ml in PBS for 10 min at 37°C. BODIPY 493/503 has an excitation wavelength of 480 nm and an emission maximum of 515 nm. Random pictures were taken using an Inverted Microscope Axio Vert.A1 (491237-0002-000, Carl Zeiss) with the appropriate fluorescence filter. Lipid droplet-positive and lipid droplet-negative cells were counted using Qupath software (Bankhead et al., 2017).

5. GLUCOSE QUANTIFICATION

Measurement of the glucose concentration of the media was performed according to the manufacturer's protocol (Abcam ab65333). Briefly, the media were obtained and added into each well with the reaction buffer. Simultaneously, a glucose standard curve was stablished and mixed with the reaction buffer. All the mixes were incubated 30 min at 37ºC. After, the fluorescence was measured at Ex/Em = 535/587nm using an Infinite M200 microplate Reader (Tecan). Data was normalized by cell number, and glucose consumption was determined by subtracting the glucose concentration of the initial (time zero) medium from each condition.

6. MIGRATION AND INVASION ASSAYS

Migration and invasion assays were performed using the Boyden chamber system. For migration assays, 1 $x10^5$ tumor cells were resuspended in DMEM 0.1% FBS in a final volume of 150 µl. Cells were seeded on the 8 µm (3422, Costar) pore size transwells and incubated for 48 h. For invasion assays, transwells were first coated with 50 µl of Matrigel 0.5 µg/µl (354230, Cultek) and incubated for at least 30 min at 37ºC. Then, 1 $x10^5$ tumor cells cells were resuspended in DMEM 0.1% FBS in a final volume of 150 µl. Cells were seeded on 8 µm (3422, Costar) pore size transwells and incubated for 48 h. In both migration and invasion assays, DMEM 10% FBS was used as chemoattractant added in the lower compartment with or without differentiated 3T3-L1 cells.

After 48 h, cells were fixed with 100% cold methanol for 20 min at -20ºC. Non-migrating and non-invading cells were removed from the upper compartment of the transwell with a cotton swab.

Migrating and invading cells were stained with Crystal Violet for 15 min at RT. After three washes with PBS, the membrane was cut with a scalpel and cells were rinsed with 30% acetic acid (300 µl). Absorbance was analyzed at 590 nm in an Infinite M200 microplate Reader (Tecan).

7. CRYSTAL VIOLET

For proliferation assays, 2 $x10^3$ AT3 cells, 1.5 $x10^3$ BTE136 cells or 2.5 $x10^3$ MCF7 cells were seeded in 96 well plates. After 24 h medium was removed and DMEM 10% FBS or d3T3L1 CM 10% FBS was added. After three days, cell proliferation was assessed using Crystal Violet staining. Similarly, 4.5 $x10^3$ MCF7 cells were seeded in 96 well plates. After 24 h medium was removed and DMEM 10% FBS was added together with Atglistatin, BMS-309403 or Etomoxir treatment. After two days, cell proliferation was assessed using Crystal Violet staining. Medium was removed, cells were washed three times with PBS, and fixed with 100% cold methanol for 20 min at -20ºC. After three washes with PBS, cells were incubated with Crystal Violet 0.25% for 15 min at RT. Finally, stained cells were washed three times with PBS and rinsed with 30% acetic acid (200 µl). Absorbance was measured at 590 nm in an Infinite M200 microplate Reader (Tecan).

8. SEAHORSE DETERMINATIONS

Approximately 4 $\times10^4$ MCF7 cells were plated on a Seahorse plate in control or treated with adipocyte conditioned media. After 48 h, cells were washed twice with Seahorse XF DMEM medium (D5030, Sigma Aldrich) supplemented with 5mM HEPES pH 7.4, 10 mM glucose (G7021, Sigma Aldrich), 100 mM sodium pyruvate

(11360039, Thermo Scientific), and 2 mM glutamine (25030-024, Thermo Scientific). Then, cells were incubated in the same media for 1 h at 37ºC without CO_2.

Oxygen consumption and ECAR were simultaneously recorded by a Seahorse XFe24 analyzer (Agilent) using the Mito Stress Test protocol, in which cells were sequentially perturbed with 1.5 µM Oligomycin (75351, Sigma Aldrich), 3 µM Carbonyl cyanide 3-chlorophenylhydrazone (CCCP, C2759, Sigma Aldrich), 1 µM Antimycin (A8674, Sigma Aldrich) and 1 µM Rotenone (R8875, Sigma Aldrich). Data was analyzed using the Seahorse Wave Desktop Software (v.2.6.3, Agilent). Data was normalized by protein concentration obtained with the BCA protein assay.

9. REACTIVE OXYGEN SPECIES (ROS) ASSAY

Approximately 6 $\times 10^4$ MCF7 cells were plated on a 96-well plate in control or treated conditions (adipocyte conditioned media). ROS production was measured using a cellular reactive oxygen species assay kit (Abcam, ab113851). Briefly, cells were labelled with DCFDA (2',7'-dichlorofluorescin diacetate), a redox sensitive fluorescent probe that it is oxidized by hydroperoxyl, peroxyl, and other ROS species (Figueroa et al., 2018). Cells were incubated for 1 h at 37ºC in the dark and fluorescence was measured at different time points. The fluorescence was measured at Ex/Em = 485/535nm using a microplate reader an Infinite M200 microplate Reader (Tecan). Data was normalized by cell number and expressed as AU (fluorescence/cell number)/ hour.

10. LIPIDOMICS

Cell supernatants were stored at -80°C until fatty acid analysis, which was performed at Hospital del Mar Research Institute (Barcelona, Spain). Sample was spiked with the internal standard (ISTD) glyceryl trinonadecanoate (Avanti, Merck) into a chloroform-resistant Eppendorf. Lipids were extracted with chloroform–methanol (2:1, v/v) containing butylated hydroxytoluene (50 mg/ml) and evaporated to dryness under N_2 at 37ºC. The lipid extract was re-dissolved in toluene and transferred to a screw-cap test-tube. Fatty acid methyl esters (FAMEs) were prepared by incubation with acidified methanol, as described (Burdge et al., 2000). FAMEs were analyzed by gas chromatography/electron ionization mass spectrometry (GC-MS), using an Agilent 6890N GC equipped with an Agilent 7683 autosampler and an Agilent 5973N mass spectrometry detector. FAMEs were separated with a J&W DB-FastFAME capillary column (30 m × 0.2 mm × 0.25 µm film thickness) (Agilent). Injections of 1 µL were performed (split ratio 25:1). FAMEs were quantified using the selected ion monitoring (SIM) mode. Based on the work of Thurnhofer and Vetter (Thurnhofer, and Vetter, 2005), several m/z ions common to saturated, monounsaturated, and polyunsaturated FAMEs were monitored. Twelve mixtures of FAME external calibration standards, spiked with C19:0-methyl ester in an equivalent amount to that included in samples as ISTD, were prepared by diluting FAME mix certified reference material (Supelco 37 Component FAME Mix, Merck) in hexane. The concentrations of 24 different FAMEs in the samples were calculated by linear regression of the peak area ratio relative to that of the ISTD. Each fatty acid was expressed as mg/L of supernatant.

11. ANIMAL STUDIES

Mice were housed in a specific pathogen-free area and fed *ad libitum* at the PRBB Animal Facility. Cycles of 12 h stable light or darkness were applied with a temperature of 22 ± 2ºC and humidity between 40-70%. All the animal procedures of the thesis were previously approved by the Animal Research Ethical Committee from the PRBB and by the Generalitat de Catalunya.

Polyoma Middle T antigen (PyMT) mice develop spontaneously Luminal B mammary gland tumors resembling human breast cancer development (Guy et al., 1992). Once tumors achieved the carcinoma stage, animals were sacrificed and tumor bearing mammary glands were extracted, 4 % PFA fixed overnight and embedded in paraffin blocks using standard histology techniques. 2.5 mm sections were sliced and hematoxylin and eosin (HE) stained.

12. STATISTICAL ANALYSIS

All data represent the relative mean of at least three independent experiments ± standard error of the mean (SEM). Data were analyzed by GraphPad Prism (v8) software (GraphPad Software, San Diego, USA). In all experiments, statistical significance was obtained using Student's t-test; p-value was represented in all the figures by * pvalue < 0.05; **, p-value < 0.01; or ***, p-value < 0.001.

13. BUFFERS AND SOLUTIONS

BODIPY 493/503: 1 mg/ml in DMSO

Crystal violet 0.25%: 0.25 g/L crystal violet (C3886, Sigma-Aldrich) in 30% methanol

Dexamethasone: 2mg/ml in DMSO

HBSS: 0.14 M NaCl, 5 mM KCl, 0.3 mM Na_2HPO_4-$2H_2O$, 0.4 mM KH_2PO_4, 6 mM D-glucose, 4 mM $NaHCO_3$ pH 7.5

IBMX: 0.1g/ml in DMSO

Insulin: 1 mg/ml in 0.01 M HCl

Laemmli sample Buffer 5X (LB): 250 mM Tris-HCl pH 6.8, 10% SDS, 0.5% bromophenol blue, 50% glycerol, 20% β-mercaptoethanol

MTT: 5 mg/ml in PBS

PBS: 137 mM NaCl, 2.7 mM KCl, 10 mM Na_2HPO_4, 1.8 mM KH_2PO_4

SDS lysis buffer: 2% SDS, 50 mM Tris pH 7.5, 10% glycerol

TBST: 25 mM Tris-HCl pH 7.5, 137 mM NaCl, 0.1% Tween-20

TGFβ1: 5 µg/ml in BSA 1 mg/ml

TGS 5X: 25 mM Tris pH 8.3, 192 mM glycine, 0.5% SDS

Transfer buffer 5X: 25 mM Tris pH 8.3, 192 mM glycine, 10% methanol

Trypan Blue: 0.4% w/v Trypan Blue (T6146, Sigma-Aldrich) in PBS

REFERENCES

Acharya, R., Shetty, S.S. and Kumari N, S. (2023) ‘Fatty Acid Transport Proteins (FATPs) in cancer’, Chemistry and Physics of Lipids, 250, 105269.

Adriá-Cebrián, J. et al. (2021) ‘MCF-7 drug resistant cell lines switch their lipid metabolism to triple negative breast cancer signature’, Cancers, 13(23), 5871.

Akhmedov, M. et al. (2019) ‘Omics Playground: A comprehensive self-service platform for visualization, analytics and exploration of Big Omics Data’, NAR Genomics and Bioinformatics, 2(1), lqz019.

Alba-Castellón, L. et al. (2016) ‘Snail1-dependent activation of cancer-associated fibroblast controls epithelial tumor cell invasion and metastasis’, Cancer Research, 76(21), 6205–6217.

Anderson, N.M. and Simon, M.C. (2020) ‘The tumor microenvironment’, Current Biology, 30(16), R921-R925.

Attané, C. and Muller, C. (2020) ‘Drilling for oil: Tumor-surrounding adipocytes fueling cancer’, Trends in Cancer, 6(7), 593–604.

Balaban, S. et al. (2017) ‘Adipocyte lipolysis links obesity to breast cancer growth: Adipocyte-derived fatty acids drive breast cancer cell proliferation and migration’, Cancer Metabolism, 5, 1.

Balaban, S. et al. (2019) ‘Extracellular fatty acids are the major contributor to lipid synthesis in prostate cancer’, Molecular Cancer Research, 17(4), 949–962.

Bankhead, P. et al. (2017) ‘QuPath: Open source software for digital pathology image analysis’, Scientific Reports, 7(1), 16878.

Barone, I. et al. (2020) ‘The weight of obesity in breast cancer progression and metastasis: Clinical and molecular perspectives’, Seminars in Cancer Biology, 60, 274–284.

Batlle, E. et al. (2000) ‘The transcription factor snail is a repressor of E-cadherin gene expression in epithelial tumour cells’, Nature Cell Biology, 2(2), 84–89.

Batlle, R. et al. (2012) ‘SNAIL1 controls TGF-β responsiveness and differentiation of mesenchymal stem cells’, Oncogene, 32(28), 3381–3389.

Baulida, J., Díaz, V.M. and García de Herreros, A. (2019) ‘Snail1: A transcriptional factor controlled at multiple levels’, Journal of Clinical Medicine, 8(6), 757.

Bazira, P.J., Ellis, H. and Mahadevan, V. (2022) ‘Anatomy and physiology of the breast’, Surgery (Oxford), 40(2), 79–83.

Bing, C. et al. (2006) ‘Adipose atrophy in cancer cachexia: Morphologic and molecular analysis of adipose tissue in tumour-bearing mice’, British Journal of Cancer, 95(8), 1028–1037.

Bochet, L. et al. (2013) ‘Adipocyte-derived fibroblasts promote tumor progression and contribute to the desmoplastic reaction in breast cancer’, Cancer Research, 73(18), 5657–5668.

Bray, et al. (2024) ‘Global cancer statistics 2022: GLOBOCAN estimates of incidence and mortality worldwide for 36 cancers in 185 countries’, CA: A Cancer Journal for Clinicians, 74(3), 229–263.

Britt, K.L., Cuzick, J. and Phillips, K.-A. (2020) ‘Key steps for effective breast cancer prevention’, Nature Reviews Cancer, 20(8), 417–436.

Broadfield, L.A. et al. (2021) ‘Lipid metabolism in cancer: New Perspectives and Emerging Mechanisms’, Developmental Cell, 56(10), 1363–1393.

Buja, A. et al. (2020) ‘Breast cancer primary prevention and diet: An Umbrella Review’, International Journal of Environmental Research and Public Health, 17(13), 4731.

Burdge, G.C. et al. (2000) ‘A method for separation of phosphatidylcholine, triacylglycerol, non-esterified fatty acids and cholesterol esters from plasma by solid-phase extraction’, British Journal of Nutrition, 84(5), 781–787.

Cai, Z. et al. (2023) ‘Adipocytes promote pancreatic cancer migration and invasion through fatty acid metabolic reprogramming’, Oncology Reports, 50(1), 141.

Calle, E.E. and Kaaks, R. (2004) ‘Overweight, obesity and cancer: Epidemiological evidence and proposed mechanisms’, Nature Reviews Cancer, 4(8), 579–591.

Calvisi, D.F. et al. (2011) ‘Increased lipogenesis, induced by AKT-mtorc1-RPS6 signaling, promotes development of human hepatocellular carcinoma’, Gastroenterology, 140(3), 1071–1083.

Cano, A. et al. (2000) ‘The transcription factor snail controls epithelial–mesenchymal transitions by repressing E-cadherin expression’, Nature Cell Biology, 2(2), 76–83.

Cass, I. et al. (2003) ‘Improved survival in women with BRCA-associated ovarian carcinoma’, Cancer, 97(9), 2187–2195.

Castelli, S. et al. (2021) ‘Lipid catabolism and Ros in cancer: A bidirectional liaison’, Cancers, 13(21), 5484.

Cave, E. and Crowther, N.J. (2018) ‘The use of 3T3-L1 murine preadipocytes as a model of adipogenesis’, Methods in Molecular Biology, 263–272.

Cawthorn, W.P. and Sethi, J.K. (2007) ‘TNF-α and Adipocyte Biology’, FEBS Letters, 582(1), 117–131.

Chan, D.S.M. et al. (2014) ‘Body mass index and survival in women with breast cancer-systematic literature review and meta-analysis of 82 follow-up studies’, Annals of Oncology, 25(10), 1901–1914.

Charrière, G. et al. (2003) ‘Preadipocyte conversion to macrophage’, Journal of Biological Chemistry, 278(11), 9850–9855.

Chen, X. et al. (2009) ‘TNF-α, a potent lipid metabolism regulator’, Cell Biochemistry and Function, 27(7), 407–416.

Clement, E. et al. (2020) ‘Adipocyte extracellular vesicles carry enzymes and fatty acids that stimulate mitochondrial metabolism and remodeling in tumor cells’, The EMBO Journal, 39(3), e102525.

Colditz, G.A. and Bohlke, K. (2015) ‘Preventing breast cancer now by acting on what we already know’, npj Breast Cancer, 1(1), 15009.

Cruz, A.L. et al. (2020) ‘Lipid droplets: Platforms with multiple functions in cancer hallmarks’, Cell Death & Disease, 11(2), 105.

Danaei, G. et al. (2005) ‘Causes of cancer in the world: comparative risk assessment of nine behavioural and environmental risk factors’, The Lancet, 366(9499), 1784–1793.

DeBerardinis, R.J. and Chandel, N.S. (2020) ‘We need to talk about the Warburg effect’, Nature Metabolism, 2(2), 127–129.

Deisenroth, C. et al. (2014) ‘Myc is an early response regulator of human adipogenesis in adipose stem cells’, PLoS ONE, 9(12), e114133.

Dhurandhar, N.V. (2022) ‘What is obesity?’, International Journal of Obesity, 46(6), 1081–1082.

Díaz, V., Viñas-Castells, R. and García de Herreros, A. (2014) ‘Regulation of the protein stability of EMT transcription factors’, Cell Adhesion & Migration, 8(4), 418–428.

Díaz, V.M. and García de Herreros, A. (2016) ‘F-box proteins: Keeping the epithelial-to-mesenchymal transition (EMT) in check’, Seminars in Cancer Biology, 36, 71–79.

Ding, X., Zhang, W., Li, S. and Yang, H. (2019). ‘The role of cholesterol metabolism in cancer’. American Journal of Cancer Research, 219–227.

Dirat, B. et al. (2011) ‘Cancer-associated adipocytes exhibit an activated phenotype and contribute to breast cancer invasion’, Cancer Research, 71(7), 2455–2465.

Dobin, A. et al. (2012) ‘Star: Ultrafast universal RNA-seq aligner’, Bioinformatics, 29(1), 15–21.

Dongre, A. and Weinberg, R.A. (2018) ‘New insights into the mechanisms of epithelial–mesenchymal transition and implications for cancer’, Nature Reviews Molecular Cell Biology, 20(2), 69–84.

Dumas, J.-F. and Brisson, L. (2020) ‘Interaction between adipose tissue and cancer cells: Role for cancer progression’, Cancer and Metastasis Reviews, 40(1), 31–46.

Düvel, K. et al. (2010) ‘Activation of a metabolic gene regulatory network downstream of mTOR complex 1’, Molecular Cell, 39(2), 171–183.

Escrivà, M. et al. (2008) ‘Repression of PTEN phosphatase by SNAIL1 transcriptional factor during gamma radiation-induced apoptosis’, Molecular and Cellular Biology, 28(5), 1528–1540.

Fares, J. et al. (2020) ‘Molecular principles of metastasis: A hallmark of cancer revisited’, Signal Transduction and Targeted Therapy, 5(1), 28.

Feng, W.W., Zuppe, H.T. and Kurokawa, M. (2023) ‘The role of CD36 in cancer progression and its value as a therapeutic target’, Cells, 12(12), 1605.

Fernyhough, M.E. et al. (2004) ‘Primary adipocyte culture: Adipocyte purification methods may lead to a new understanding of adipose tissue growth and development’, Cytotechnology, 46(2–3), 163–172.

Figueroa, D., Asaduzzaman, M. and Young, F. (2018) ‘Real time monitoring and quantification of reactive oxygen species in breast cancer cell line MCF-7 by 2′,7′–dichlorofluorescin diacetate (DCFDA) assay’, Journal of Pharmacological and Toxicological Methods, 94, 26–33.

Friedenreich, C.M., Neilson, H.K. and Lynch, B.M. (2010) ‘State of the epidemiological evidence on physical activity and cancer prevention’, European Journal of Cancer, 46(14), 2593–2604.

Ganesh, K. and Massagué, J. (2021) ‘Targeting metastatic cancer’, Nature Medicine, 27(1), 34–44.

García de Herreros, A. (2024) ‘Dual role of SNAIL1 as transcriptional repressor and activator’, Biochimica et Biophysica Acta (BBA) - Reviews on Cancer, 1879(1), 189037.

Giulitti, F. et al. (2021) ‘Anti-tumor effect of oleic acid in hepatocellular carcinoma cell lines via autophagy reduction’, Frontiers in Cell and Developmental Biology, 9, 629182.

Green, H. and Kehinde, O. (1975) ‘An established preadipose cell line and its differentiation in culture II. Factors affecting the adipose conversion’, Cell, 5(1), 19–27.

Griesel, B.A. et al. (2021) ‘Pfkfb3-dependent glucose metabolism regulates 3T3-L1 adipocyte development’, The FASEB Journal, 35(7), e21728.

Guaita-Esteruelas, S. et al. (2016) ‘Exogenous Fabp4 increases breast cancer cell proliferation and activates the expression of fatty acid transport proteins’, Molecular Carcinogenesis, 56(1), 208–217.

Guaita-Esteruelas, S. et al. (2018) ‘The peritumoural adipose tissue microenvironment and cancer. The roles of fatty acid binding protein 4 and fatty acid binding protein 5’, Molecular and Cellular Endocrinology, 462, 107–118.

Guerrero-Rodríguez, S.L. et al. (2022) ‘Role of CD36 in cancer progression, stemness, and targeting’, Frontiers in Cell and Developmental Biology, 10, 1079076.

Gustafson, B. and Smith, U. (2010) ‘Activation of canonical wingless-type MMTV integration site family (Wnt) signaling in mature adipocytes increases β-catenin levels and leads to cell dedifferentiation and insulin resistance’, Journal of Biological Chemistry, 285(18), 14031–14041.

Guy, C.T., Cardiff, R.D. and Muller, W.J. (1992) ‘Induction of mammary tumors by expression of polyomavirus middle T oncogene: A transgenic mouse model for metastatic disease’, Molecular and Cellular Biology, 12(3), 954–961.

Gyamfi, J. et al. (2018) ‘Interleukin-6/STAT3 signalling regulates adipocyte induced epithelial-mesenchymal transition in breast cancer cells’, Scientific Reports, 8(1), 8859.

Gyamfi, J. et al. (2021) ‘Interaction between CD36 and FABP4 modulates adipocyte-induced fatty acid import and metabolism in breast cancer’, npj Breast Cancer, 7(1), 129.

Han, J. et al. (2018) ‘Interleukin-6 induces fat loss in cancer cachexia by promoting white adipose tissue lipolysis and browning’, Lipids in Health and Disease, 17(1), 14.

Hanahan, D. (2022) ‘Hallmarks of cancer: New dimensions’, Cancer Discovery, 12(1), 31–46.

Hanahan, D. and Weinberg, R.A. (2000) ‘The hallmarks of cancer’, Cell, 100(1), 57–70.

Hanahan, D. and Weinberg, R.A. (2011) ‘Hallmarks of cancer: The next generation’, Cell, 144(5), 646–674.

Hänzelmann, S., Castelo, R. and Guinney, J. (2013) ‘GSVA: Gene set variation analysis for microarray and RNA-Seq Data’, BMC Bioinformatics, 14(1), 7.

Harbeck, N. et al. (2019) ‘Breast cancer’, Nature Reviews Disease Primers, 5(1), 66.

Herranz, N. et al. (2008) ‘Polycomb Complex 2 is required for E-cadherin repression by the SNAIL1 transcription factor’, Molecular and Cellular Biology, 28(15), 4772–4781.

Hirano, H. et al. (2020) ‘Impact of pretreatment total cholesterol level is associated with metastasis of prostate cancer’, American Journal of Men’s Health, 14(2), 1557988320918788.

Hoy, A.J., Balaban, S. and Saunders, D.N. (2017) ‘Adipocyte–tumor cell metabolic crosstalk in breast cancer’, Trends in Molecular Medicine, 23(5), 381–392.

Hoy, A.J., Nagarajan, S.R. and Butler, L.M. (2021) ‘Tumour fatty acid metabolism in the context of therapy resistance and obesity’, Nature Reviews Cancer, 21(12), 753–766.

Hsieh, A.L. et al. (2015) ‘Myc and metabolism on the path to cancer’, Seminars in Cell & Developmental Biology, 43, 11–21.

Hu, W. et al. (2019) ‘Lung cancer-derived extracellular vesicles induced myotube atrophy and adipocyte lipolysis via the extracellular il-6-mediated STAT3 pathway’, Biochimica et Biophysica Acta (BBA) - Molecular and Cell Biology of Lipids, 1864(8), 1091–1102.

Jones, S.A. and Jenkins, B.J. (2018) ‘Recent insights into targeting the IL-6 cytokine family in inflammatory diseases and cancer’, Nature Reviews Immunology, 18(12), 773–789.

Kalluri, R. and Weinberg, R.A. (2009) ‘The basics of epithelial-mesenchymal transition’, Journal of Clinical Investigation, 119(6), 1420–1428.

Kami, D. et al. (2016) ‘Cardiac mesenchymal progenitors differentiate into adipocytes via KLF4 and c-myc’, Cell Death & Disease, 7(4), e2190.

Kaufhold, S. and Bonavida, B. (2014) ‘Central role of SNAIL1 in the regulation of EMT and resistance in cancer: A target for therapeutic intervention’, Journal of Experimental & Clinical Cancer Research, 33(1), 62.

Kim, N.H. et al. (2017) ‘Snail reprograms glucose metabolism by repressing phosphofructokinase PFKP allowing cancer cell survival under metabolic stress’, Nature Communications, 8(1), 14374.

Kocianova, E., Piatrikova, V. and Golias, T. (2022) ‘Revisiting the Warburg effect with focus on lactate’, Cancers, 14(24), 6028.

Kolberg, L. et al. (2023) ‘g:Profiler—interoperable web service for Functional Enrichment Analysis and gene identifier mapping (2023 update)’, Nucleic Acids Research, 51(W1), W207-W212.

Kopelman, P.G. (2000) ‘Obesity as a medical problem’, Nature, 404(6778), 635–643.

Koppenol, W.H., Bounds, P.L. and Dang, C.V. (2011) ‘Otto Warburg’s contributions to current concepts of cancer metabolism’, Nature Reviews Cancer, 11(5), 325–337.

Kothari, C., Diorio, C. and Durocher, F. (2020). The Importance of Breast Adipose Tissue in Breast Cancer. International Journal of Molecular Sciences, 21(16), 5760.

La Camera, G. et al. (2021) 'Adipocyte-derived extracellular vesicles promote breast cancer cell malignancy through hif-1α activity', Cancer Letters, 521, 155–168.

Laurent, V. et al. (2019) 'Periprostatic adipose tissue favors prostate cancer cell invasion in an obesity-dependent manner: Role of oxidative stress', Molecular Cancer Research, 17(3), 821–835.

Law, C.W. et al. (2014) 'Voom: precision weights unlock linear model analysis tools for RNA-seq read counts', Genome Biology, 15(2), R29.

Lazar, I. et al. (2016) 'Adipocyte exosomes promote melanoma aggressiveness through fatty acid oxidation: A novel mechanism linking obesity and cancer', Cancer Research, 76(14), 4051–4057.

Leone, K., Poggiana, C. and Zamarchi, R. (2018) 'The interplay between circulating tumor cells and the immune system: From immune escape to cancer immunotherapy', Diagnostics, 8(3), 59.

Li, B. and Dewey, C.N. (2011) 'RSEM: Accurate transcript quantification from RNA-seq data with or without a reference genome', BMC Bioinformatics, 12(1), 323.

Li, J. et al. (2017) 'Lipid desaturation is a metabolic marker and therapeutic target of ovarian cancer stem cells', Cell Stem Cell, 20(3), 303–314.

Li, S. et al. (2020) ‘Obesity promotes gastric cancer metastasis via diacylglycerol acyltransferase 2-dependent lipid droplets accumulation and redox homeostasis’, Redox Biology, 36, 101596.

Liang, Y. et al. (2018) ‘CD36 plays a critical role in proliferation, migration and tamoxifen-inhibited growth of ER-positive breast cancer cells’, Oncogenesis, 7(12), 98.

Liotti, A. et al. (2018) ‘Oleic acid promotes prostate cancer malignant phenotype via the G protein-coupled receptor FFA1/GPR40’, Journal of Cellular Physiology, 233(9), 7367–7378.

Liu, K. and Czaja, M.J. (2012) ‘Regulation of lipid stores and metabolism by lipophagy’, Cell Death & Differentiation, 20(1), 3–11.

Liu, W. et al. (2021) ‘Dysregulated cholesterol homeostasis results in resistance to ferroptosis increasing tumorigenicity and metastasis in cancer’, Nature Communications, 12(1), 5103.

Liu, X.-Z. et al. (2022) ‘C/EBPB-dependent adaptation to palmitic acid promotes tumor formation in hormone receptor negative breast cancer’, Nature Communications, 13(1), 69.

Liu, Y. and Cao, X. (2016) ‘Characteristics and significance of the pre-metastatic niche’, Cancer Cell, 30(5), 668–681.

Mahdavi, M. et al. (2018) ‘Hereditary breast cancer; genetic penetrance and current status with BRCA’, Journal of Cellular Physiology, 234(5), 5741–5750.

Mani, S.A. et al. (2008) ‘The epithelial-mesenchymal transition generates cells with properties of stem cells’, Cell, 133(4), 704–715.

Martin-Perez, M. et al. (2022) ‘The role of lipids in cancer progression and metastasis’, Cell Metabolism, 34(11), 1675–1699.

Massagué, J. and Obenauf, A.C. (2016) ‘Metastatic colonization by circulating tumour cells’, Nature, 529(7586), 298–306.

Mayer, N. et al. (2013) ‘Development of small-molecule inhibitors targeting adipose triglyceride lipase’, Nature Chemical Biology, 9(12), 785–787.

Mehlen, P. and Puisieux, A. (2006) ‘Metastasis: A question of life or death’, Nature Reviews Cancer, 6(6), 449–458.

Mele, L. et al. (2018) ‘A new inhibitor of glucose-6-phosphate dehydrogenase blocks pentose phosphate pathway and suppresses malignant proliferation and metastasis in vivo’, Cell Death & Disease, 9(5), 572.

Mendes, C. et al. (2019) ‘Unraveling Fatp1, regulated by ER-β, as a targeted breast cancer innovative therapy’, Scientific Reports, 9(1), 14107.

Mestre-Farrera, A. et al. (2021) ‘Glutamine-directed migration of cancer-activated fibroblasts facilitates epithelial tumor invasion’, Cancer Research, 81(2), 438–451.

Meyer, N. and Penn, L.Z. (2008) ‘Reflecting on 25 years with MYC’, Nature Reviews Cancer, 8(12), 976–990.

Migita, T. et al. (2008) ‘ATP citrate lyase: Activation and therapeutic implications in non–small cell lung cancer’, Cancer Research, 68(20), 8547–8554.

Miranda, F. et al. (2016) ‘Salt-inducible kinase 2 couples ovarian cancer cell metabolism with survival at the adipocyte-rich metastatic niche’, Cancer Cell, 30(2), 273–289.

Mollinedo, F. and Gajate, C. (2020) ‘Lipid rafts as signaling hubs in cancer cell survival/death and invasion: Implications in tumor progression and therapy’, Journal of Lipid Research, 61(5), 611–635.

Morigny, P. et al. (2021) ‘Lipid and glucose metabolism in white adipocytes: pathways, dysfunction and therapeutics’, Nature Reviews Endocrinology, 17(5), 276–295.

Mukherjee, A. et al. (2020) ‘Adipocyte-induced FABP4 expression in ovarian cancer cells promotes metastasis and mediates carboplatin resistance’, Cancer Research, 80(8), 1748–1761.

Mukherjee, A., Bilecz, A.J. and Lengyel, E. (2022) ‘The adipocyte microenvironment and cancer’, Cancer and Metastasis Reviews, 41(3), 575–587.

Nagarajan, S.R., Butler, L.M. and Hoy, A.J. (2021) ‘The diversity and breadth of cancer cell fatty acid metabolism’, Cancer & Metabolism, 9(1), 2.

Nath, A. and Chan, C. (2016) ‘Genetic alterations in fatty acid transport and metabolism genes are associated with metastatic progression and poor prognosis of human cancers’, Scientific Reports, 6(1), 18669.

Nelson, D. L., Cox, M. and Hoskins, A. et al. (2021) ‘Glycolysis, Gluconeogenesis, and the Pentose Phosphate Pathway’, *Lehninger Principles of Biochemistry*, NY: Macmillan International, 1964-2131.

Nelson, E.R. et al. (2013) '27-hydroxycholesterol links hypercholesterolemia and breast cancer pathophysiology', Science, 342(6162), 1094–1098.

Nieman, K.M. et al. (2011) 'Adipocytes promote ovarian cancer metastasis and provide energy for rapid tumor growth', Nature Medicine, 17(11), 1498–1503.

Nieman, K.M. et al. (2013) 'Adipose tissue and adipocytes support tumorigenesis and Metastasis', Biochimica et Biophysica Acta (BBA) - Molecular and Cell Biology of Lipids, 1831(10), 1533–1541.

Nieto, M.A. et al. (2016) 'EMT: 2016', Cell, 166(1), 21–45.

Oh, D.Y. and Bang, Y.J. (2020) 'HER2-targeted therapies — a role beyond breast cancer', Nature Reviews Clinical Oncology, 17(1), 33–48.

Okuyama, H. et al. (2010) 'Downregulation of c-MYC protein levels contributes to cancer cell survival under dual deficiency of oxygen and glucose', Cancer Research, 70(24), 10213–10223.

Pandaya, S. and Moore, R. (2011). Breast Development and Anatomy. Clinical Obstetrics & Gynecology, 54(1), 91-95.

Pascale, R.M. et al. (2020) 'The Warburg effect 97 years after its discovery', Cancers, 12(10), 2819.

Pascual, G. et al. (2021) 'Dietary palmitic acid promotes a prometastatic memory via Schwann cells', Nature, 599(7885), 485–490.

Pati, S. et al. (2023) 'Obesity and Cancer: A Current Overview of Epidemiology, Pathogenesis, Outcomes, and Management', Cancers, 15(2), 485.

Patra, K.C. and Hay, N. (2014) ‘The pentose phosphate pathway and cancer’, Trends in Biochemical Sciences, 39(8), 347–354.

Peláez-García, A. et al. (2015) ‘A proteomic analysis reveals that snail regulates the expression of the nuclear orphan receptor nuclear receptor subfamily 2 group F member 6 (NR2F6) and interleukin 17 (IL-17) to inhibit adipocyte differentiation’, Molecular & Cellular Proteomics, 14(2), 303–315.

Pepino, M.Y. et al. (2014) ‘Structure-function of CD36 and importance of fatty acid signal transduction in fat metabolism’, Annual Review of Nutrition, 34(1), 281–303.

Piskounova, E. et al. (2015) ‘Oxidative stress inhibits distant metastasis by human melanoma cells’, Nature, 527(7577), 186–191.

Polyak, K., 2007. Breast cancer: origins and evolution. The Journal of Clinical Investigation, 117(11), 3155-3163.

Quail, D.F. and Dannenberg, A.J. (2018) ‘The obese adipose tissue microenvironment in cancer development and progression’, Nature Reviews Endocrinology, 15(3), 139–154.

Riboli, E. (2000) ‘The European prospective investigation into cancer and nutrition: perspectives for cancer prevention’, Cancer & Nutrition, 4, 117–133.

Rinaldi, S. et al. (2006) ‘Relationship of alcohol intake and sex steroid concentrations in blood in pre- and post-menopausal women: the European Prospective Investigation into Cancer and Nutrition’, Cancer Causes & Control, 17(8), 1033–1043.

Ritchie, M.E. et al. (2015) ‘Limma powers differential expression analyses for RNA-sequencing and Microarray Studies’, Nucleic Acids Research, 43(7), e47.

Romieu, I.I., Amadou, A. and Chajes, V. (2017) ‘The role of diet, physical activity, body fatness, and breastfeeding in breast cancer in young women: Epidemiological evidence’, Clinical and Translational Investigation, 69(4), 193-203.

Ruan, H. et al. (2003) ‘Standard isolation of primary adipose cells from mouse epididymal fat pads induces inflammatory mediators and down-regulates adipocyte genes’, Journal of Biological Chemistry, 278(48), 47585–47593.

Rybinska, I. et al. (2021) ‘Cancer-associated adipocytes in breast cancer: Causes and consequences’, International Journal of Molecular Sciences, 22(7), 3775.

Schneider, C.A., Rasband, W.S. and Eliceiri, K.W. (2012) ‘NIH image to Imagej: 25 years of image analysis’, Nature Methods, 9(7), 671–675.

Schug, Z.T., Vande Voorde, J. and Gottlieb, E. (2016) ‘The metabolic fate of acetate in cancer’, Nature Reviews Cancer, 16(11), 708–717.

Shen, L. et al. (2023) ‘Leptin secreted by adipocytes promotes EMT transition and endometrial cancer progression via the JAK2/STAT3 signalling pathway’, Adipocyte, 13(1), e2293273.

Slamon, D.J. et al. (1987) ‘Human breast cancer: correlation of relapse and survival with amplification of the HER-2/neu oncogene’, Science, 235(4785), 177–182.

Stemmler, M.P. et al. (2019) ‘Non-redundant functions of EMT transcription factors’, Nature Cell Biology, 21(1), 102–112.

Sun, Y.-S. et al. (2017) ‘Risk factors and preventions of breast cancer’, International Journal of Biological Sciences, 13(11), 1387–1397.

Swinnen, J.V. et al. (2001) ‘Overexpression of fatty acid synthase is an early and common event in the development of prostate cancer’, International Journal of Cancer, 98(1), 19–22.

TeSlaa, T. et al. (2023) ‘The pentose phosphate pathway in health and disease’, Nature Metabolism, 5(8), 1275–1289.

Thurnhofer, S. and Vetter, W. (2005) ‘A gas chromatography/electron ionization−mass spectrometry−selected ion monitoring method for determining the fatty acid pattern in food after formation of fatty acid methyl esters’, Journal of Agricultural and Food Chemistry, 53(23), 8896–8903.

Toledo, E. et al. (2015) ‘Mediterranean diet and invasive breast cancer risk among women at high cardiovascular risk in the PREDIMED trial: A Randomized Clinical Trial’, JAMA Internal Medicine, 175(11), 1752–1760.

Tzavlaki, K. and Moustakas, A. (2020) ‘TGF-β Signaling’, Biomolecules, 10(3), 487.

Vander Heiden, M.G., Cantley, L.C. and Thompson, C.B. (2009) ‘Understanding the Warburg effect: The metabolic requirements of cell proliferation’, Science, 324(5930), 1029–1033.

Vasseur, S. and Guillaumond, F. (2022) ‘Lipids in cancer: A global view of the contribution of lipid pathways to metastatic formation and treatment resistance’, Oncogenesis, 11(1), 46.

Wang, Y. and Patti, G.J. (2023) ‘The Warburg effect: A signature of mitochondrial overload’, Trends in Cell Biology, 33(12), 1014–1020.

Wang, Y.Y. et al. (2017) ‘Mammary adipocytes stimulate breast cancer invasion through metabolic remodeling of tumor cells’, JCI Insight, 2(4), e87489.

Wang, T. et al. (2018) ‘JAK/STAT3-Regulated Fatty Acid β-Oxidation Is Critical for Breast Cancer Stem Cell Self-Renewal and Chemoresistance’, Cell Metabolism, 27(1), 136–150.e5.

Warburg, O. (1956) ‘On the origin of Cancer Cells’, Science, 123(3191), 309–314.

Wei, L. et al. (2016) ‘Leptin promotes epithelial-mesenchymal transition of breast cancer via the upregulation of pyruvate kinase M2’, Journal of Experimental & Clinical Cancer Research, 35(1), 166.

Wu, K. et al. (2024) ‘The pleiotropic functions of reactive oxygen species in cancer’, Nature Cancer, 5(3), 384–399.

Yang, J. et al. (2020) ‘Guidelines and definitions for research on epithelial–mesenchymal transition’, Nature Reviews Molecular Cell Biology, 21(6), 341–352.

Yang, J.H. et al. (2020) ‘Snail augments fatty acid oxidation by suppression of mitochondrial ACC2 during cancer progression’, Life Science Alliance, 3(7), e202000683.

Yin, N. et al. (2004) ‘Molecular mechanisms involved in the growth stimulation of breast cancer cells by leptin’, Cancer Research, 64(16), 5870–5875.

Yu, H. et al. (2014) ‘Revisiting STAT3 signalling in cancer: new and unexpected biological functions’, Nature Reviews Cancer, 14(11), 736–746.

Zhang, M. et al. (2018) ‘Adipocyte-derived lipids mediate melanoma progression via FATP proteins’, Cancer Discovery, 8(8), 1006–1025.

Zhang, M., Lee, A. and Rosen, J.M. (2017). The Cellular Origin and Evolution of Breast Cancer. Cold Spring Harbor Perspectives in Medicine, 7(3), a027128.

Zhang, S. et al. (2022) ‘The regulation, function, and role of lipophagy, a form of selective autophagy, in metabolic disorders’, Cell Death & Disease, 13(2), 132.

Zhao, C. et al. (2020) ‘Cancer-associated adipocytes: Emerging supporters in breast cancer’, Journal of Experimental & Clinical Cancer Research, 39(1), 156.

Zhao, W. et al. (2016) ‘Candidate Antimetastasis Drugs Suppress The Metastatic Capacity of Breast Cancer Cells by Reducing Membrane Fluidity’, Cancer Research, 76(7), 2037–2049.

Zhou, B.P. et al. (2004) ‘Dual regulation of snail by GSK-3β-mediated phosphorylation in control of epithelial–mesenchymal transition’, Nature Cell Biology, 6(10), 931–940.

Zhu, Q. et al. (2022) ‘Adipocyte mesenchymal transition contributes to mammary tumor progression’, Cell Reports, 40(11), 111362.

Zou, X. et al. (2022) ‘Targeting the PDGF/PDGFR signaling pathway for cancer therapy: A Review’, International Journal of Biological Macromolecules, 202, 539–557.